Role for the Peripheral Benzodiazepine Receptor in Neuroinflammation of Neurodegenerative disorders

by

Sriram Venneti

M.D. Bangalore Medical College, Bangalore University, India 1998

Submitted to the Graduate Faculty of the School of

Medicine, Department of Neurobiology, in partial fulfillment

of the requirements for the degree of

Doctor of Philosophy

University of Pittsburgh

2006

UNIVERSITY OF PITTSBURGH

SCHOOL OF MEDICINE

This thesis/dissertation was presented

by

Sriram Venneti

It was defended on

March 14th 2006

and approved by

Committee Chair: Donald DeFranco, Ph.D., Professor, Department of Pharmacology

Patrick J. Card, Ph.D., Associate Professor, Department of Neuroscience

Charleen T. Chu, M.D., Ph.D., Associate Professor, Departmental of Pathology

Michael J. Zigmond, Ph.D., Professor, Department of Neurology

External Examiner: Eliezer Masliah, M.D., Professor of Pathology and Neuroscience,

University of San Diego, California.

Thesis Dissertation Advisor: Clayton A. Wiley, M.D., Ph.D., Professor, Department of Pathology

Role for the Peripheral Benzodiazepine Receptor in Neuroinflammation of Neurodegenerative disorders

Sriram Venneti, M.D.

University of Pittsburgh, 2006

Neuroinflammation is a major component of several neurodegenerative disorders such as Alzheimer's disease, HIV-associated dementia, Multiple sclerosis and Parkinson's disease. Although the primary pathology underlying each of these diseases is vastly different, neuroinflammation, consisting of chronic activation of brain macrophages, is a significant factor that contributes to neuronal damage in all these conditions. Were it possible to image chronic activation of brain macrophages, it would be possible to monitor developing neuroinflammation and assess the efficacy of therapies that are targeted at modulating CNS inflammation.

The goal of this thesis is to determine if activated brain macrophages can be imaged in vivo using positron emission tomography. *We propose to take advantage of increased expression of the peripheral benzodiazepine receptor in activated brain macrophages and hypothesize that ligands that bind specifically to this receptor will label activated brain macrophages in vivo using positron emission tomography.* The peripheral benzodiazepine receptor is normally expressed at low levels in the central nervous system in astrocytes and brain macrophages and is hypothesized to increase specifically on brain macrophages in neuroinflammation.

We show that PK11195, a specific ligand to the peripheral benzodiazepine receptor, shows increased binding to brain macrophages in HIV encephalitis and that PK11195 can be used to image brain macrophages in vivo using positron emission tomography in a macaque model of HIV encephalitis. PK11195 binding is also increased in activated brain macrophages in Alzheimer's disease and shows age dependent increases in transgenic mice models of Alzheimer's disease. Finally we compare binding characteristics of DAA1106, a novel peripheral benzodiazepine receptor ligand, with PK11195 to show that DAA1106 binds with greater affinity in rat models of neuroinflammation both in brain tissues as well as in vivo. These data suggest that ligands of the peripheral benzodiazepine receptor specifically label activated brain macrophages and may be used to image neuroinflammation in vivo using positron emission tomography.

TABLE OF CONTENTS

LIST OF TABLES

LIST OF FIGURES

ACKNOWLEDGEMENTS

This work was not possible without the guidance, vision, and exceptional mentorship provided by Dr. Clayton A. Wiley. Always a source of inspiration and wisdom, whether viewing slides on the microscope or heatedly discussing recently published results, Clayton has gone above and beyond requirements in his careful attention to both my projects and my career. He will continue to serve as the role model in all my professional and scientific endeavors. I'd like to thank the members of my thesis committee, Prof. Donald DeFranco, Dr. Patrick Card, Dr. Charleen Chu, Prof. Eliezer Masliah and Prof. Michael Zigmond for their guidance during this project.

During the evolution of this work, I have accumulated many debts, only a proportion of which I have the space to acknowledge here. I thank the present and past members of the Wiley lab for their help, support and friendship. Special thanks are due to Guoji Wang for her help and mastery with the confocal microscope. I would like to thank Stephanie Bissel who shared the journey of graduate school with me and was a constant source of humor, energy and camaraderie. I would like to thank members of the PET center at UPMC, especially Brain Lopresti, Prof. Chester A. Mathis, James Ruszkiewicz and Susan Slagel who made the PET studies possible. I would like to thank members of the Division of Neuropathology, especially Karen Weber, Jonette Werley, Arlene Carbone-Wiley, and Dr. Ronald Hamilton. I would like to thank members of Dr. Micheal Murphy-Corb's lab for their help with the primates. I would like to thank my parents and my family for their constant patience and love.

Finally, I would like to thank my partner Dennis Pozega who is my soul mate, constant source of support and whose remarkable sense of humor can bring the sun out on the grayest Pittsburgh day.

ABBREVIATIONS

[11C]	Crabon-11 labeled ligand
[3H]	Tritium labeled ligand
6-OHDA	6-Hydroxy Dopamine
AD	Alzheimer's Disease
AIDS	Acquired Immunodeficiency Syndrome
Akt	Serine/threonine protein kinase downstream of PI3K
ANT	Adenine Nucleotide Transporter
APP	Amyloid Precursor Protein
Aβ	Amyloid Beta
Bmax	Maximal bound Receptors
CD 4+ T cell	Cluster Differentiation type 4 T lymphocyte
CD68	Lysosomal marker for activated macrophages
CNS	Central Nervous System
Con	Control
CSF	Cerebrospinal Fluid
DAA1106	(N-(2,5-Dimethoxybenzyl)-N-(5-fluoro-2-phenoxyphenyl)acetamide)
dCAMP	Dibutyryl Cyclic Adenosine Mono Phosphate
F 4/80	Marker for activated mouse macrophages
Fc	Constant Fragment of Antibody
GFAP	Glial Fibrillary Acidic Protein (marker for astrocytes)
HAART	Highly Active Antiretroviral Therapy
HEPES	4-(2-hydroxyethyl)-1-piperazineethanesulfonic acid, 4-(2-hydroxyethyl)-1-piperazineethanesulphonic acid- Buffer
HIV	Human Immunodeficiency Virus
HIVE	Human Immunodeficiency Virus Encephalitis

IL	Interleukin
INF-γ	Interferon-gama
kd	Dissociation Constant
LPS	Lipopolysaccaride
LY294002	Inhibitor of PI3K
MAP-2	Microtubule Associated Protein
MCMD	Minor Cognitive Motor Disorder
MCP-1	Monocyte Chemoattractant Protein-1
MDM	Monocyte Derived Macrophages
MIP-1a	Macrophage Inflammatory Protein-1alpha
MIP-1b	Macrophage Inflammatory Protein-1beta
MRI	Magnetic Resonance Imaging
NGF	Nerve Growth Factor
NSAID	Non Steroidal Antiinflammatory Drugs
PBR	Peripheral Benzodiazepine Receptor
PET	Positron Emission Tomography
PI3K	Phosphatidylinositol-3-kinase
PK11195	[1-(2-chlorophenyl)-N-methyl-N-(1methylpropyl)-3-isoquinolinecarboxamide]
PS	Presenilin
SDF-1	Stromal cell-Derived Factor (SDF)-1
SIV	Simian Immunodeficiency Virus
SIVE	Simian Immunodeficiency Virus Encephalitis
SYN	Synaptophysin
T cell	T (thymic)-lymphocyte Cell
Tg	Transgenic mice
TH	Tyrosine Hydroxylase
TNF-α	Tumor Necrosis factor alpha
U0126	Inhibitor of MEK1/2
VDAC	Voltage Dependent Anion Channel

1.0 INTRODUCTION

In the following section, I discuss the role played by brain macrophages in health and disease, then discuss their role in HIV related dementia and Alzheimer's disease and the applicability of labeling the peripheral benzodiazepine receptor to image brain macrophages in vivo.

1.1 BRAIN MACROPHAGES IN HEALTH AND DISEASE

1.1.1 Brain macrophages: origin and function

Microglia constitute 5-10% of the total cell population in the brain and are the resident macrophages that function as phagocytes, clearing debris around damaged neurons and synapses (168). Recognition of microglia as pathologically important cells in the CNS is ascribed to Del RioHortega, who is also credited with coining their name (70). It is generally accepted that microglia are derived from cells of the monocyte lineage from the embryonic mesoderm that migrate from the bone marrow into the CNS (196). Alternate views assign a neuroectodermal origin to microglia based on tissue culture experiments (83). However, the functions of microglia and the expression of cell surface markers are very similar to bone marrow derived macrophages, favoring a mesodermal origin.

Microglia undergo changes from a resting phenotype to an activated phenotype in response to CNS insults that enable them to function as phagocytes (93). This change in morphology has been best documented in the facial-nerve axotomy model, which results in microglial activation assessed by the expression of several surface markers,

morphological changes and proliferation of these cells around the motor neurons of the facial nucleus (135).

In addition to activation of resident brain microglia, monocytes migrate from the vascular compartment into the CNS during CNS-inflammation and differentiate to form macrophages (197). These cells have been referred to as perivascular macrophages. Experiments conducted in chimeric mice suggest that these cells are regularly replaced from the bone marrow (116). Although, these two populations of cells may be viewed as separate, it is possible that cells from the perivascular regions may traffic into the parenchymal space and vice versa. Macrophages derived from the periphery also have similar morphology and function as activated brain microglia. Besides, current immunohistochemical markers are unable to distinguish between these two populations of cells. *Due to their similar embryonic origin and function and the absence of current markers to differentiate peripheral macrophages that infiltrate into the brain and resident microglia, these cells will be collectively referred to as brain macrophage henceforth.*

Resident brain macrophages were previously thought to be quiescent and non-motile in the resting state. However, recent evidence imaging fluorescently labeled resident brain macrophages in transgenic mice using two photon microscopy shows that these cells are far from static (67, 180). These cells showed highly ramified processes that were highly motile and displayed cycles of formation, extension and withdrawal. Each of these processes also showed foot-like appendages that formed and withdrew. These authors hypothesized that resident brain macrophages serve a housekeeping function, enabling them to sample and maintain homeostasis of local environments. Following injury induced using a laser, time-lapse imaging showed rapid movement of ramified processes to the site of injury, which fused to form an area of containment between healthy and injured tissues within about 30 seconds, suggesting that resident brain macrophages may represent the first line of defense in CNS injury (67, 86, 180).

The phagocytic function of brain macrophages is mediated in a receptor dependent fashion. Brain macrophages express receptors for Fc (constant fragment of antibodies) and complement, which enable them to engulf antibody-coated cells and opsonized antigen (48, 240, 247). Brain macrophages also express MHC II that enable

them to present antigen to CD4-T cells (93). In addition, brain macrophages also express costimulatory substances such as B7-1, B7-2 and CD40 that enable them to stimulate T cells (102). These functions of phagocytosis and antigen presentation enable brain macrophages to serve an immune surveillance function in the CNS.

1.1.2 Brain macrophages: role in neurodegeneration

Activation of brain macrophages is seen in several neurodegenerative disorders. Neuritic plaques, which constitute the central pathology in Alzheimer's disease (AD), are surrounded by activated macrophages (162). In multiple sclerosis, areas of demyelination are rich in activated brain macrophages (25). HIV-dementia is characterized by viral infection of brain macrophages (255), and other neurodegenerative diseases such as Parkinson's disease (161), Creutzfeldt-Jakob disease (173) and Amyotrophic Lateral Sclerosis (214) are also associated with activated brain macrophages.

A wealth of literature suggests that activated brain macrophages produce toxins, that are detrimental to neurons. Several studies report that these cells synthesize and secrete several neurotoxins, which may cause neuronal damage or aggravate the underlying pathology. These neurotoxins include cytokines such as interleukin-1 (96), interleukin-6 (208) and tumor necrosis factor α (53), chemokines such as MIP-1α (175), MIP-1β (164) and MCP-1(64), free radicals (52), nitric oxide (51), proteinases (61) and eicosanoids (114). Although some of these studies are based on tissue culture systems and remain to be confirmed in vivo, it is generally accepted that activated brain macrophages can produce a complexarray of neurotoxins.

Further, inhibition of brain macrophage activation using non-steroidal anti-inflammatory drugs or minocyclin reduces the extent of neuronal damage in animal models of Parkinson's disease (76) and AD (143). Activation of brain macrophages also inhibits neurogenesis in the hippocampus in rats that are irradiated or injected with lipopolysaccaride. Hippocampal regeneration was restored in these conditions by blocking brain macrophage activation with either indomethacin (170) or minocyclin (77). These studies suggest that activation of brain macrophages is indeed a perpetuator of pathology in degenerative disorders.

However, recent evidence suggests that activated macrophages may also serve more positive roles. For example, in therapeutic immunization protocols in AD, activation of brain macrophages is thought to play a role in the clearance of Aβ from the CNS by activation of phagocytic mechanisms (155, 179, 218). In fact, the efficacy of antibodies in clearance of plaques from the brain correlated with the affinity of the antibody for the Fc receptor on brain macrophages (21). It has also been suggested that brain macrophages can exist in different states of activation depending on the microenvironment, with some states favoring the secretion of substances damaging neurons and other states favoring a phagocytic role such as in immunization protocols in Alzheimer's disease (172).

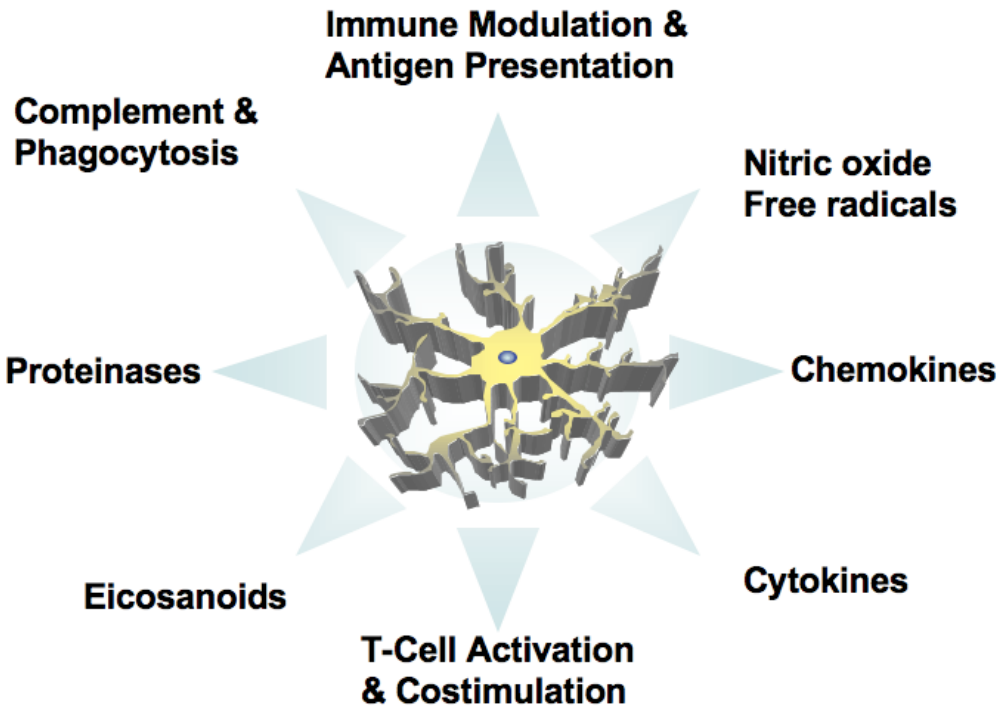

Figure 1 Brain macrophages in health and disease

The main function of brain macrophages is to defend the CNS against pathogens by immune surveillance, phagocytosis and antigen presentation to T cells. Brain macrophages transform from a resting state to an activated state in response to CNS pathologies. Activation enables these cells to carry out their immune surveillance functions. Chronic activation of brain macrophages results in the production of several substances, including cytokines like TNF α and interleukins, chemokines such as MIP-1α which may recruit other immune cells into the CNS, free radicals, nitric oxide, eicosanoids and proteinases which are toxic to neurons and may exacerbate the disease specific pathology.

1.2 NEUROINFLAMMATION IN HIV ENCEPHALITIS

It has been about 25 years since initial reports of patients suffering from previously rare diseases such as Kaposi's sarcoma and pneumocystitis pneumonia heralded the AIDS epidemic. In 1983, a retrovirus later called the human immunodeficiency virus-1 was identified as the primary cause of acquired immunodeficiency syndrome (AIDS) in humans (23). Since then, AIDS has grown to be one of the greatest challenges that mankind has ever faced.

HIV associated dementia arises in 25 % of terminally ill AIDS patients due to direct consequences of HIV-infection and inflammation of the CNS termed HIV encephalitis (HIVE), discussed in detail below.

1.2.1 The HIV epidemic

The United Nations AIDS program estimates that 40 million people around the world are currently living with HIV infection with five million new infections in 2004 (see http://www.unaids.org) (241). The HIV epidemic is a devastating public health issue in Africa and Asia, which together hold more than 70% of the world population living with AIDS (241). The several ways that HIV can be transmitted is through unprotected sex with infected partners, infected blood or blood products, sexual fluids, sharing of un-sterilized injection materials previously used by infected persons and materno-fetal routes (141).

The natural life cycle of HIV in humans displays two phases, acute infection and chronic infection that then progresses to AIDS (141). Acute infection presents with symptoms and signs very similar to infectious mononucleosis including, fever, myalgia, nausea, headache, sore throat, fatigue and lymphadenopathy (141). Acute infection is mainly characterized by high viral replication and a decrease in $CD4^+$ T cell counts (82). The "latency period" or "window period" is largely asymptomatic and is characterized by a decreased rate, but continued viral replication due to host immune responses that may last from months to years (189). The chronic phase of infection is characterized by progressive declines in $CD4^+$ T cell counts that culminates in AIDS (82). Based on

criteria defined by the Center for Disease Control and the World Health Organizations, patients with AIDS display fever, diarrhea, lymphadenopathy, cachexia, and several opportunistic infections including Kaposi's sarcoma, pnuemocystitis pneumonia, toxoplasmosis, candidiasis, cytomegalovirus retinitis, cryptosporidiosis, listeriosis, Burkitt's lymphoma, progressive multifocal leukoencephalopathy, atypical mycobacterial infections and histoplasmosis (141).

HIV productively infects cells that express the CD4 receptor and the CXCR4 or CCR5 co-receptors which are expressed mainly on CD4 + T cells and macrophages respectively (75, 84, 131). Although in tissue culture systems, viral stains can be classified into T-cell tropic and macrophage tropic depending on the preferred cell type infected, most viral strains *in vivo* are able to use both receptors for entry with varying efficiency (9, 75). The life span of CD4 T cells is significantly shortened by viral infection as opposed to macrophages, which may act as a reservoir for persistent viral infection and produce chronic inflammation and tissue damage (11, 12).

1.2.2 HIV associated dementia

One in four immunosuppressed patients infected with HIV develop a neurodegenerative syndrome clinically characterized as HIV-associated dementia (HIVD) (3, 38, 57, 74, 158). This syndrome is characterized by cognitive impairments such as memory and concentration deficits, motor abnormalities such as tremors and limb weakness, and psychiatric symptoms such as depression, apathy and social withdrawal (98, 198, 201). Patients with terminal AIDS often also develop various CNS opportunistic infections and neoplasia such as cytomegalovirus encephalitis, cryptococcal meningitis, toxoplasmosis, B cell lymphomas and progressive multifocal leukoencephalopathy (10). These diseases may present with similar clinical signs and symptoms to HIVD; thus, the diagnosis of HIV associated dementia is one of exclusion of these conditions. The more definitive diagnosis obtained on autopsy, is characterized by the presence of classic immunohistochemical pathologic features termed HIV encephalitis (HIVE) (252).

1.2.3 HIV encephalitis

HIV encephalitis is considered to be the pathological substrate of HIV associated dementia (154, 252). HIVE is characterized by the presence of microglial nodules, multinucleated giants cells, and abundant HIV-infected and activated macrophages (39, 40, 178, 253). Microglial nodules are regional aggregations of HIV-infected and activated brain macrophages. Fusion of HIV-infected macrophages are thought to form multinucleate giant cells (223, 255). Infiltration of HIV-infected and activated macrophages is seen in perivascular and brain parenchymal compartments of the CNS in both subcortical gray and white matter regions (166, 181). The predominant cell types infected with HIV in the CNS are brain macrophages, including resident brain macrophages and macrophages derived from monocytes trafficking into the CNS (255). It is thought that these monocytes act as "Trojan horses" that bring the virus into the CNS (68, 195, 250). This hypothesis draws support from immunohistochemical, *in vitro* studies and several reports suggesting that the main viral strains isolated from the CNS are macrophage tropic (104).

1.2.4 Brain macrophages are central to the pathology of HIVE

Current hypotheses implicate HIV infected and activated macrophages infiltrating into the brain as central players in the pathogenesis of HIV-associated dementia (128). Evidence from in vitro studies, animal models and postmortem studies suggest that macrophages are the main group of cells that are productively infected with virus in the CNS and mediate neuropathology in an indirect fashion by producing toxic secretory products and viral proteins (128, 255).

Controversy exists regarding the relative contributions of activated macrophages versus HIV infected macrophages towards the neurodegenerative process (97). Initial studies suggest that the severity of dementia, assessed ante mortem correlate with the extent of macrophage staining in post mortem tissue but correlate poorly with the extent of HIV gp41 immunoreactive cells (97). These data suggest that dementia may correlate better with the abundance of activated macrophages than the abundance of HIV infected

cells. However, HIVgp41 positive cells correlate with decreases in immunoreactivity of a dendritic protein MAP-2 suggesting a role for both activated and HIV infected macrophages in synaptic damage (153). More recent data from the primate model of HIVE suggest that loss of synaptic proteins correlate with both infected and activated macrophages (32).

Toxins derived from macrophages are generally classified into two groups: viral proteins and toxic host secretory products. While, the relative contributions of either group of toxins are continuously debated, it is conceivable that the toxic effects of both viral proteins and secretary products may not be mutually exclusive. Viral proteins derived from macrophages include HIV envelope proteins such as gp41 and gp120 that may interact with the HIV receptor and coreceptors that may be expressed in neurons (213). Other viral proteins implicated in neuronal toxicity and dysfunction includes Tat, Vpr, Nef, Vpu, and Rev (177).

Neurotoxic secretory products including cytokines such as TNF-α (107) and interleukins (2), chemokines such as SDF-1 (261) and MCP-1 (101), free radicals generated by activation of NADPH oxidase and reactive nitrogen intermediates (4) and eicosanoids such as quinolinic acid products (115). These substances may cause neuronal dysfunction directly by triggering pathways that decrease neuronal viability and alter synaptic plasticity or indirectly through affects on glial cells (128).

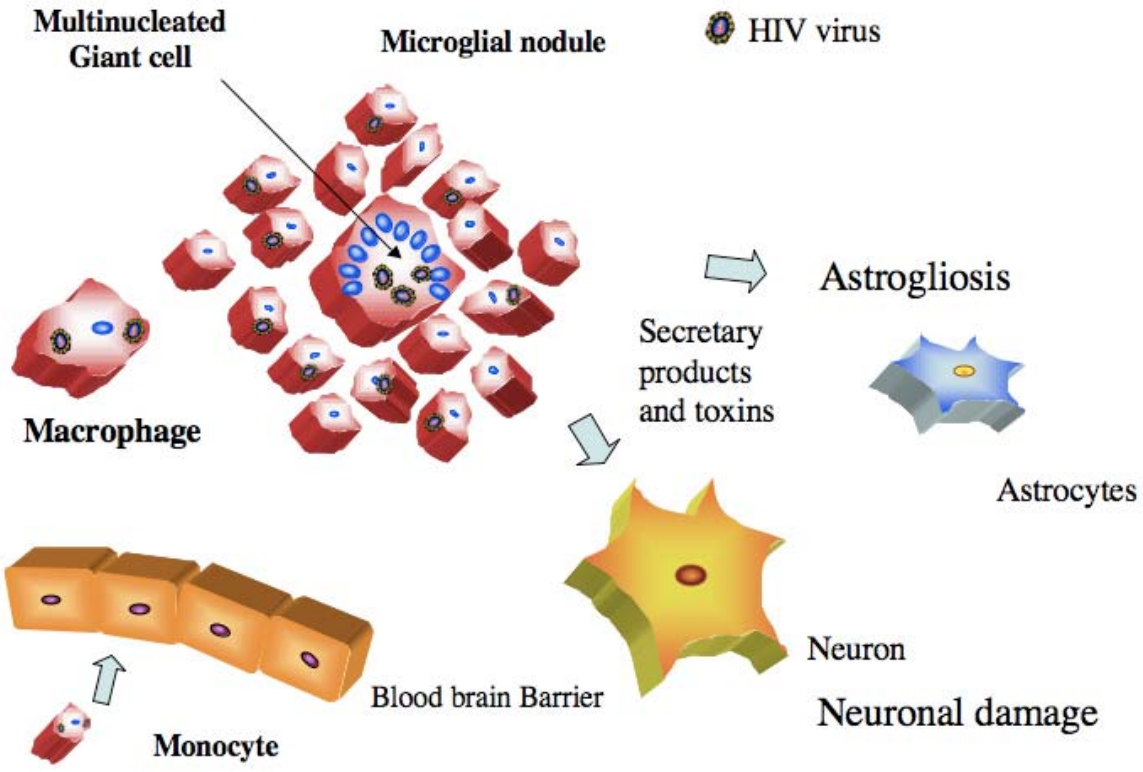

Figure 2 Pathogenesis of HIV Encephalitis

Monocytes harboring the HIV virus cross the blood brain barrier and differentiate to form macrophages in the central nervous system. Neuroinflammation then recruit, infect and activate other macrophages (both resident brain macrophages and macrophages from the periphery). These cells may then aggregate to form microglial nodules and may fuse to form multinucleated giant cells. Secretary products and toxins derived from HIV infected and activated macrophages may cause neuronal damage and activate astrocytes to cause astrogliosis.

1.2.5 Neuronal damage in HIVE

Although, it is generally accepted that activated and HIV infected macrophages are the central mediators of neuronal damage in HIVE, the mechanisms of neuronal damage and degeneration are continuously debated. Despite the absence of convincing evidence supporting productive neuronal infection, neuronal damage and loss are reported in HIVE. Dementia may arise from loss of pyramidal neurons (254) and specific decreases

in clabindin staining neurons in the cortex (79). However, cognitive abnormalities in these patients seem to correlate better with decreases in neuronal synaptic proteins rather than decreases in neuronal numbers suggesting that synaptic damage plays a central role in HIV-associated dementia (156). Both presynaptic and postsynaptic neuronal damage have been reported in HIVE and animal models of this disease (32, 153). Presynaptic changes have been mainly studied by documenting changes in a 38kd calcium-binding, synaptic vesicle protein named synaptophysin (SYN) (153). Postmortem decreases in SYN staining in HIVE are interpreted as damage to presynaptic terminals and correlate with poor ante mortem neuropsychological performance in HIV-infected cognitively impaired patients (79). Similarly, decreases in a dendritic protein called microtubule-associated protein-2 (MAP-2), reflective of postsynaptic damage, have also been observed in HIVE and correlate with poor ante-mortem cognitive testing (156). These data suggest that neurocognitive dysfunction may arise as a direct result of synaptic damage.

1.2.6 Effect of HAART on HIV dementia and neuroinflammation

Highly active antiretroviral therapy (HAART) was introduced in 1995 and since then markedly decreased the mortality associated with HIV infection (13). HAART consists of multiple anti-HIV drugs including one nucleoside analogue, one protease inhibitor and either a second nucleoside analog or a non-nucleoside reverse transcription inhibitor that target different aspects of the HIV life cycle (reviewed in (203)). The incidence of several opportunistic infections along with HIV associated dementia has decreased with the advent of HAART. In fact, the incidence of HIV associated dementia is thought to have decreased by 10%. However, it has been suggested that the prevalence of HIV associated dementia will increase due to the longer life spans of HIV infected patients on HAART (94, 242). Despite the observation that few antiretroviral drugs attain effective concentrations in the CNS, the incidence of HIVE has decreased in patients on HAART (105, 106). With HAART, abundant HIV infected macrophages are still observed in brains with HIVE but are associated with a more subtle degeneration of dendritic arbors

and interneuron populations (139). Interestingly, the clinical neurological symptoms in patients treated with HAART are reported to be less severe than frank dementia and are termed minor cognitive motor disorder (MCMD) (1). MCMD differs from HIV associated dementia in that; the symptoms of higher cortical dysfunctions such as disorientation, memory losses, and executive skill dysfunctions are milder. It has been estimated that 25-30% of HIV infected patients on HAART suffer from MCMD (55, 211).

1.2.7 Primate model of HIV encephalitis

The simian model of lentiviral infection closely resembles the human disease with a variable percentage of infected macaques developing neurological disease (24). Histopathologic hallmarks of both HIV and SIV encephalitis (HIVE or SIVE) include abundant brain tissue infiltration by macrophages, multinucleated giant cells, microglial nodules and perivascular chronic inflammatory cells (39, 137).

The macaque model of HIVE has been extensively used to understand the pathogenesis of HIVE. As in the human disease the predominant strain of SIV in the CNS of macaques with SIVE is macrophage-tropic (63). Macaque models have been extensively studied to determine correlates of encephalitis that can be translated to the human disease. Some of the factors associated with the development of encephalitis in macaques include, rapid progression to AIDS (182, 251), high levels of CSF viral loads (264), elevated CSF monocyte chemotactic protein (MCP)-1 concentrations (58, 263) and low anti-SIV antibody titers 1 month after infection (182).

SIV in macaques is a natural pathogen and the natural disease course of SIV, including the development of encephalitis, closely resembles HIV infection in humans. The macaque model thus continues to serve a key role in understanding the pathogenesis of HIVE.

1.3 NEUROINFLAMMATION IN ALZHEIMER'S DISEASE

1.3.1 Pathology of Alzheimer's disease

Approximately 50% of individuals over 85 years of age and over 10% of individuals over 65 years of age suffer from Alzheimer's disease (AD), making it the leading causes of dementia (8). Clinically, AD is characterized by progressive memory and cognitive impairment and behavioral abnormalities. The disease begins as a decrease in short term memory, followed by a progressive impairment of mental functions and daily activities, accompanied by behavioral changes such as social withdrawal and depression (110). Terminally ill patients are usually bed ridden, incontinent and completely dependent on custodian care with death occurring at an average of nine years after diagnosis (26). AD is a major public health problem from the devastating nature of the disease on patients and resources available to health providers and patient attendants (174). Current therapies available are at best palliative and do not address the underlying pathogenesis of AD.

The pathology of Alzheimer's disease is first seen in the cerebral cortex and subsequently spreading to more subcortical structures. Limbic structures such as the hippocampal formation are one of the first regions to degenerate (152).

Two main features characterize the neuropathology of AD: the formation of intraneuronal neurofibrillary tangles and extracellular Aβ deposition (167). Aβ deposition leads to the formation of diffuse plaques that are believed to progress to neuritic plaques with a dense core of β-amyloid protein (Aβ), dystrophic neurites, astrocytes, and activated brain macrophages (161). Neurofibrillary tangles are intraneuronal inclusion bodies found with the cell soma, proximal dendrites, distal axon terminals and synaptic terminals (134). These inclusion bodies consist mainly of hyperphosphorylated isoforms of the microtubule-associated protein Tau, causing it to form paired helical filaments that are insoluble which consequently aggregate (99). The major constituent of neuritic plaques was identified to be the Aβ peptide nearly 20 years ago (157). It is now generally accepted that Aβ is formed due to abnormal cleavage of the amyloid precursor protein (APP) by the two enzymes β and γ-secretase (221).

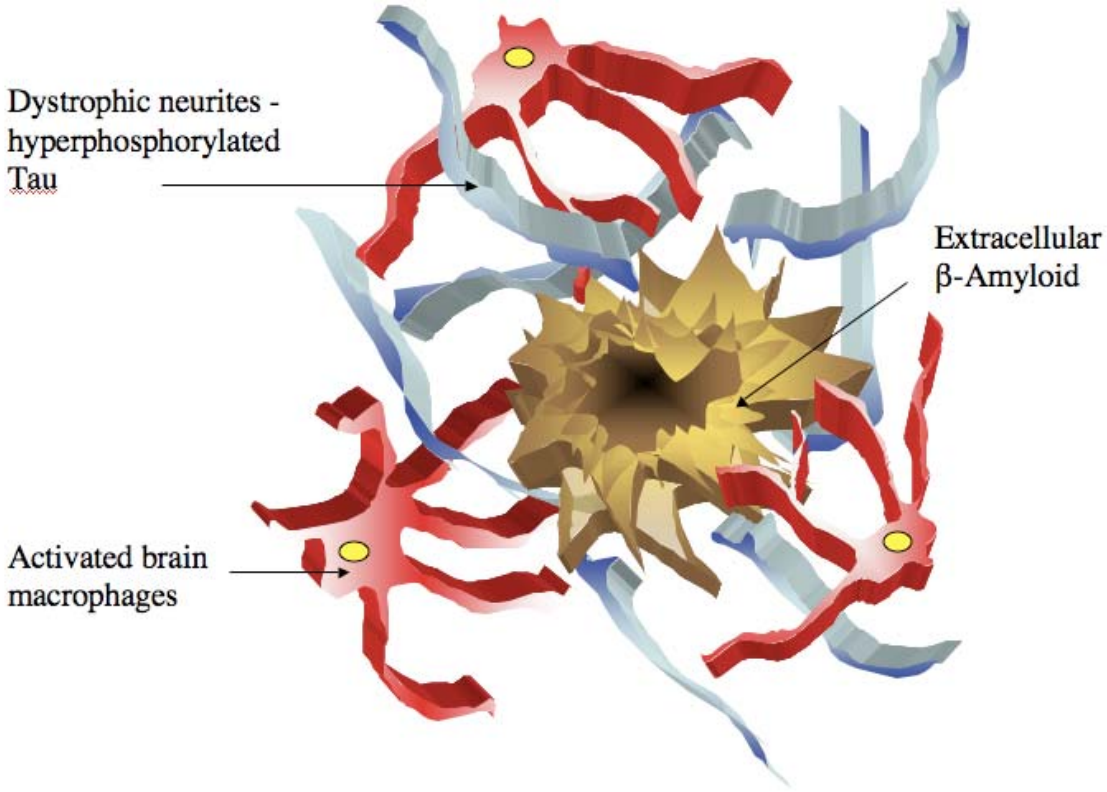

Figure 3: Schematic depiction of a neuritic plaque

Neuritic plaques consist of a dense core of β-amyloid (brown) surrounded by dystrophic neurites (blue) containing hyperphosphorylated Tau, activated brain macrophages (red) and activated astrocytes (not shown in the figure).

While several studies show that Aβ may initiate neuronal damage through various mechanisms, the relative contributions of Aβ and Tau to disease pathogenesis and progression are continuously debated. The amyloid hypothesis suggests that overproduction of Aβ, or failure to clear this peptide, leads to the formation of Aβ deposits, which cause the formation of neurofibrillary tangles; these abnormalities then cause neuronal damage and death (111). Several arguments and experiments, beyond the scope of this thesis, favor or oppose this hypothesis and it remains to be either conclusively proved or disproved.

1.3.2 Transgenic mouse models of AD

Transgenic mice have been created that express various mutations related to AD. These include mice that express Familial-APP mutations (such as Swedish, Indiana, and 717) presenilins-1 (PS1), combinations of mutant APP and PS1 (258), and more recently, the triple transgenic mouse expressing mutant APP, PS1 and Tau (P301L) (183). Various aspects of the disease pathology are seen in these mice including deposition of extracellular Aβ, dystrophic neurites, memory deficits, hippocampal synaptic abnormalities, mild neuronal loss and glial activation. The degree to which each of these models displays AD pathology depends on the level of the transgene and the specific mutation. Activation of brain macrophages is more variable depending again on the transgene expressed, but is reported to be lower than the human disease overall (72).

Transgenic mice have revolutionized the study of AD and other neurodegenerative disorders by providing models suitable to study therapeutics and mechanistic hypotheses in vivo. However, studies utilizing transgenic models have to be interpreted with caution in terms of applicability to the human disease. Levels of expression of aberrant proteins may far exceed actual pathological condition in the human disease. Further, transgenic mice may not model all the aspects of a complex chronic human neurodegenerative disease. For example, mice that model Huntington's disease and Alzheimer's disease rarely show frank neuronal loss (258). Also mice expressing the APP and PS1 mutations mice show decreased retention of the PIB-amyloid PET ligand as compared to human AD subjects, which may be due to differences in the secondary structure of the deposited Aβ (133).

1.3.3 Brain macrophage activation in Alzhiemer's disease

Aβ is the main protein in the dense core of neuritic plaques and is formed by abnormal protein cleavage of the amyloid precursor protein (APP). Aβ deposits are thought to activate brain macrophages that then surround the neuritic plaque (165). Evidence for this hypothesis comes from cultured brain macrophages which when exposed to the Aβ

peptide show upregulation of MHC-II, complement receptor, chemokines, expression of cytokines such as TNFα and interleukins and other acute phase proteins similar to changes seen in activated brain macrophages in AD postmortem brain tissue (16, 102, 209).

Transgenic mice overexpressing human APP show deposits of Aβ surrounded by activated brain macrophages (28, 89, 143, 229). Mice injected with fibrillar Aβ also show activated brain macrophages (88). Aberrant chemokine and cytokine expression may also recruit and activate other macrophages from the periphery (209). The mechanisms by which Aβ causes brain macrophages activation are not clearly understood. Several receptors and pathways have been implicated, but it has not been clearly demonstrated that binding to such receptors is the principal mediator of activation (148).

1.3.4 Role of activated brain macrophages in Alzhiemer's disease

While the biochemical processes related to Aβ processing have been studied extensively, the role of activated brain macrophages in the pathogenesis of AD is not well understood and is continuously debated. One hypothesis is that brain macrophages are primarily activated to serve a phagocytic function in response to deposited Aβ (219). Ultrastructural studies suggest that intracytoplasmic Aβ fibrils may be found in activated brain macrophages in AD and transgenic mouse brain tissue (7, 142, 229). However, a recent study suggests that these amyloid fibrils may be extensions of extracellular amyloid forming finger-like channels into the brain macrophages cytoplasm, but not directly contained within it (228). Evidence from in vitro experiments suggest that activated brain macrophages are capable of ingesting Aβ, but may be defective in their phagocytic capacity due to poor degradation of ingested amyloid within brain macrophages (87, 192). Also, no phagocytosis is observed when brain macrophages are incubated with AD frozen sections containing Aβ, but is enhanced by incubation with specific Aβ antibodies (21).

Brain macrophages are sources of several neurotoxins that may enhance the neurodegenerative process seen in AD and several other chronic neurological disorders.

On activation, brain macrophages express several proteins that may accentuate the neurodegenerative process (30, 225, 236). Activated macrophages produce cytokines such as TNF-α and interleukins, free radicals generated by activation of NADPH oxidase, reactive nitrogen intermediates, eicosanoids, complement associated proteins, antigen presentation and co-stimulatory molecules and matrix metaloproteinases which have been implicated in disease pathogenesis (30, 225, 236). These substances are thought to trigger various cellular processes including cell death cascades in neurons. Further, Non Steroidal Anti-Inflammatory Drugs (NSAIDs) which are associated with a decrease in the incidence of AD (119) may reduce the extent of brain macrophages activation in animal models (143, 260). These studies suggest a detrimental role for activated brain macrophages in AD.

1.3.5 Therapeutic approaches to AD

Current standards of medical care include acetylcholine esterase inhibitors in mild to moderate AD and the NMDA antagonist, Memantine, in advanced AD (33, 73). These therapies although reported to have improvements in cognition, do not address the underlying pathology in AD. Other therapies include mood stabilizers and antipsychotics used to manage behavioral abnormalities seen in AD (73). No current FDA approved therapies have disease-modifying effects and are of limited use in the clinic.

Several therapeutic approaches target various aspects of AD pathology. These include the use of neurotrophic factors like NGF targeted to increased neuronal survival, drugs that potentially interfere with Aβ aggregation or modulate enzymes that process APP, anti inflammatory compounds and immunotherapies targeted at clearing Aβ from the brain. Nerve growth factor (NGF) is a neurotrophic factor that promotes survival of cholinergic neurons (reviewed in) (59). Cholinergic neurons in the basal nucleus of mynert are the first group of neurons to degenerate in early stages of AD (147). Clinical trials delivering NGF to the CNS show initial promise, however, the widespread involvement of neurons including non-cholinergic neurons in AD may preclude significant clinical improvement in advanced AD (36). Aβ-42 is generated by sequential

cleavage of APP by two enzymes called β-secretase and γ-secretase. A third enzyme called α-secretase competes with β-secretase and may decrease the production of $A\beta_{42}$ (221). Therapies targeted at either inhibiting β-secretase and γ-secretase or stimulating α-secretase activity may be beneficial in decreasing Aβ production and are currently under active research (reviewed in)(243).

1.3.5.1 Immunization aganist Abeta

Both active and passive immunizations in animal models have proved promising in clearing Aβ loads from the brain and improving behavioral/memory tests (22, 120, 171, 218). PDAPP mice immunized with Aβ peptides over a six-month period show generation of antibodies against Aβ, clearance of Aβ brain deposits and improvements in cognitive testing. Passive immunization utilizing antibodies targeted against the Aβ peptides cross the blood brain barrier and clear Aβ deposits from the CNS. Immunization against Aβ in aged vervets, which shows Aβ deposition in older age groups, also clears plaques (140). Active immunizations in human subjects have generated both positive and negative outcomes. Postmortem studies from 3 immunized patients showed clearance of Aβ from the brain, however ~5% of subjects developed severe T-cell encephalitis on immunization (85, 155, 179). Despite mixed enthusiasm, immunization against Aβ shows great promise in the treatment of AD (219).

Several mechanisms have been proposed for $A\beta$ clearance with immunization. Some of these hypotheses propose that (1) antibodies generated against $A\beta$ interfere with fibrillogenesis and neurotoxicity of Aβ (163, 226), (2) clearance of amyloid by transfer to the CSF/vascular compartment which act as a "peripheral sink" (71) and (3) phagocytosis of Aβ by activated brain macrophages via Fc and non-Fc dependent mechanisms (66, 217). Clearance of CNS $A\beta$ may occur through one or more of these processes, however the observation that the clearance of Aβ is consistently associated with activation of brain macrophages raises the possibility that the efficacy of immunizations is related to the extent of activation of brain macrophages.

1.3.5.2 Brain macrophages in Aβ immunization

Brain macrophage activation is seen with both active and passive immunization and is consistently associated with "collapsed" plaques in both animal models and human subjects (22, 85, 155, 179, 218). Phagocytosis is enhanced with the addition of antibodies to cultured brain macrophages in the presence of Aβ (22). Further, the efficacy of clearance with passive immunization correlated with the ability of the antibody to bind Fc receptors on activated brain macrophages rather than binding to Aβ (21), suggesting a central role for activated brain macrophages in Aβ clearance. However, mice deficient in the Fc-receptor, which plays a role in Aβ phagocytosis by brain macrophages, crossed with amyloid precursor protein transgenic mice show efficient clearance with immunization against Aβ (66). This raises the possibilities of other mechanisms, such as the peripheral sink hypothesis, playing a more important role in Aβ clearance than Fc dependent phagocytosis by brain macrophages. Alternatively, phagocytosis in brain macrophages may also be mediated by scavenger receptors or other FC independent mechanisms (66). Although, both active and passive immunization protocols are associated with brain macrophage activation, the exact role of these cells in clearance of Aβ remains to be understood.

1.4 THE PERIPHERAL BENZODIAZEPINE RECEPTOR

1.4.1 The peripheral benzodiazepine receptor-structure and function

Two pharmacologically distinct benzodiazepine receptors exist in the CNS: the central and the peripheral benzodiazepine receptors. The central benzodiazepine receptor is a part of the ionotropic GABA receptor located on the plasma membrane of GABA-ergic neurons (232). The peripheral benzodiazepine receptor (PBR), on the other hand is located on the outer mitochondrial membrane of astrocytes and brain macrophage (45). It is part of a hetero-oligomeric complex comprised of the voltage-dependent anion channel

and an adenine nucleotide carrier forming the mitochondrial permeability transition pore (160).

The functions of this receptor in the CNS are not entirely known. It is thought to be involved in neurosteroid synthesis by serving to transport cholesterol from the outer to the inner mitochondrial membranes (190). As a constituent of the mitochondrial permeability transition pore it is thought to regulate cell death (160) and mitochondrial respiration (117). Although the functions of this receptor in the resting CNS have not been entirely elucidated, several studies have focused on changes in PBR expression in CNS diseases.

1.4.2 PBR in CNS diseases

After early reports that the PBR was present in the CNS, several studies have focused on determining changes in PBR expression in CNS disease. These studies mainly utilize the isoquinoline carboxamide derivative PK11195, a specific pharmacological ligand that binds to PBR with high affinity. [3H](R)-PK11195 was first used to label giloma cell lines implanted into mice brains using autoradiography (230). Several binding studies using homogenized brain tissue and autoradiography studies have now shown increased [3H](R)-PK11195 binding (reflecting increases in PBR protein expression) in a wide variety of neurological diseases such as multiple sclerosis (20, 246), experimental autoimmune encephalitis (246), stroke (231), brain trauma (204), facial nerve transaction (19, 92), and SIVE (151). In the majority of these studies cellular localization of increased PBR expression is specific to activated brain macrophage elements, but not astrocytes as discussed below.

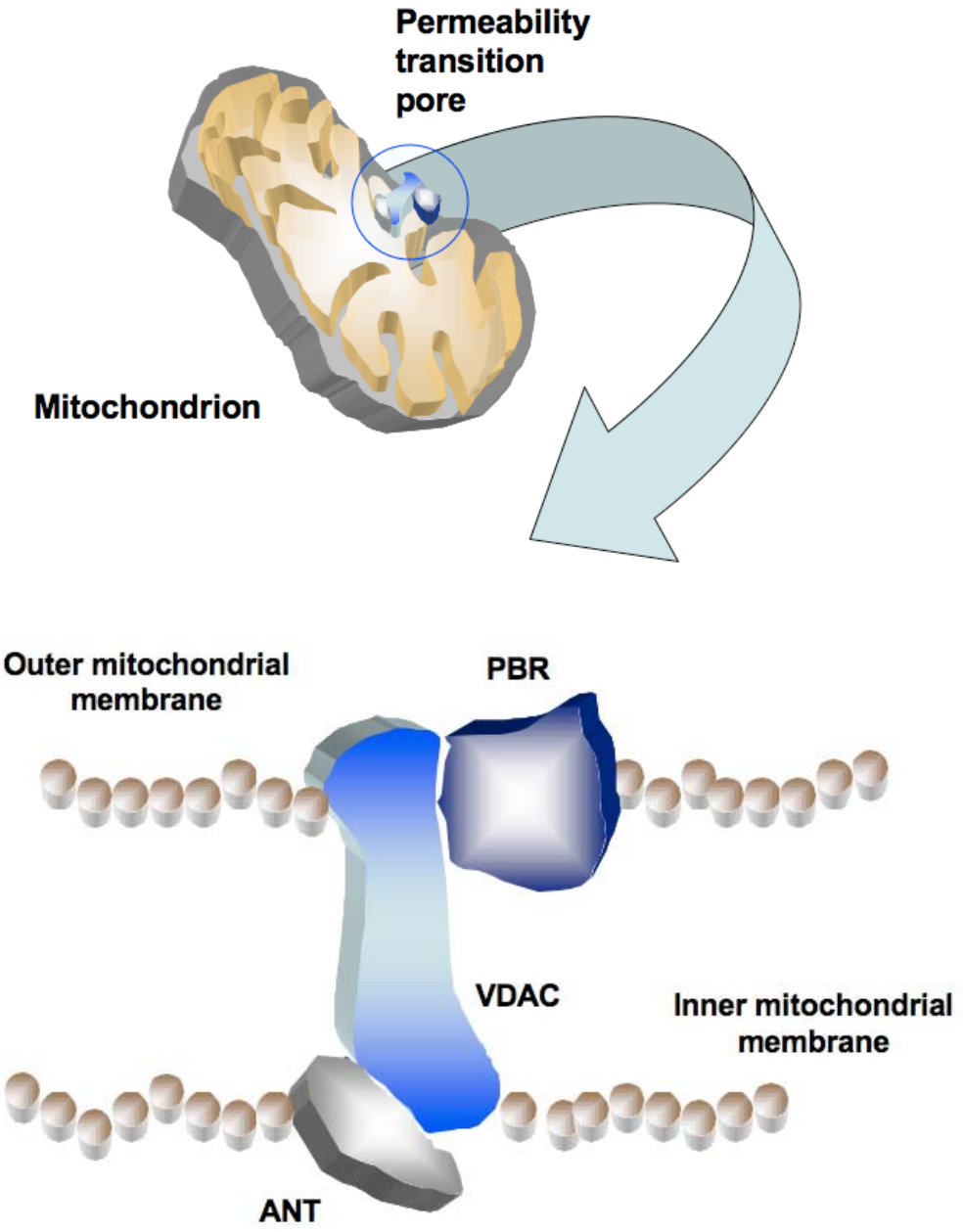

Figure 4 Structure of the mitochondrial permeability transition pore showing the location of the peripheral benzodiazepine receptor

The mitochondrial permeability transition pore consists mainly of the voltage dependent anion channel (**VDAC**), the adenine nucleotide transporter (**ANT**) and the peripheral benzodiazepine receptor (**PBR**). Note that **PBR** is situated on the outer mitochondrial membrane.

1.4.3 PBR is increased specifically in brain macrophages during disease

In the resting CNS, PBR was first reported to localize to ependymal cell lining the ventricles, the olfactory bulb and the choroids plexsus (248). Subsequently PBR was found to be expressed in low levels in glial cells including astrocytes and brain macrophages and was increased specifically in brain macrophages in a rat model of stroke (176). This phenomenon has been confirmed in other CNS pathologies associated with gliosis such as models of ischemia in rats (231), experimental autoimmune encephalitis (246), multiple sclerosis (20), facial nerve axotomy in rats (19), brain trauma in rats (204) and SIV encephalitis in macaques (151). However, some studies report increased astrocyte expression of PBR following an initial increase in brain macrophages in rodents treated with the neurotoxin trimethyltin (136) and cuprizone (54). In vitro studies also suggest that neurons may express PBR (121), but not in brain tissues in vivo. It is, however, generally accepted that increase in PBR is specific to glial cells.

1.4.4 Potential functions for PBR in brain macrophages

The effects of increased PBR expression in macrophages are unknown. The association of PBR with the mitochondrial permeability transition pore suggests a role in the regulation of cell death. At the mitochondrial permeability transition pore, PBR interacts with several resident mitochondrial proteins including the voltage dependent anion channel and the adenine nucleotide carrier which in turn interact with proteins regulating apoptosis (160). Interestingly, PBR prevents myxoma-infected macrophages from apoptosis (80, 81). In these studies, forced macrophage-PBR overexpression prevented these cells from undergoing myxoma virus-mediated apoptosis. Forced PBR expression in neurons in *vivo* and jurkat cells *in vitro* protects these cells against apoptosis (125, 234). PBR upregulation in testicular leydig cells protects them from cytokine-induced toxicity (207, 237). This is also seen in blood phagocytic cells where PBR protects against oxidant induced cell death (44). Macrophage specific PBR expression may thus protect these cells from various toxins including the cytopathic effects of HIV, contributing to longer macrophage life spans in the brain.

1.4.5 Potential mechanisms for PBR upregulation in brain macrophages

The mechanisms responsible for increased PBR expression in macrophage elements in the CNS are not known. In pancreatic islet cells, the cytokines TNF-α, IFN-γ and IL-1β cause an increase in PBR mRNA and [3H](R)-PK11195 binding in a transcription dependent manner (20). Similar results are seen in testicular leydig cell exposed to TNF-α (237). In the CNS, rats injected with IL-1, or TNF-α, or LPS resulted in increased [3H](R)-PK11195 binding to macrophages, reflecting increased PBR expression in these cells (31, 35). IL-1 and TNF-α also increase [3H](R)-PK11195 binding in cultured astrocytes (184). In experimental autoimmune encephalitis, IL-6 and TNF-α expression profiles correlate with increase in spinal cord [3H](R)-PK11195 binding (5). These data suggest that cytokines increase PBR expression in various cell types including macrophages. However, the mechanisms mediating this increase are not known. It has been proposed that cellular upregulation of PBR in these systems may serve as a protective strategy against cytokine toxicity. Since activated brain macrophages themselves are sources of cytokines, increase in PBR expression would be an autocrine-paracrine phenomenon.

Since PBR upregulation is associated with cell survival, it is possible that cell pathways that promote survival regulate PBR expression. One of the major pathways that regulates cell survival is the Phosphatidylinositol-3-kinase (PI3K)/Akt pathway. PI3K is a lipid kinase essential for the activation of Akt, which plays a pivotal role in cell survival and proliferation (187). PI3K/Akt activation is an important survival-regulation pathway in brain macrophages (129), peripheral macrophages and other hemopoietic cell (169, 239). Activation of PI3K/Akt protects against toxicity induced by multiple cytokines (100, 169). Further, inhibition of PI3K pathway in peripheral macrophages causes cell death by loss of mitochondrial transmembrane potential by mechanisms not fully understood (144). Since PBR is a constituent of the permeability transition pore and may play a role in maintaining mitochondrial transmembrane potential, it is possible that PBR is directly regulated by activation of the PI3K/Akt pathway.

1.4.6 PBR ligands may be used to image activated brain macrophages in vivo

Several ligands have been synthesized that bind specifically to PBR. Labeling these ligands with [3H] and [11C] has enabled their use in autoradiography and PET respectively. Of these ligands PK11195, a lipid soluble isoquinoline carboxamide, has been the most extensively characterized (17). [11C](R)-PK11195 has been used to label activated brain macrophages in patients with multiple sclerosis (20, 69) Rasmussen's encephalitis (18), stroke (206), Herpes encephalitis (43), gliomas (191), multiple system atrophy (95), animal models of HIV encephalitis (245) and AD (41).

Studies in AD patients showed high [11C](R)-PK11195 binding in the entorhinal, temporoparietal and cingulate cortices, brain regions which show the highest degree of AD pathology (41). However, this study also reported high levels of [11C](R)-PK11195 binding in regions not involved in AD, such as the thalamus and the brainstem (41). Similarly, a recent study using [11C](R)-PK11195 to image activated brain macrophages in amyotrophic lateral sclerosis (ALS) patients showed high binding in the occipital cortex, regions of the prefrontal cortex, and the thalamus, which are areas that are not traditionally implicated in ALS pathology (238). Both these studies were not followed up by neuropathologic assessments and the presence of activated brain macrophages in brain regions usually not involved in the disease pathology cannot be ruled out. However, these findings may be attributed to some degree of non-specific binding of PK11195, underscoring the importance of using a ligand with high specific binding to PBR.

DAA1106 [N-(2,5-dimethoxybenzyl)-N-(4-uoro-2-phenoxyphenyl) acetamide], an aryloxyanilide derivative, is a recently synthesized ligand that binds selectively and with higher affinity to PBR (47). DAA1106 shows a higher affinity to PBR compared to PK11195 suggested by the differences in the dissociation constants. The K_d (dissociation constant) of PK11195 ranges between 4nM to 20nM, while the K_d of DAA1106 is around 0.1nM (dissociation constant being inversely proportional to binding affinity) (47, 185). Due to a high affinity, DAA1106 may serve as a better ligand to label PBR both *ex vivo* and *in vivo* (149, 262). This may also address some of the issues related to nonspecific binding seen in studies with PK11195.

2.0 SPECIFIC AIMS

Activated brain macrophages play a significant role in several neurodegenerative diseases including HIV-associated dementia, Alzheimer's disease and Parkinson's disease. Neurotoxins such as cytokines and free radicals produced from activated brain macrophages are thought to promote the degenerative process by causing neuronal damage. Several therapies such as anti inflammatory drugs and immunization protocols in Alzheimer's disease target activated macrophages. Were it possible to detect the presence of brain macrophages in vivo, in may be possible to monitor the development and progression of neuroinflammation as well as determine the efficacy of therapies targeted at altering neuroinflammation.

The peripheral benzodiazepine receptor is abundant on activated brain macrophages and expressed in low levels in the normal brain. We investigated the feasibility of imaging activated brain macrophages using Positron Emission Tomography (PET) by taking advantage of elevated levels of peripheral benzodiazepine receptor expression (PBR) on brain macrophages. ***We tested the overall hypothesis that selective ligand to PBR will specifically label activated brain macrophages in neuroinflammation.*** We propose to use the extensively characterized peripheral benzodiazepine ligand PK11195 to image brain macrophages in vivo using animal models of HIV encephalitis and Alzheimer's disease. We also propose to characterize DAA1106, a novel ligand that binds with high affinity and specificity to the peripheral benzodiazepine. Accordingly, the following four specific aims are proposed.

Subhypothesis1: PK11195 will selectively label brain macrophages in a macaque model of HIV encephalitis in vivo, using PET.

SPECIFIC AIM 1: Determine if (1); [3H](R)-PK11195 shows higher specific binding in SIVE brain tissue compared to SIV infected, non encephalitic tissue, and

control uninfected tissue, (2); [11C](R)-PK11195 can label brain macrophages in vivo in SIVE.

In this specific aim, we will utilize PET imaging with [11C](R)-PK11195 to compare binding characteristics in macaques infected with SIV that develop encephalitis with macaques that do not develop encephalitis. We will also use filtration-binding techniques to compare [3H](R)-PK11195 binding in SIVE with SIV infected, non-encephalitis, and control uninfected brain tissue derived from macaques that have been PET imaged. PET finding will be correlated with histopathology and filtration binding data to determine if PK11195 can label brain macrophages in vivo in SIVE.

Subhypothesis2: PK11195 will selectively label brain macrophages in HIV encephalitis.

SPECIFIC AIM 2: Determine (1); if [3H](R)-PK11195 shows higher specific binding in HIVE brain tissue compared to HIV infected, non encephalitic tissue, and control uninfected tissue, (2); if activated macrophages show higher specific binding with [3H](R)-PK11195 compared to astrocytes *in vitro*, (3); if HIV infected macrophages show higher specific binding of [3H](R)-PK11195 compared to astrocytes treated with supernatants derived from HIV infected macrophages *in vitro,* and (4) determine the cell signaling pathways that mediate upregulation of PBR in macrophages.

In this aim, we will confirm data obtained from SIVE in aim 1 in HIVE postmortem tissue. We will also use cell culture systems to determine the effects of activation and HIV infection in primary human macrophages. We will also use pharmacologic blockers of the PI3K/Akt and the MAP-kinase pathways to determine if these pathways are responsible for upregulation of PBR in macrophages.

Subhypothesis3: PK11195 will selectively label brain macrophages in Alzheimer's disease postmortem tissue and transgenic mice models of Alzheimer's disease in vivo.

SPECIFIC AIM 3: We will compare (1); [3H](R)-PK11195 binding in postmortem Alzheimer's disease brain tissue from Alzheimer's disease patients with age matched controls using filtration binding assays, and (2); [3H](R)-PK11195 binding in brain tissue derived from APPSwe/PS1dE9 mice with wild type controls and (3);

[11C](R)-PK11195 binding in APPSwe/PS1dE9 mice with wild type age matched controls *in vivo.*

In this aim we will compare data obtained from filtration binding techniques, PET imaging, and immunohistochemistry in postmortem tissue obtained from Alzheimer's disease and transgenic mice to determine if PK11195 can label brain macrophages in Alzheimer's disease in vivo.

Subhypothesis4: DAA1106 will bind to regions of neuroinflammation with higher affinity compared to PK11195

SPECIFIC AIM 4: We will compare the binding characteristics of the novel PBR ligand [3H]-DAA1106 with [3H](R)-PK11195 in (1); normal human and rat brain tissue, and (2); rat models of neuroinflammation. We will also use ex-vivo autoradiography to compare binding characteristics of [11C]-DAA1106 with [11C](R)-PK11195 in rat models of neuroinflammation in vivo.

In this aim we will use two extensively characterized models of neuroinflammation, rat injected with lipopolysaccaride and 6-hydroxy dopamine to compare binding characteristics of DAA1106 with PK11195.

In the first three aims, we will test if PK11195, a specific ligand that binds to the PBR, will label activated brain macrophages in post mortem tissue and animals models of HIV encephalitis and Alzheimer's disease. In the final aim, we will characterize a newer ligand, DAA1106, which binds to PBR with higher affinity compared to PK11195, in normal brain tissue as well as rat models of neuroinflammation. These studies will help determine if ligands to PBR will label brain macrophages in HIV encephalitis and Alzheimer's disease.

3.0 RESULTS

3.1 PET IMAGING OF BRAIN MACROPHAGES USING THE PERIPHERAL BENZODIAZEPINE RECEPTOR IN A MACAQUE MODEL OF NEUROAIDS.

3.1.1 Abstract

HIV infection in humans and simian immunodeficiency virus (SIV) infection in macaques results in an encephalitis in approximately one-quarter of infected individuals, and is characterized by infiltration of the brain with infected and activated macrophages. PK11195 is a ligand specific for the peripheral benzodiazepine receptor abundant on macrophages and expressed in low levels in the non-infected brain. We hypothesized that [11C](R)-PK11195 positron emission tomography (PET) could image brain macrophages and hence the development of encephalitis in vivo. [11C](R)-PK11195 binding was assessed in the brain using PET in eleven SIV infected macaques, six of which showed increased binding in vivo. Postmortem examination of the brain in these six macaques demonstrated encephalitis, while macaques that did not show an increase in [11C](R)-PK11195 binding did not develop SIV encephalitis. Brain tissue from SIV encephalitic macaques also showed increased [3H](R)-PK11195 binding compared to binding in non-encephalitic macaques. Increased PK11195 binding in vivo and in postmortem brain tissue correlated with abundance of macrophages but not astrocytes. Our results suggest that PET [11C](R)-PK11195-imaging can detect the presence of macrophages in SIV encephalitis in vivo and may be useful to predict the development of HIV encephalitis and in studies of the pathogenesis and treatment of HIV dementia.

3.1.2 Introduction

Approximately one quarter of immunosuppressed AIDS patients develop a neurodegenerative disorder clinically characterized as HIV associated dementia complex (37, 57, 74, 158). Early neurological symptoms appear to be reversible; however, later a progressive neurological deficit becomes fixed (202). The simian model of lentiviral infection closely resembles the human disease with a variable percentage of infected macaques developing neurological disease (24). Histopathologic hallmarks of both HIV and SIV encephalitis (HIVE or SIVE) include abundant brain tissue infiltration by macrophages, multinucleated giant cells, microglial nodules and perivascular chronic inflammatory cells (39, 137). The pathogenesis of neurodegeneration is unknown. Current hypotheses implicate viral proteins and toxins derived from both HIV infected and activated macrophages that cause neuronal damage (128).

Several imaging modalities have been used to assess central nervous system (CNS) changes associated with lentiviral infection (14, 194, 200). While X-ray computed tomography has been considered relatively insensitive, magnetic resonance imaging (MRI) has demonstrated a spectrum of lesions including white matter abnormalities and brain atrophy in demented HIV-infected subjects (15 , 159, 199, 205 , 227, 249). Functional imaging studies using PET with the fluorine-18 labeled glucose analog [^{18}F]2-fluoro-2-deoxyglucose, single-photon emission computed tomography, magnetic resonance spectroscopy, and functional MRI have offered tantalizing insights into lentiviral infection, but no definitive relationship between abnormalities and onset of neurological disease has been observed (49, 50, 78, 193, 210). If HIVE could be evaluated during life, it would be possible to identify developing neurological damage and monitor efficacy of therapy before development of fixed deficits. Since activated and infected macrophages are the *sine qua non* of HIVE and SIVE (39, 128), it may be possible to monitor the progression of HIVE if it were possible to monitor the presence of macrophages in vivo.

Radiolabeled ligands have been recently synthesized that selectively bind to the peripheral benzodiazepine receptor (PBR), which is abundantly expressed on brain macrophages (17, 42). The isoquinoline carboxamide derivative PK11195 [1-(2-

chlorophenyl)-N-methyl-N- (1-methylpropyl)-3-isoquinolinecarboxamide] is a specific ligand for PBR. Because PBR is expressed only at low levels in the normal brain, several in vitro and in vivo studies have examined whether PK11195 can be used to radiolabel activated macrophages in the diseased CNS. Autoradiographic studies have demonstrated increased binding of [^{3}H](R)-PK11195 to macrophages in a wide variety of neurological diseases such as multiple sclerosis and experimental autoimmune encephalitis (20, 246), stroke (231) and brain trauma (204). Several studies have utilized PET with [11C](R)-PK11195 to detect activated macrophages in the CNS of patients with multiple sclerosis (20, 69, 246), Rasmussen's encephalitis (18), Herpes encephalitis (43), Alzheimer's disease (41) and Multiple System Atrophy (95). In the current study we used both in vivo PET imaging and binding analysis of post mortem tissues to demonstrate increased specific binding of both [11C](R)-PK11195 and [3H](R)-PK11195 to macrophages in SIV encephalitic macaques. Increased PK11195 specific binding in SIVE suggests that PET utilizing [11C](R)-PK11195 may permit in vivo monitoring of the evolution and treatment of HIV dementia.

3.1.3 Methods

Animals

All animals were housed and maintained according to strict standards of the Association for Assessment and Accreditation of Laboratory Animal Care, and experiments were approved by the University of Pittsburgh Institutional Animal Care and Use Committee. Fourteen macaques: 4 pigtail macaques (Macaca nemestrina) and 10 rhesus macaques (Macaca mulatta) varying from ages 84 to 168 months were challenged with SIVDeltaB670 (SIVDB670) with the length of infection varying from 56 to 1622 days (Table 1).

We used six CD8 T-cell depleted macaques (to compress the disease time course) and eight non-depleted macaques in this study. Preliminary studies from our laboratory have shown that the CD8 T-cell depleted macaques develop encephalitis (unpublished data). CD8 T-cell depletion was performed using protocols analogous to those previously

described (220) using the CD8 T-cell specific antibody cM-T807 (gift from Dr. Keith Reinman). Eleven macaques were available for PET scanning after infection.

Macaques were sacrificed at pre-specified time points or when moribund with AIDS (**Table 1**). Complete neuropathological microscopic analysis was performed in all macaques and no opportunistic infections were identified in the CNS. SIVE was diagnosed and classified as mild, moderate or severe on the basis of distribution of perivascular and parenchymal macrophage infiltrates, microglial nodules, multinucleated giant cells and abundant macrophages that immunostained for SIV envelope protein (assessed in multiple10X and 40X fields per brain region) in various brain regions (137) (**Table 2**). Brain tissue from two non-infected macaques served as additional controls.

Table 1 Macaque experimental parameters.

Macaque number	Species	CD8 T-cell depletion	Virus	Length of infection, days	PET scan	Filtration binding analysis in post mortem brain tissue	Time of sacrifice
1259	Pigtailed	Yes	SIVDB670	66	Yes	Yes	Moribund with AIDS
2263	Rhesus	Yes	SIVDB670	80	Yes	No	Moribund with AIDS
2265	Rhesus	Yes	SIVDB670	56	Yes	Yes	Moribund with AIDS
2266	Rhesus	Yes	SIVDB670	56	Yes	Yes	Moribund with AIDS
1220	Pigtailed	No	SIVDB670	171	Yes	No	Moribund with AIDS
0222	Pigtailed	No	SIVDB670	121	Yes	No	Moribund with AIDS
9240	Rhesus	No	SIVDB670	64	Yes	No	Timed sacrifice
9244	Rhesus	No	SIVDB670	1622	Yes	No	Moribund with AIDS
9243	Rhesus	No	SIVDB670	408	Yes	No	Moribund with AIDS
2229	Rhesus	No	SIVDB670	722	No	Yes	Moribund with AIDS
9231	Rhesus	No	SIVDB670	351	Yes	No	Timed sacrifice
2233	Rhesus	No	SIVDB670	1062	No	Yes	Moribund with AIDS
1260	Pigtailed	Yes	SIVDB670	70	Yes	No	Timed sacrifice
2264	Rhesus	Yes	SIVDB670	69	No	Yes	Moribund with AIDS
7405	Rhesus	No	NA	NA	No	Yes	Not infected
7421	Rhesus	No	NA	NA	No	Yes	Not infected

Time of sacrifice indicates if macaques were sacrificed at predetermined time points or sacrificed when moribund with AIDS. SIVDB670 - SIVDeltaB670, NA - Not applicable.

PET imaging

High specific activity [11C](R)-PK11195 ([N-methyl-^{11}C]-PK11195) was produced at the UPMC PET Facility using methods similar to those previously described by the Hammersmith PET Group (222), except that the methylation was performed at room temperature for 2 min to minimize the dechlorination side reaction (60). Chemical and radiochemical purities were ≥95% with specific activities ≥2.0 Ci/μmol at the end of a 40 min synthesis. Typical end of synthesis yields of high purity [11C](R)-PK11195 were in the range of 40-100 mCi.

Chronically infected macaques were imaged using PET with [11C](R)-PK11195 either pre-mortem (non CD8 T-cell depleted animals) or before SIV infection and at two months post infection (CD8 T-cell depleted animals). After a 10-min transmission scan using rotating ^{68}Ga/^{68}Ge rod sources, approximately 5 mCi (average dose 4.92±0.6 mCi, range 3.33 mCi – 5.92 mCi) of high specific activity [11C](R)-PK11195 in 5 ml of sterile isotonic saline was injected intravenous, into each macaque. PET data were acquired in 3-D imaging mode using an ECAT HR+ PET scanner (CTI PET Systems, Inc., Knoxville, TN). This instrument simultaneously acquired 63 image planes (15.2 cm field of view) with a reconstructed image resolution of 5.8 mm FWHM (ramp filter). A dynamic series of PET scans was acquired over 90 min in 33 frames. Emission data were corrected for attenuation, dead time, scatter, and radioactive decay.

[11C](R)-PK11195 PET scans of each macaque were co-registered to the baseline PET scan using the Automated Image Registration algorithm (259). Regions of interest were defined on summed PET images (0-8 min post-injection) and applied to the dynamic PET images to generate time-activity curves for the midfrontal cortex, basal ganglia, cerebellum, occipital cortex and hippocampal (mesial temporal lobe) brain regions. In the non CD8 T-cell depleted animals, the regional brain radioactivity concentration summed over the scan frames at various time points was normalized to both the injected dose of [11C](R)-PK11195 and the body mass of the animal (%ID/Kg*g) to represent a semi-quantitative measure of [11C](R)-PK11195 binding.

In the CD8 T-cell depleted macaques, we used the reference-Logan graphical analysis method to determine the specific binding of [11C](R)-PK11195 (146). [11C](R)-PK11195 PET scans obtained prior to SIV infection allowed each animal to serve as its own control because of the difficulty of identifying a consistent brain region devoid of disease pathology to serve as reference tissue.

MRI

Imaging was performed using a 3.0 Tesla whole body MRI scanner (General Electric Medical Systems, Milwaukee, WI) operating under version VH3 of the scanning software. The scanner has peak gradient strength of 4 Gauss/cm and peak slew rate of 15,000 Gauss/cm/sec. A custom-built, quadrature, birdcage extremity coil (15cm diameter, 32 legs) was used for scanning the animals, placed supine on the imaging table. Data acquisition was performed using an imaging protocol of standard imaging sequences used for the evaluation of anatomical detail, followed by the acquisition of a high-resolution gradient echo data set to be used for MRI PET co-registration and a dynamic, contrast-enhanced EPI acquisition.

High Resolution Spoiled Gradient-Recalled (SPGR) Acquisition: Three-dimensional gradient echo images were acquired prior to contrast injection to provide a high-resolution data set for MRI-PET co-registration. This SPGR data set was acquired using a TE, TR and flip angle combination (7 ms, 25 ms and 40^{o}, respectively) chosen to maximize contrast between brain tissue and its surroundings (including meninges and CSF). Contrast-enhanced Gradient Echo EPI: Multi-slice (21 axial slices, 3.0 mm thick, no gap, 80 images per slice) gradient recalled, single shot, EPI images (Flip = 60^{o}) were acquired one minute before and one minute after bolus venous injection (3 ml saline solution with 0.1 mM/kg of contrast agent, duration = one second) of Gadodiamide (Omniscan, Nycomed, Princeton, NJ). These data were acquired after collection of all other MR data sets. Volume measurements were determined as described before using the MORPH software (123, 124).

Autoradiography

Autoradiography was performed using 15 μm thick frozen sections obtained from the frontal cortex (204). Brain sections were placed on Superfrost^{Tm} glass slides (Sigma, St Louis, MO) and incubated in ice-cold 50 mM TRIS-HCl (pH 7.4) containing 1 nM [3H](R)-PK11195 (sp. Act., 89.9 Ci/mmol; NEN Life Sciences Products, Boston, MA) for 30 min. Specificity of binding was ensured by the inclusion of 10 μM PK11195 (Sigma, St Louis, MO) in parallel sections. The sections were mounted with a layer of autoradiographic LM-1 emulsion (Amersham, UK) using a wire loop, following which they were developed after 4 weeks and imaged on the confocal microscope.

Filtration radioligand binding assays

Brain tissue from various regions was dissected, weighed and homogenized in ice-cold 50 mM Tris-HCl buffer (pH 7.4). Homogenates were washed four times by centrifugation at 40,000 g for 20 min at 4^0C. Total binding (per mg tissue) was determined by incubating tissue (total protein concentration ranging from 150 to 200 μg determined using the BCA protein assay kit; Pierce, Rockford, IL) with 1 nM [3H](R)-PK11195 (except in saturation binding experiments where 0.5-80 nM [3H](R)-PK11195 was used) at 4^0C for 2 hr in a final volume of 250 μl of Tris-HCl. Nonspecific binding was determined by the inclusion of 10 μM PK11195. Specific binding (in fmoles per mg protein incubated in each test tube) was defined as the difference between total and nonspecific binding (204). The reaction was terminated by the addition of ice-cold buffer in a vacuum cell harvester (Brandel, Gaithersburg, MD). All samples were run in duplicate.

Immunohistochemical labeling and confocal microscopic quantification

Immunostaining and laser confocal microscopic quantification was performed as described before (32, 126). Sections were stained with antibodies to GFAP (mouse monoclonal, DAKO, Carpinteria, CA), or CD68 (mouse monoclonal, DAKO), or SIV gp110 (a gift from Dr. Kelly Stephano-Cole and Dr. Ronald Montelaro) or MAP2 (SMI 52; Sternberger Monoclonals Inc., Lutherville, MD) used at concentrations 1:500, 1:100, 1:100 and 1:1000 respectively. Sections were then incubated with Cy5-conjugated goat

anti-mouse or Cy3-conjugated anti-rabbit IgG at a concentration of 1:200 (Jackson Immunoresearch Laboratories Inc., West Grove, PA). Different anatomic regions were identified using a dissection microscope and marked on the slides. Immunostained sections were scanned and quantified on a laser confocal microscope (LSM 150, Zeiss, Heidelberg, Germany). This scope is equipped with an argon laser with 458 nm, 477 nm, 488 nm and 514 nm primary emission lines. Each section was scanned along the *z*-axis to define the middle optical plane used in quantification (262,144 pixels/plane; 1 pixel= 0.25 μm^2). Image analysis was performed on a Silicon Graphics computer (Windows NT 4.0 operating system, Microsoft, Redmond, Washington) using the LSM software (version 3.0, Zeiss). Scanning parameters such as laser power aperture, gain, and photomultiplier tube settings were kept constant for each wavelength.

In each anatomic region, an individual blinded to the experimental design imaged 10 areas (40X) encompassing 106,100 μm^2. For each cell phenotype scanned, contribution to signal intensity from autofluorescence was minimized using a threshold that was kept constant. In each area the average pixel fluorescence along with the pixel counts for a given cell phenotype marker that exceeded the threshold were enumerated. The average pixel fluorescence was multiplied by the total number of pixels to measure the total florescence for that cell phenotype marker in that area. The total fluorescence values determined from the 10 scanned areas in one brain region were averaged to represent a measure of the cell phenotype in that brain region.

To evaluate cellular localization of [3H](R)-PK11195 binding in SIVE brain tissue we combined immunostaining with autoradiography. Sections were first immunostained, subjected to autoradiography (see above) and then imaged on the confocal microscope.

Statistical analysis

Data were analyzed using PRISM software (Graphpad, San Diego, CA). Student's *t* tests or one-way ANOVA tests with post-test Bonferroni correction and 95% confidence intervals were used to analyze data. Correlations using 95% confidence intervals were performed to quantify the relationship between PK11195 binding and macrophages or

astrocytes. Results from correlational analyses are represented by *r*, the Spearman's coefficient.

3.1.4 Results

[11C](R)-PK11195 PET binding is higher in macaques that develop SIV encephalitis

To test if PET imaging of macaques using [11C](R)-PK11195 correlates with the development of SIVE, we compared PET findings in SIVDB670 infected macaques immediately prior to sacrifice with neuropathological features**.** Our macaque cohort consisted of fourteen animals (six animals were CD8 T-cell depleted to compress the disease time course and eight were non CD8 T-cell depleted) (**Table 1**). Eleven of these macaques were imaged using 3D PET (**Tables 1 and 2**). Six of the eleven SIV infected macaques (four CD8 T-cell depleted and two non CD8 T-cell depleted macaques) demonstrated increased uptake and retention of [11C](R)-PK11195 with PET compared to the other macaques ($p<0.03$, **Table 2 and Figure 5**).

Brain histopathology was assessed in all macaques after PET imaging. SIVE was defined by the presence of parenchymal and perivascular macrophages, multinucleated giant cells, microglial nodules and abundant macrophages that stained for the SIV envelope protein. The six macaques that demonstrated increased [11C](R)-PK11195 PET binding showed various degrees of SIVE (**Table 2**). Macaque 9231 showed some macrophage infiltration in the basal ganglia without other classical histopathological features of SIVE, which corresponded to a 29%, increase in [11C](R)-PK11195 specific binding in vivo in the basal ganglia (**Table 2**) and might represent a pre-encephalitic stage of disease. The remaining macaques either showed subtle inflammatory changes in the form of perivascular mononuclear cell infiltrates, or failed to show any significant abnormalities and were therefore considered non-encephalitic controls. These macaques showed marginal or no PET [11C](R)-PK11195 uptake and binding (**Table 2**). Increased [11C](R)-PK11195 specific binding in vivo correlated with the post mortem diagnosis of SIVE.

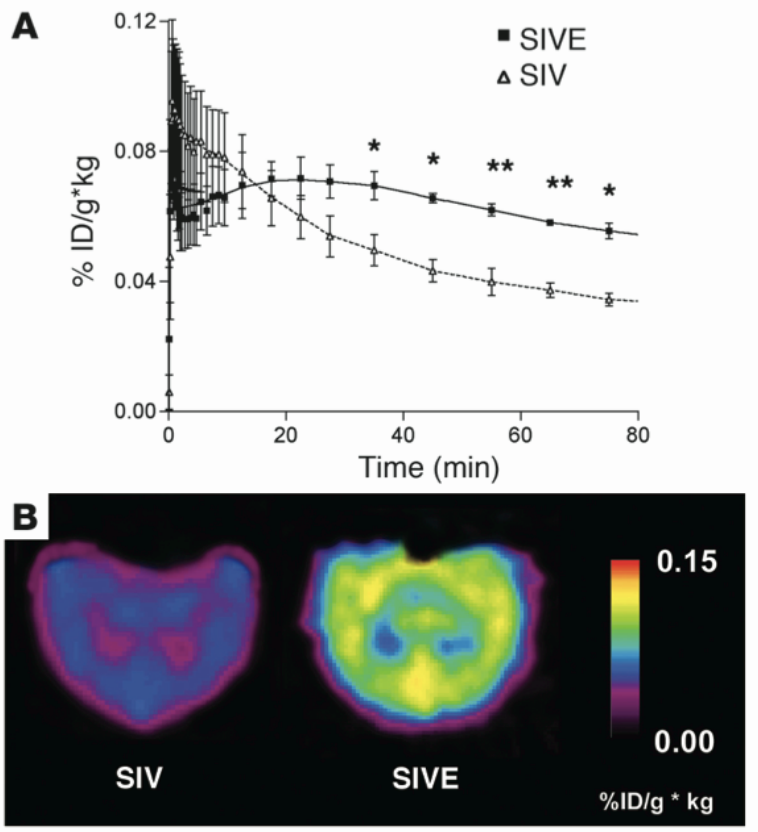

Figure 5 [11C](R)-PK11195 specific binding is higher in macaques that develop SIVE in vivo compared to SIV infected macaques that do not develop encephalitis.

(**A**) Time Activity curve of [11C](R)-PK11195 specific binding in the mesial temporal lobe of non CD8 T-cell depleted macaques imaged before necropsy. [11C](R)-PK11195 specific binding is represented as radioactivity concentrations summed over the scan frames and normalized to both the injected dose of [11C](R)-PK11195 and the body mass of the animal (%ID/g*kg, y-axis) and is plotted against time in minutes (x-axis). Macaques were then classified into SIV encephalitic (SIVE, n=2, black squares) and control SIV infected, non-encephalitic groups (SIV, n=4, clear triangles) based on histopathology (Table 2). [11C](R)-PK11195 specific binding determined prior to neuropathological evaluation was compared in these two macaque groups. SIVE macaques show increased [11C](R)-PK11195 retention and specific binding over time in the late scan frames (40-90 min) compared to SIV infected, non-encephalitic macaques. Data was analyzed using students *t* test with 95% confidence intervals **, $p < 0.004$, *, $p < 0.03$.

(**B**) Representative horizontal-section parametric images of [11C](R)-PK11195 specific binding in SIV encephalitic (SIVE) and SIV infected, non-encephalitic (SIV) macaques. SIVE macaque brains show increased [11C](R)-PK11195 specific binding compared to SIV infected, non-encephalitic macaques.

Table 2 Increased [11C](R)-PK11195 binding in vivo corresponds to the presence of SIVE and increased [3H](R)-PK11195 binding in post mortem brain tissue.

Macaque number	PET binding value (% increase over control)	Histopathology	Post mortem tissue binding (% increase over control)
1259	313	Severe SIVE	104
2263$^{\delta}$	213	Mild SIVE$^{\delta}$	NA
2265	122	Moderate SIVE	71
2266	174	Severe SIVE	37
1220	55	Severe SIVE	NA
0222	39	Moderate SIVE	NA
9240	11	No encephalitis	NA
9244	0	No encephalitis	NA
9243	0	No encephalitis	NA
2229	NA	No encephalitis	0
9231*	29*	No encephalitis*	NA
2233	NA	No encephalitis	9
1260	0	No encephalitis	NA
2264	NA	No encephalitis	1

Representative data obtained from the basal ganglia of fourteen SIV infected macaques (similar results were observed in other areas). Eleven SIV infected macaques were imaged with 3D PET using [11C](R)-PK11195 prior to sacrifice, following which they were grouped into mild, moderate or severe SIV encephalitic (SIVE) or SIV infected, non-encephalitic (SIV) categories based on the histopathology (frequency of distribution of multinucleated giant cells, microglial nodules, abundant activated and SIV infected macrophages, perivascular chronic inflammation per 10X and 40X field in different brain regions). An increase in [11C](R)-PK11195 specific binding (represented as % increase in specific binding over controls) corresponded with the post mortem diagnosis of SIV encephalitis. Macaques that did not exhibit increased [11C](R)-PK11195 binding did not exhibit SIVE. **™**Macaque 2263 showed a densely focal but low frequency of distribution of microglial nodules and macrophages and was classified as mild SIVE. *****Macaque 9231 had macrophage (staining negative for SIV antigen) infiltration in the basal ganglia (without other histopathological features of SIVE, that might represent a pre-encephalitic state) may have resulted in the 29% increase in [11C](R)-PK11195 binding. **NA**- Not assessed.

MRI imaging of the macaques

Four macaques underwent head MRI with and without contrast administration. Each animal was scanned pre-infection and then at one month post-infection and the day before sacrifice. MRI findings were compared to histopathological findings at post mortem examination as described before.

In these macaques, no structural abnormalities were observed in any of the scans at baseline pre-infection (**Figures 6A and 6C**). No qualitatively appreciable contrast enhancement was observed at any time in any animal. At autopsy the macaque without significant neuropathology and the macaque with mild SIVE (**Figures 6A and 6B**) showed no appreciable structural differences between pre- and post-infection scans with any of the MRI sequences. The macaques with moderate and severe SIVE showed no appreciable structural abnormalities at one month post-infection. Scans immediately prior to sacrifice, however, showed mild atrophy with ventricular dilatation (average increase in ventricular volume of 47% relative to pre-infection scans, data not shown) best appreciated with T-2 sequences (**Figures 6C and 6D**).

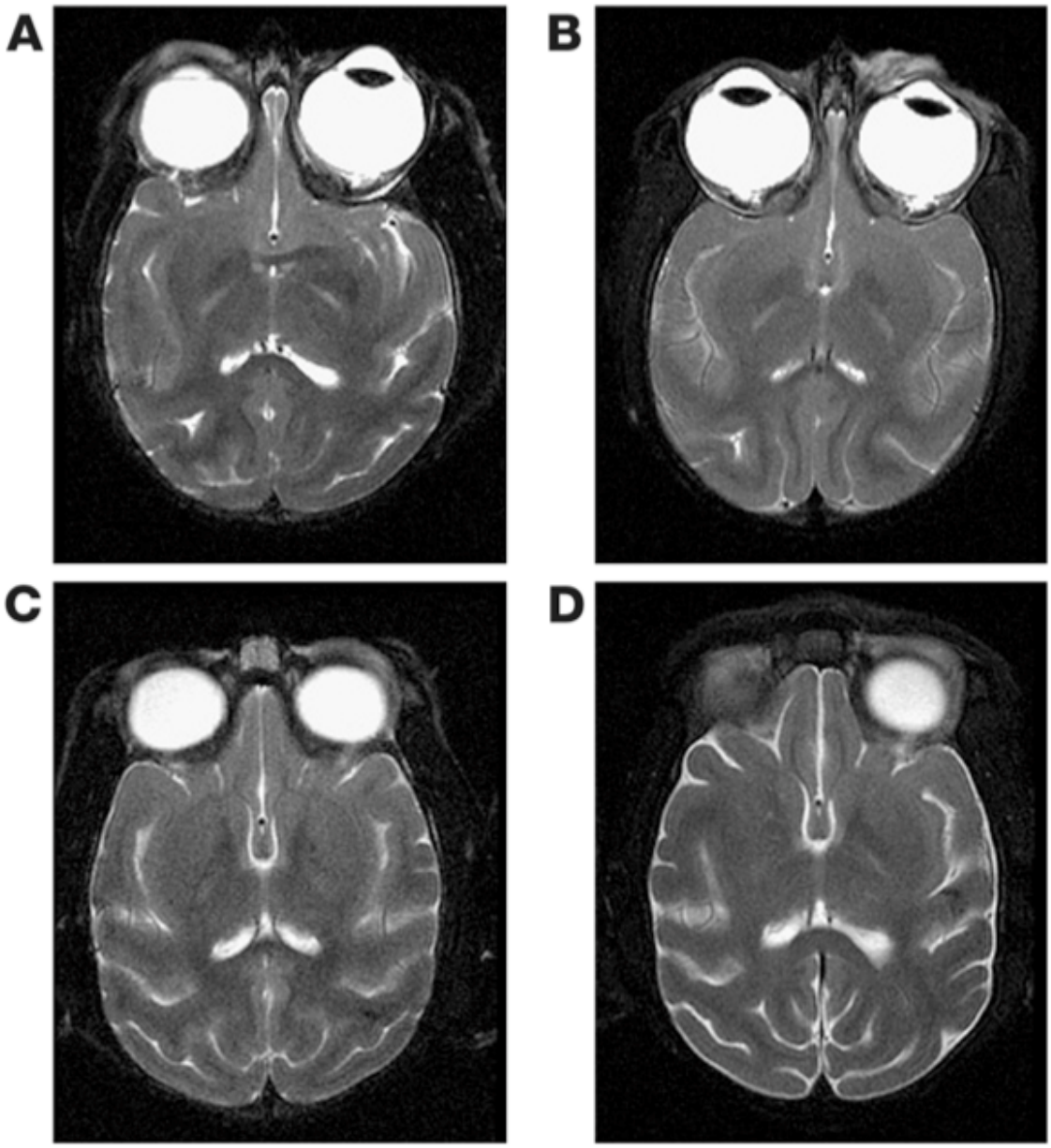

Figure 6 Comparison of pre and post infection MRI scans in SIVE macaques.

Head MRI scans from 2 macaques pre-infection (left, A and C) and immediately before autopsy (right, B and D).

(**A,B**) Images from a macaque that demonstrated mild SIVE at autopsy. No significant changes were observed between pre-infection and post infection images.

(**C,D**) Images from a macaque that demonstrated severe SIVE at autopsy. Mild increase in CSF space and parenchymal atrophy were observed in the macaque. No contrast enhancement was observed in any brain at any time.

[3H](R)-PK11195 binding is higher in SIV encephalitic brain tissue

To confirm increased PK11195 binding in SIVE macaques we used filtration binding and autoradiographic analyses to compare [3H](R)-PK11195 specific binding in SIVE brain tissue with controls. [3H](R)-PK11195 specific binding (per mg protein) was defined as the difference between total binding (determined by incubation of brain tissue with 1nM [3H](R)-PK11195) and nonspecific binding (determined by including 10μM PK11195). Specific binding was significantly higher in the frontal white and gray matter, basal ganglia and hippocampal areas of encephalitic macaques ($p<0.004$) compared to binding in these regions in SIV infected, non-encephalitic and non-infected macaque brain tissue (**Figure. 7A and Table 2**). The cerebellum and occipital cortex of encephalitic macaques did not show a significant difference in specific binding over these regions in control macaques (**Figure. 7A**). For autoradiography, frozen brain sections obtained from the frontal cortex were incubated with 1 nM [3H](R)-PK11195 with non-specific binding determined by the inclusion of 10 μM PK11195. SIVE brain tissue showed higher [3H](R)-PK11195 binding compared to the non-encephalitic control brain tissue (**Figure 8A-B**). [3H](R)-PK11195 binding in encephalitic tissue appeared more intense and corresponded to the distribution of microglial nodules (**Figure 8A**) in contrast to the diffuse, less intense binding seen in SIV infected, non-encephalitic tissue in all observed fields (**Figure 8B**). Increased [3H](R)-PK11195 specific binding in postmortem brain tissue also corresponded to an increase in [11C](R)-PK11195 binding in encephalitic macaques in vivo (**Table 2**).

Increased PK11195 binding in SIVE macaques may be due to increases in PBR expression (*Bmax*/ binding sites) or due to alterations in receptor-PK11195 affinity (*Kd*). We used [3H](R)-PK11195 saturation binding experiments (range 0.5 nM to 80 nM) to compare the total number of binding sites (*Bmax*) and ligand affinity (*Kd*) in SIVE with SIV infected, non-encephalitic and non-infected controls. SIVE macaques showed a significant increase in [3H](R)-PK11195 binding sites (*Bmax*, **Figure 7B**) ($p=0.009$) with no significant difference in ligand affinity (*Kd,* **Figure 7C**) ($p=0.488$).

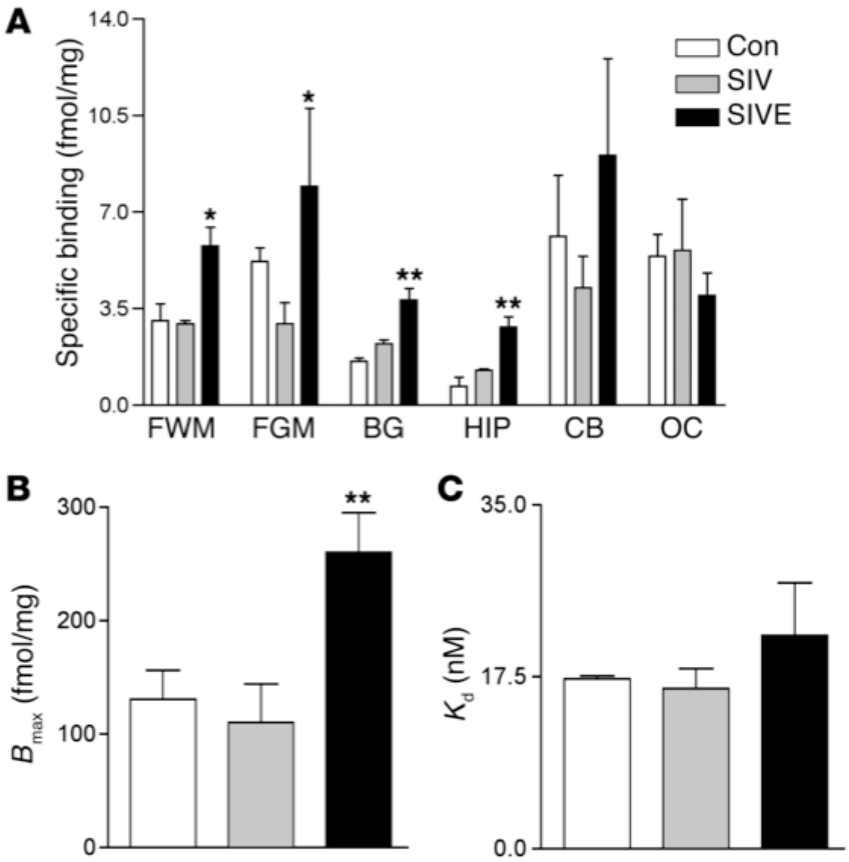

Figure 7 [3H](R)-PK11195 specific binding is higher in SIVE brain tissue compared to controls.

A. [3H](R)-PK11195 specific binding (fmoles/mg protein, Y-axis) is higher in the frontal cortical white matter (FWM), frontal cortical gray matter (FGM), basal ganglia (BG) and hippocampus (HIP) in SIVE macaques (n=3, black bars) compared to non-infected controls (Con, n=2, clear bars) and SIV infected, non-encephalitic (SIV, n=3, hatched bars) macaques. No significant difference was seen in the cerebellum (CB) and the occipital cortex (OC). Data analyzed using one-sided ANOVA, **, $p< 0.0002$, *, $p< 0.004$.

B. [3H](R)-PK11195 (0.5nM to 80nM) saturation binding experiments indicate that increase in specific binding is due to an increase in total number of [3H](R)-PK11195 binding sites (*Bmax*, fmoles/mg protein, Y-axis) in SIVE (n=3, black bars) as compared to non-infected controls (Con, n=2, clear bars) and SIV infected, non-encephalitic (SIV, n=3, hatched bars) frontal cortical brain tissue. Data analyzed using one-sided ANOVA, **, $p=0.009$.

C. Saturation binding experiments indicate no significant increase in [3H](R)-PK11195 binding affinity (*Kd*, nM, Y-axis) in SIVE (n=3, black bars) as compared to non-infected controls (Con, n=2, clear bars) and SIV infected, non-encephalitic (SIV, n=3, hatched bars) frontal cortical brain tissue. Data analyzed using one-sided ANOVA, $p=0.488$.

[3H](R)-PK11195 binding in SIV encephalitic brain tissue localizes to macrophages

PBR is expressed mainly on astrocytes and brain macrophages (20, 45) and at lower levels in neurons (121). We wanted to determine the relative contributions of these cell types to [3H](R)-PK11195 binding. We addressed this question in two ways. First, we combined immunostaining for astrocytes (GFAP) and activated macrophages (As a macrophage lysosomal marker, CD68 is increased on activation, and is useful to label activated macrophages/microglia) with [3H](R)-PK11195 autoradiography on frozen brain sections obtained from the frontal cortex of SIVE macaques. [3H](R)-PK11195 binding in SIVE overlapped with regions rich in activated macrophages and microglial nodules (aggregates of macrophages) (**Figure. 8C**). [3H](R)-PK11195 binding did not overlap with GFAP labeled astrocytes in encephalitic brain tissue (**Figure. 8D**).

Second, we tested whether [3H](R)-PK11195 binding in homogenized brain tissue correlated with the abundance of astrocytes or activated macrophages or neurons. Astrocytes, activated macrophages and neuronal elements were immunostained for GFAP, CD68 and MAP2 respectively, and quantified in SIVE and SIV infected, non-encephalitic brain tissue using laser confocal microscopy by an individual blinded to the experimental design. Each cell type marker was then correlated with [3H](R)-PK11195 filtration binding values obtained from the corresponding brain regions in the same macaques. Results of correlations are represented by Spearmen's correlation coefficient *r* (**Table 3**). [3H](R)-PK11195 binding correlated with the abundance of CD68 stained activated macrophages (r = 0.5285, p= 0.0066) but not with the abundance of GFAP stained astrocytes (r = 0.1991, p = 0.2915) or with the abundance of MAP2 stained neuronal elements (r = 0.0709, p = 0.6767) (Table 3).

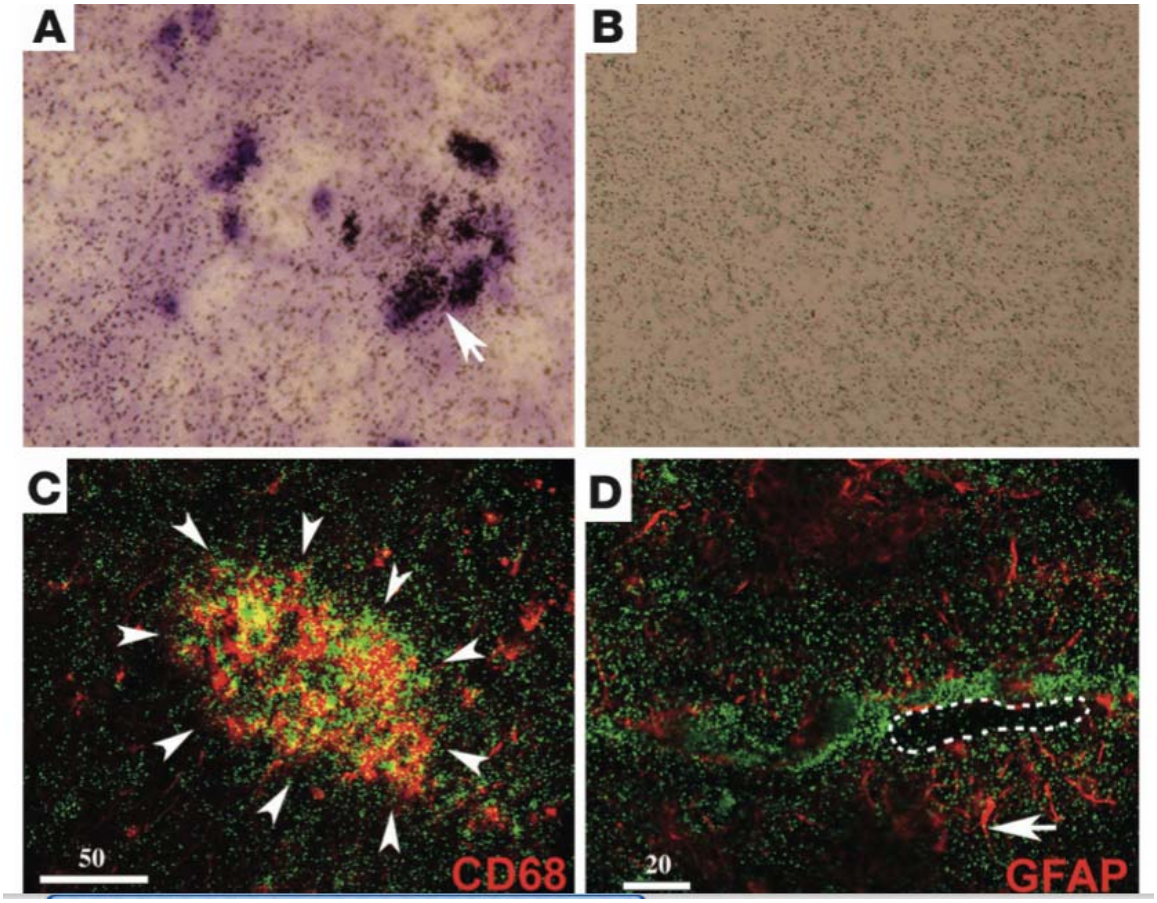

Figure 8 [3H](R)-PK11195 specific binding in SIVE corresponds to activated macrophages but not astrocytes.

(**A,B**) [3H](R)-PK11195 autoradiograms (black grains) with light hematoxylin counter stain of sections from frontal cortex show higher specific binding in SIVE (8A) compared to SIV infected, non-encephalitic macaques (8B). Arrow in A shows a region of numerous grains overlying a microglial nodule.

(**C,D**) Combined [3H](R)-PK11195 autoradiography (green grains) and immunostaining for activated macrophages (C, CD68, Red) or astrocytes (D, GFAP, Red) in SIVE frontal cortex. [3H](R)-PK11195 specific binding overlaps with CD68 (C) and not with GFAP (D) immunostaining. Arrowheads in (C) surround a microglial nodule, dotted line in (D) showing the lumen of a blood vessel and arrow in (D) showing astrocytic end processes (red). Vessels in SIVE are frequently surrounded by mononuclear infiltrates interdigitated between astrocytic processes in regions with abundant [3H](R)-PK11195 grains in green. Scale bar in microns.

[11C](R)-PK11195 binding in SIV encephalitis in vivo correlates with the presence of activated macrophages

We correlated [11C](R)-PK11195 specific binding in vivo with the presence of astrocytes, activated macrophages or neuronal elements in selected brain regions of SIVE and SIV infected, non-encephalitic macaques. Astrocytes, activated macrophages and neurons were immunostained and quantified using laser confocal microscopy as above and compared to in vivo estimates of [11C](R)-PK11195 specific binding in the corresponding brain regions in the same macaques. [11C](R)-PK11195 binding correlated with the abundance of CD68 stained activated macrophages (r = 0.6424, p= 0.0013) but did not correlate with the presence of astrocytes (r = -0.1692, p=0.5630) or neurons (r = 0.0574, p = 0.563) (**Table 3**).

Table 3 [3H](R)-PK11195 binding in post mortem tissue and [11C](R)-PK11195 binding in vivo correlate with immunostaining for activated macrophages but not astrocytes.

Spearman's coefficient (r) with [3H](R)-PK11195 binding in post mortem tissue.		Spearman's coefficient (r) with [11C](R)-PK11195 binding in vivo.	
Activated macrophages (CD68)	Astrocytes (GFAP)	Activated macrophages (CD68)	Astrocytes (GFAP)
0.5285**	0.1991	0.6424 **	-0.1692

Activated macrophages and astrocytes were quantified by immunostaining for CD68 (lysosomal marker for activated macrophages) and GFAP (astrocytic marker) in the frontal cortex, basal ganglia, hippocampus, cerebellum and occipital cortex of SIVE (n=3) and SIV infected, non-encephalitic (n=3) macaques, using confocal laser microscopy. Each cell phenotype marker was then correlated with [3H](R)-PK11195 binding in post mortem tissue or [11C](R)-PK11195 PET binding in vivo in the corresponding brain regions in the same macaques. PK11195 binding in post mortem tissue and in vivo correlated with activated macrophages but not astrocytes, **p<0.006.

3.1.5 Discussion

We examined binding of the PBR ligand PK11195 in a macaque model of HIV encephalitis. In vivo ligand binding was assessed using [11C]-labeled (R)-PK11195 with PET in SIV infected macaques. Out of eleven-imaged SIV infected macaques, six showed higher levels of [11C](R)-PK11195 binding (**Figure 5 and Table 2**). Increased binding corresponded to the presence of SIV encephalitis on post mortem examination (**Table 2**). Macaques that did not show an increase in [11C](R)-PK11195 binding did not exhibit SIVE (**Table 2**). In four macaques comparison of MRI before infection and two months after infection showed mild brain atrophy and increase in ventricular size only in the moderate to severe SIVE cases (**Figure 6** and data not shown). Brain post mortem [3H](R)-PK11195 binding was significantly higher in SIVE macaques from controls due to an increase in the number of binding sites (*Bmax*) with no significant changes in binding affinity (*Kd*) (**Figure 7**) and correlated with in vivo binding measured with PET just before sacrifice (**Table 2** and data not shown). Brain regions with elevated PK11195 binding on PET and filtration assays correlated with abundant activated macrophages but not with activated astrocytes or neurons quantified by laser confocal microscopy (**Table 3**). Finally, combined autoradiography and immunostaining identified macrophages, but not astrocytes as the cells with highest [3H](R)-PK11195 binding (**Figure 8**).

Our study involves the use of two different species of macaques utilizing two different protocols (with and without CD8 T-cell depletion) to induce disease. While this is a limitation based on macaque availability and continual evolution of the primate model, baseline pre-infection PET studies in animals of the two different species did not indicate significant differences (Average PET [11C](R)-PK11195 binding in the basal ganglia of Rhesus macaques: 0.06±0.01 %ID/Kg*g versus Pigtail macaques: 0.08±0.02 %ID/Kg*g, p=0.217. Similarly, other brain regions including the frontal cortex, cerebellum, occipital cortex and hippocampus showed no significant differences between the two species). Thus data from all control animals were grouped together. However, we cannot rule out the possibility of differences resulting from species in the extent of CNS

disease. Further, it has been suggested the CD8 T-cell depletion results in an increase in the severity of CNS disease by Williams and Hickey (256) and this was the impetus to our using this model. Preliminary histopathological comparisons of our two groups of animals did not indicate any major differences (**Table 2**). However, we are unable to draw any conclusions regarding this issue due to the small number of CD8 T-cell depleted macaques used in this study.

In the frontal cortex, mesial temporal lobe and the basal ganglia of SIVE macaques [3H](R)-PK11195 binding in post mortem tissue correlated with PET [11C](R)-PK11195 binding in vivo (**Table 2** and data not shown). In the cerebellum and occipital cortex PET [11C](R)-PK11195 binding showed significant increases which we did not see in post mortem tissue (**Figures 5, 7** and data not shown). Further, while macaque 2263 showed 213 percent increase in PET binding from control in the basal ganglia, it demonstrated mild but densely focal encephalitis on postmortem examination in this region. These discrepancies may be due to differences in resolution and sampling size between PET, post mortem tissue-filtration binding analyses, and histopathological assessment. Neuropathological studies are performed on a section of a given brain region and post mortem binding analysis is restricted to a small mass of brain tissue (~100 mg) in contrast to larger regions of the brain involved in PET analyses with more limited spatial resolution. However, in both post mortem tissue and in vivo PET, PK11195 binding closely correlated with the histopathological abundance of macrophages (**Table 3 and Figure 8**).

Comparing pre-infection MRI scans with scans at autopsy in four infected macaques showed mild atrophy with ventricular dilatation only in macaques with moderate and severe SIVE. The macaque with mild SIVE did not show any structural changes on comparing pre- and post- infection scans but showed regional increases in vivo PK11195 binding corresponding with macrophage infiltration. This suggests that PET [11C](R)-PK11195 imaging may be more sensitive than structural MRI in assessing neurologic disease in SIVE, although all of the eleven PET scanned macaques were not imaged using MRI.

The distribution of lesions in SIVE is multifocal without a prominent or consistent neuroanatomical distribution (32). This diffuse and multifocal distribution

hinders identification of a consistent reference region for application of PET reference-tissue based analyses. To overcome this issue, the segmentation of dynamic PET images into clusters of image voxels with similar concentration time-activity curves has been proposed as a viable means to extract a reference ligand kinetic without *a priori* knowledge of the brain distribution of PBR sites (109). This reference kinetic, though not necessarily derived from a uniform brain region, has been demonstrated to be capable of providing a reasonable estimate of free and non-specific binding and has been successfully employed in the study of multiple sclerosis patients with [11C](R)-PK11195 (20).

Although all macaques with increased [11C](R)-PK11195 binding showed encephalitis, the percent increase in [11C](R)-PK11195 binding from controls was higher in CD8 T-cell depleted SIVE macaques (174% - 313%) vis-à-vis the non-CD8 T-cell depleted macaques (39-55%) (Table 2). These two groups of encephalitic macaques did not show significant neuropathological differences (**Table 2**). We attribute this discrepancy to the incommensurability of the two parameters used to estimate specific binding. In the non-CD8 T-cell depleted animals, a semi-quantitative measure of [11C](R)-PK11195 binding was defined to be the regional brain radioactivity concentration summed over the late scan frames (**Figure 5**: 40-90 minutes post-injection) and normalized to both the injected dose of [11C](R)-PK11195 and the body mass of the animal (%ID/Kg*g). In contrast [11C](R)-PK11195 specific binding in the CD8 T-cell depleted animals was determined using each macaque's regional baseline (pre-infection) [11C](R)-PK11195 time-activity curve as the reference kinetic for regional post-infection assessments based on the reference-Logan graphical analysis method (20, 108, 138)**.** Because the reference tissue kinetic provides an estimate of both free and nonspecifically bound radiotracer, the binding potential parameter derived by this method of analysis from the CD8 T-cell depleted macaques represents a more accurate measure of specific binding. This is in contrast to the more qualitative estimates of specific binding (regional brain radioactivity concentrations without subtraction of the free and non specific binding) obtained over the summed late PET scan frames from the first group of non-CD8 T-cell depleted macaques.

We also found that in the CD8 T-cell depleted group, normalized regional brain radioactivity concentrations (%ID/kg*g) were considerably more variable than in non-CD8 depleted animal (data not shown). Such a discrepancy could be explained by differences in systemic infection with variation in non-CNS macrophage proliferation and subsequent specific binding of [11C](R)-PK11195 outside the CNS. Such sites of systemic binding of [11C](R)-PK11195 could be expected to decrease the partitioning of the ligand in the brain with a varying proportion of the injected dose being taken up into these non CNS sites of systemic infection.

A recent report by Lockhart et. al.(145) has shown that the concentration of PBR sites in the whole blood of healthy human volunteers to be on the order of 10nM, with approximately 85% of the ligand bound in plasma and 15% bound to blood cells. These investigators demonstrated that [11C](R)-PK11195 binds with high affinity to α1-acid glycoprotein (AGP), which is present in varying degrees in serum. It is possible that binding of [11C](R)-PK11195 to AGP is higher with CD8 T-cell depletion in SIV infection, contributing to the unstable kinetic behavior of [11C](R)-PK11195 in plasma. Future studies defining an arterial input function for the injected PK11195 might clarify these modeling problems.

Our results in SIVE are in accordance with previous reports where PK11195 binding (as determined using post mortem tissue and PET) has been used as a marker for brain macrophages and a surrogate marker for neuronal damage (42, 151). To determine if PK11195 binding correlated better with SIV infected macrophages, we correlated PK11195 binding with SIV antigen gp110 quantified using immunostaining in selected brain regions of SIV infected macaques. The abundance of the viral antigen varied in different regions of the brain, consistent with the multifocal nature of the disease (32, 97). Regions with high viral antigen showed high PK11195 binding, but, high PK11195 binding was also seen in regions that did not show high viral antigen (data not shown), thus correlating better with activated macrophages. This is presumably due to the more general distribution of activated macrophages in SIV encephalitis than viral infection, which is more multifocal (32, 97). Our findings support the hypothesis that PK11195 binding may be a surrogate marker of activated macrophages and active loci of neurodegenerative disease in lentivirus encephalitis.

Our results in SIV infected macaques show that PET assessment of [11C](R)-PK11195 binding can distinguish macaques with and without SIV encephalitis (defined at post mortem analysis) in vivo. We are currently conducting serial PET experiments in SIV infected macaques to determine the earliest time period where this distinction can be made. Importantly, our macaque data can be extended to PET studies in HIV-infected humans. One in four late-stage AIDS patients is afflicted by HIV encephalitis in the absence of opportunistic infections (37). Its clinical diagnosis requires the presence of irreversible clinical symptoms and signs**.** Traditional imaging studies such as CT and MRI have not been of much assistance in the diagnosis of AIDS dementia and dementia in general (66)**.** Current methodologies, such as structural MRI assessment of brain volume are insensitive late measures of neurological damage and the diagnosis by neurocognitive tests is possible only after irreversible neuronal damage has occurred. Effective therapy requires early intervention at the onset of neuronal injury prior to the appearance of irreversible signs and symptoms. PET imaging of macrophages in HIV encephalitis before the onset of signs and symptoms may enable early diagnosis and therapeutic interventions.

To design therapies for neurodegenerative disorders, it is critical to be able to monitor their success in arresting the progression of neurological disease. Monitoring therapeutic efficacy of any such treatments is also complicated by the fact that one can only assess absence of disease progression and not recovery of function. Any attempt to develop therapy for AIDS dementia will require some means of monitoring the primary pathogenic process, activated macrophages. Issues of CNS drug penetrance and the absence of good markers of treatment effectiveness complicate monitoring the course of HIV encephalitis. Imaging macrophages may provide a better index of disease progression during treatment with antiretroviral and other potentially neuroprotective drugs. [11C] (R)-PK11195 PET imaging of macrophages may be able to help in the early prediction of HIV encephalitis, monitor the severity and progression of the disease, and help evaluate the effectiveness of CNS therapies.

3.2 THE PERIPHERAL BENZODIAZEPINE RECEPTOR IS SPECIFICALLY INCREASED IN MACROPHAGES IN A PI3-KINASE DEPENDENT FASHION IN HIV ENCEPHALITIS

3.2.1 Abstract

HIV encephalitis is a neurodegenerative disease seen in approximately one in four terminally infected patients. Macaques infected with the simian immunodeficiency virus develop encephalitis (SIVE) very similar to the human disease. Neurodegeneration in both these conditions is hypothesized to occur mainly from the effects of toxins derived from HIV infected and activated brain macrophages. Our goal is to label brain macrophages in vivo by taking advantage of potential increases in the peripheral benzodiazepine receptor in these cells. Using the peripheral benzodiazepine receptor specific ligand PK11195, we have previously shown increases in the peripheral benzodiazepine receptor in the SIVE model. In this report, we show that human brain tissue derived from HIV encephalitis shows similar increases in binding compared to controls with the peripheral benzodiazepine receptor ligands [3H](R)-PK11195 and [3H](R)-DAA1106. We further dissect out the cell specific contributions to increased PK11195 binding by reporting that primary human macrophage cultures show an increases in [3H](R)-PK11195 and [3H](R)-DAA1106 binding on activation with lipopolysaccaride or interferon-γ. Macrophages infected with HIV-1 ADAM show an increase in [3H](R)-PK11195 binding, which peaks at 14 days post infection. Astrocyte cultures treated with LPS or activated with dibutyryl Cyclic AMP or treated with supernatants derived from HIV-infected macrophages do not show a significant change in ligand binding. Finally, increases in [3H](R)-PK11195 binding on activation with LPS in

macrophage cultures is reversed on blocking the PI3K/Akt pathway, but is not affected by blocking the MEK-1/2 MAP-kinase pathway. Our results suggest that activated and HIV-infected macrophages in HIVE show increased [3H](R)-PK11195 binding due to specific increases in [3H](R)-PK11195 binding in a PI3K/Akt dependent fashion.

3.2.2 Introduction

About 25% of immunosuppressed patients infected with HIV develop a neurodegenerative syndrome clinically diagnosed as HIV-associated dementia (3, 38, 57, 74, 158). This syndrome is characterized by cognitive impairments, motor abnormalities and behavioral symptoms (98, 198, 201). HIV encephalitis is considered to be the pathological substrate of HIV associated dementia (252). HIVE is characterized by the presence of microglial nodules, multinucleated giants cells formed by fusion of HIV infected macrophages, and abundant HIV-infected and activated macrophages (39). Macrophage elements (including brain microglia and infiltrating macrophages, hence forth referred to as macrophages) constitute the cell type productively infected with HIV in the brain (255). Macrophages are hypothesized to be central to neurodegeneration as the sources of virus and toxic substances that initiate synaptic damage and neuronal death (128).

The macaque model for HIVE closely resembles the human disease. Like humans, only a percentage (dependent on the species) of macaques infected with Simian Immunodeficiency Virus (SIV) will develop encephalitis that is very similar to HIVE (24, 137). We have previously shown that brain tissue derived from SIVE macaques shows higher peripheral benzodiazepine receptor (PBR) expression, as measured by binding with a PBR specific ligand PK11195. Increased PK11195 binding has been reported in several studies including multiple sclerosis and experimental autoimmune encephalitis (20, 69, 246), stroke (231), brain trauma (204), Rasmussen's encephalitis (18), Herpes encephalitis (41), Alzheimer's disease (41) and Multiple System Atrophy (95). In the normal brain, PBR is expressed on astrocytes and brain macrophages in low levels, and is hypothesized to specifically increase in brain macrophages in response to pathology (17). In this study we examine the relative contributions of astrocytes and

macrophages to increases in PBR in the context of HIV encephalitis. We utilize PK11195 and DAA1106, a newer ligand that binds to PBR with high affinity (47), to show increased ligand binding in HIVE. Using primary human macrophage and astrocytes cultures, we show increased [3H](R)-PK11195 and [3H]-DAA1106 in activated macrophage cultures and HIV-infected macrophage cultures, but not in activated astrocytes cultures or astrocytes cultures exposed to HIV. Finally, we show that increased [3H](R)-PK11195 binding in macrophages is dependent on activation of the PI3K/Akt pathway. Our results suggest that PBR expression is increased specifically in activated and HIV infected macrophages in a PI3K/Akt dependent fashion in HIVE.

3.2.3 Methods

Human postmortem tissue

Postmortem brain tissue was obtained from HIV-infected patient and age matched controls from the University of Pittsburgh brain bank. HIVE was defined on neuropathologic analysis by the presence of microglial nodules; multinucleated giant cell and HIV infected macrophages defined by the staining for the viral protein gp41. Five cases were defined as HIVE and six cases as HIV infected without encephalitis using these criteria. Brain tissue from three non-infected, age-matched controls were included as additional controls. Brain tissue from the fontal cortex was dissected out from each of these cases and used in filtration binding experiments.

Macaque model of HIVE

Archival tissue was obtained from Rhesus macaques that were infected with SIVDeltaB670 that developed encephalitis. Tissue obtained from animals that did not develop encephalitis served as controls. Histopathologic criteria used for HIV infected human tissue were also applied to macaque tissue. Archival frozen brain tissue from the frontal cortex of three SIVE, three SIV infected non encephalitic and two non-infected macaques were dissected out and used for saturation binding experiments and autoradiography.

Tissue culture experiments

Human peripheral blood mononuclear cells (PBMC) were isolated freshly from HIV and Hepatitis B seronegative buffy coats obtained from the blood bank (Central Blood Bank, Pittsburgh, PA), using histopaque (Sigma, St. Louis, MO). PBMC were counted and plated in T-150 flasks (Corning, NY) at a density of 75 x 10^6 per ml. PBMC were grown for 5 days in complete medium consisting of AIM-V medium (Gibco BRL, Grand Island, NY), 10% heat inactivated-fetal calf serum (Gibco BRL, Grand Island, NY) and 1% penicillin-streptomycin (Gibco BRL, Grand Island, NY). Non-adherent cells were washed thoroughly after 5 days and adherent macrophages were cultured for an additional two days in complete medium. Macrophage cultures were activated with either 1μg/ml LPS (Sigma, St. Louis, MO) or 300 units of interferon-γ (Sigma, St. Louis, MO) for 48hrs (29). Primary macrophage cultures were infected with HIV-1 ADAM for 24 hrs following which cells were washed thoroughly. Infected macrophage cultures were harvested at 7, 14 and 21 days post infection. HIV-1 p24 levels using ELISA (Beckman Coulter Inc., Fullerton, CA) were assessed to confirm productive HIV-infection in macrophage and astrocyte (described below) cultures.

Primary human embryonic brain cultures.

Brain tissue was gathered according to the standards of the University of Pittsburgh ethics and biosafety guidelines. Human fetal brain tissue was washed thrice and minced in ice cold DMEM F12 medium (Gibco BRL, Grand Island, NY), incubated in 0.05% trypsin-EDTA (Gibco BRL, Grand Island, NY) for 30 minutes and then triturated with graded pasture pipettes to get tissues into single cell suspension. The cell suspension was then filtered serially through 100 μm, 70 μm and 40 μm microfilters (Fischer scientific) and plated in T-150 tissue culture flasks (Corning, NY) at a density of 7 X 10^6 cells per flask in DMEM with 10 % human serum and 1% penicillin-streptomycin. Shaking the cultures overnight at 200 rpm separated Microglial cells out. Astrocytes were then passaged thrice and purity of cultures was determined to be between 98-99% by staining with GFAP. Mitochondrial extracts were obtained from primary human macrophages and astrocytic cultures utilizing a kit according to guidelines provided by the manufactures (Pierce, Rockford, IL).

Filtration radioligand binding assays

Tissue was weighed and homogenized in ice-cold 50 mM HEPES buffer (pH 7.4). Homogenates were washed four times by centrifugation at 40,000 g for 20 min at 4^0C. Protein values were determined in each sample by the BCA protein assay kit (Pierce, Rockford, IL). [3H]-DAA1106 was custom synthesized and was of specific activity 80 Ci/mmol (American Radiolabeled Chemical, St Lousi, MO). Mitochondrial extracts were incubated with 1nM [3H]-DAA1106 and nonspecific binding was excluded by the inclusion of 1μM DAA1106. Saturation binding experiments were performed by incubating tissue (total protein concentration ranging from 150 to 200 μg) with 0.5-64 nM [3H](R)-PK11195 (sp. Act., 89.9 Ci/mmol; NEN Life Sciences Products, Boston, MA) or 0.2-20 nM [3H]-DAA1106 at 4^0C for 2 hr in a final volume of 250 μl of HEPES. Nonspecific binding was determined by the inclusion of 10 μM PK11195 or 10 μM DAA1106 respectively in saturation binding experiments. The reaction was terminated by the addition of ice-cold buffer in a vacuum cell harvester (Brandel, Gaithersburg, MD). All samples were run in duplicate. Bmax in fmoles per mg protein and kd in nM were determined using PRISM software (Graphpad, San Diego, CA).

Autoradiography

Autoradiography was performed as described earlier (245). Briefly, 15 μm thick frozen sections obtained from the frontal cortex were placed on Superfrost^{Tm} glass slides (Sigma, St Louis, MO) and incubated in ice-cold 50 mM TRIS-HCl (pH 7.4) containing 1 nM [3H](R)-DAA1106 (Sp. Act., 80 Ci/mmol; American Radiolabeled Chemical, St Lousi, MO) for 30 min. Specificity of binding was ensured by the inclusion of 1 μM DAA1106 in parallel sections. The sections were mounted with a layer of autoradiographic LM-1 emulsion (Amersham, UK), following which they were developed after 4 weeks and imaged on the confocal microscope.

Statistical analysis

Data were analyzed using PRISM software (Graphpad, San Diego, CA). Student's *t* tests or one-way ANOVA tests with post-test Bonferroni correction and 95% confidence intervals were used to analyze data.

3.2.4 Results

[3H](R)-PK11195 and [3H](R)-DAA1106 binding is higher in HIVE compared to controls

We used saturation filtration binding to compare [3H](R)-PK11195 and [3H]-DAA1106 specific binding, reflective of PBR expression, in HIVE with age-matched controls. Brain tissue from the frontal cortex was dissected from five cases of HIVE; six HIV-infected non-encephalitic controls and three age-matched controls. HIVE in postmortem tissue was defined by the presence of microglial nodules; multinucleated giant cells and HIV infected macrophages defined by the staining for the viral protein gp41. Tissue was homogenized and incubated with 0.5-64 nM [3H](R)-PK11195 or 0.2-20 nM [3H]-DAA1106 to obtain total binding values. Nonspecific binding was determined in parallel by including 10μM PK11195 or 10μM DAA1106 respectively. Specific binding at each given concentration of [3H]-ligand was defined as the difference between total binding and nonspecific binding. Bmax and kd values reflective of the total number of binding sites per mg protein and binding affinity of ligand to PBR respectively were determined using PRISM software.

Bmax was significantly higher in the frontal cortex of HIVE brain tissue compared to HIV-infected non-encephalitic and non-infected controls assessed with both [3H](R)-PK11195 ($p=0.0006$) and [3H]-DAA1106 ($p=0.0003$) **(Figure 9, A and C)**. The affinity of either ligand to PBR reflected by the kd did not differ between HIVE and controls **(Figure 9, B and D).**

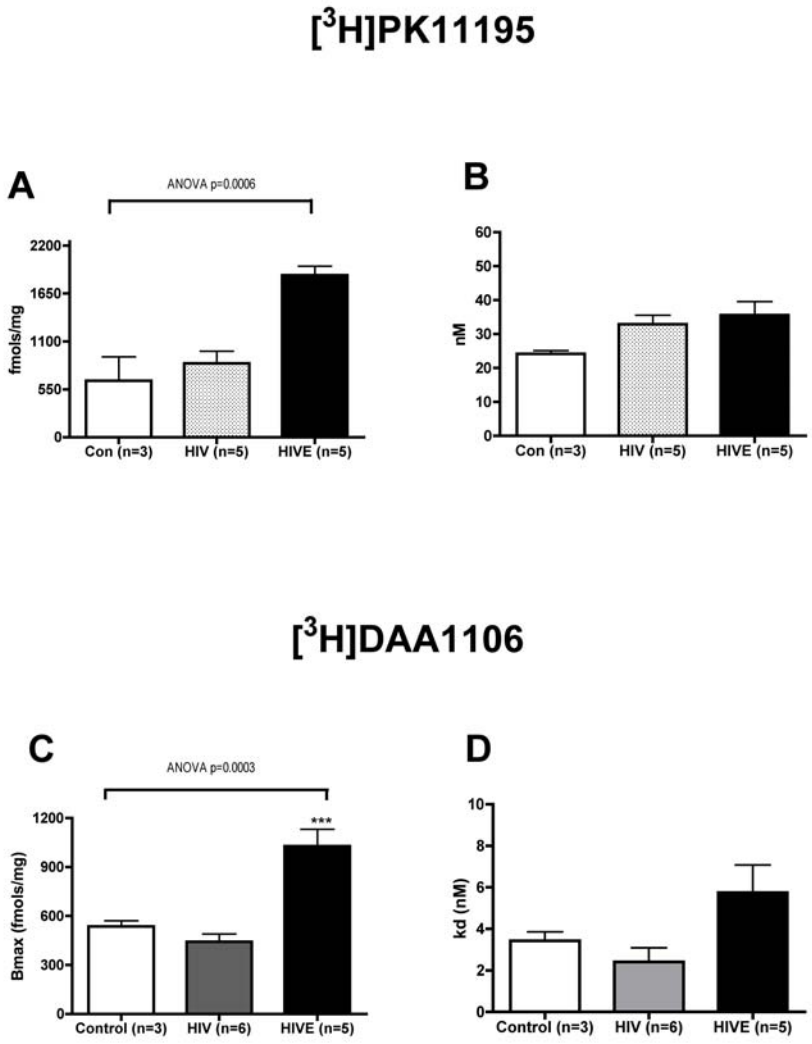

Figure 9 HIVE brain tissue shows increased [3H](R)-PK11195 and [3H]-DAA106 binding compared to controls

Filtration binding was assessed in frontal cortical brain tissue obtained from 5 HIVE, 6 HIV infected non-encephalitic (HIV) and 3 age matched controls. The Bmax, reflective of the total number of binding sites is shown in the left panel (A & C) and the kd reflective of the binding affinity of the ligand to PBR is shown in the right panel (B & D). Data analyzed using one-sided ANOVA.

(**A, B**) Bmax with [3H](R)-PK11195 was significantly higher in HIVE compared to controls (A), p=0.0006. The kd was not significantly different between HIVE and controls (B), p=0.2293.

(**C, D**) Bmax with [3H]-DAA1106 was significantly higher in HIVE compared to controls (C), p=0.0003. The kd was not significantly different between HIVE and controls, (D) p=0.0712.

[3H](R)-PK11195 and [3H]-DAA1106 binding is higher in activated macrophages compared to controls.

Since PBR is expressed on both astrocytes and brain macrophages (20, 45), we wanted to compare the relative changes in PBR binding in both cell types on activation. Primary human macrophages and primary human embryonic astrocytes were cultured for 5 days and 14 days respectively. Macrophage cultures were activated with 1 μg/ml LPS or 300 IU/ml interferon-γ for 48 hrs. TNF-α secretion was assessed using ELISA to confirm activation (data not shown). Activated macrophages also displayed a change in morphology from a more rounded to a spindle like morphology (**Figure 10 B and D**) compared to controls (**Figure 10 A and C**). Primary human astrocytes were activated with dibutyryl cyclic AMP (dCAMP) 100 μM as described in the literature (188). Activation in astrocytes was assessed by changes from a flat morphology (**Figure 10 E and G**) to cells that displayed multiple processes (**Figure 10 F and G**). Astrocytes treated with 1 μg/ml LPS for 48 hrs served as an addition control. Saturation binding experiments were conducted on homogenized cells using [3H]-PK11195. Bmax, reflective of PBR expression, was significantly higher in macrophages activated with either LPS or interferon-γ, compared to non-activated macrophages, dCAMP activated astrocytes, LPS treated astrocytes and control astrocytes ($p<0.0001$) (**Figure 11 A**). Affinity of [3H](R)-PK11195 to PBR reflected by the kd did not significantly change in any of these conditions (**Figure 11 B**).

Since PBR is a mitochondrial receptor, we assessed [3H]-DAA1106 binding in mitochondrial extracts derived from control macrophages, macrophages activated with 1 μg/ml LPS for 48 hrs, control astrocytes and astrocytes activated with 100 μM dCAMP. Mitochondrial extracts were incubated with 1 nM [3H]-DAA1106 and non-specific binding was excluded by the inclusion of 1 μM DAA1106. Mitochondrial extracts derived from LPS activated macrophages showed significantly higher binding compared to macrophage and astrocyte controls ($p=0.0008$) (**Figure 11 C)**

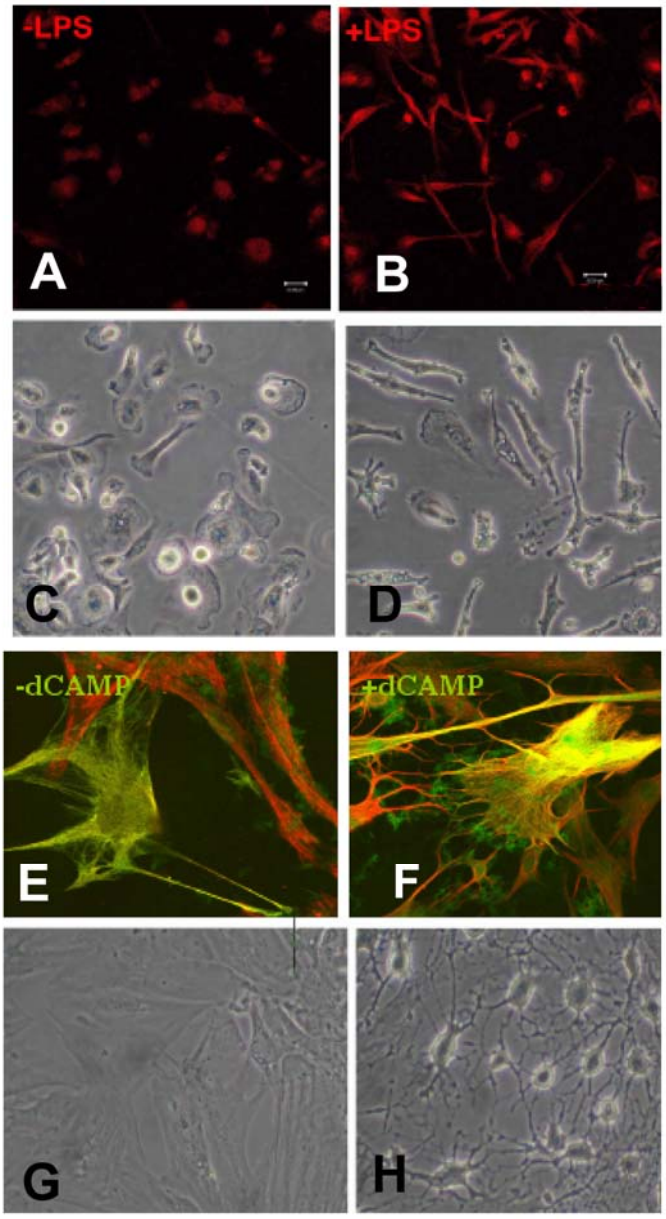

Figure 10 Primary human macrophages and human embryonic astrocytes activated with LPS and dCAMP respectively.

(**A-D**) Primary human macrophages were cultured for 5 days and activated with 1 μg/ml LPS for 48 hrs. (A-B) Macrophages cultures were stained with CD68 (red), (C-D) Phase contrast images of macrophages. On activation with LPS, macrophages show and increase in CD68 staining (B), and changes in morphology (D), compared to non-stimulated cultures (A) and (C).

(**E-H**) Primary human embryonic astrocytes were cultured for 14 days and activated with 100 μM dCAMP for 48 hrs. (E-F) Astrocyte cultures were stained with GFAP (green) and vimentin (red), (C-D) Phase contrast images of astrocytes. On activation with dCAMP, astrocytes show changes in morphology with the appearance of several spindle shaped processes (F & H), compared to non-activated cultures (E & H).

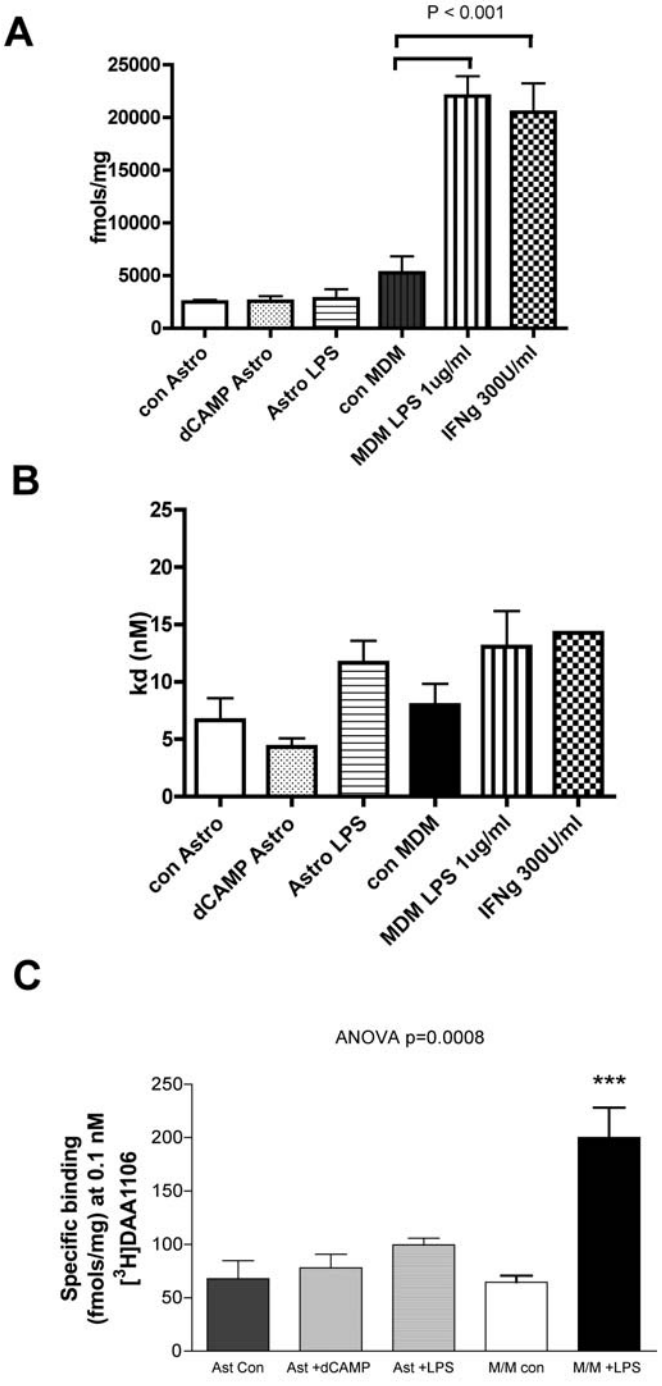

Figure 11 Activated macrophages show higher binding with [3H](R)-PK11195 and [3H]-DAA106 when compared to controls.

(**A, B**) Filtration binding was assessed in primary human macrophages (*denoted by MDM, monocyte derived macrophages*) and primary human astrocyte cultures with [3H](R)-PK11195. Macrophage (MDM) cultures were activated with LPS (1μg/ml) or INF-γ (300U/ml) for 48 hrs. Astrocytes were treated with LPS (1μg/ml) or activated with dCAMP (100 μg/ml) for 48 hrs. The Bmax, reflective of the total number of binding sites is shown in the upper panel and was found to be significantly higher ($p<0.0001$) in macrophages (MDM) activated with either LPS or INF-γ compared to non-activated controls, astrocytes activated with dCAMP, non-activated astrocytes or astrocytes treated with LPS (A). The kd reflective of the binding affinity of the ligand to PBR is shown in the right panel and did not differ in all the conditions ($p=0.3963$) (B). Data analyzed using one-sided ANOVA.

(**C**) [3H]-DAA1106 binding using 1nM of the ligand (non-specific binding was excluded by 1μM DAA1106) was determined in mitochondrial preparations from the above conditions. [3H]-DAA1106 binding was significantly higher in mitochondrial preparations obtained from macrophages (MDM) activated with LPS compared to controls, $p=0.0008$.

[3H](R)-DAA1106 binding in SIV encephalitic brain tissue localizes to macrophages

Our in vitro data suggesting increases in PBR-ligand binding in macrophages were confirmed in brain tissue obtained from SIVE macaques. We compared [3H]-DAA11106 binding in frontal cortical tissue obtained from SIVE (n=3) with SIV infected no-encephalitic tissue (n=3) and non-infected macaques (n=2). [3H]-DAA1106 binding was significantly higher in SIVE compared to controls (**Figure 12 A)**. For autoradiography, frozen brain sections obtained from the frontal cortex were incubated with 1 nM [3H]-DAA11106 with non-specific binding determined by the inclusion of 1 μM DAA1106. SIVE brain tissue showed higher [3H]-DAA1106 binding compared to the non-encephalitic control brain tissue (**Figure 12 D-C**). [3H](R)-PK11195 binding in encephalitic tissue appeared more intense and corresponded to the distribution of microglial nodules (**Figure 12 D**) in contrast to the diffuse, less intense binding seen in SIV infected, non-encephalitic tissue in all observed fields (**Figure 12 C**). Autoradiography with [3H]-DAA1106 combined with immunohistochemistry on frozen brain sections obtained from the frontal cortex of SIVE macaques showed [3H]-DAA1106 binding overlapping with regions rich in activated macrophages and microglial

nodules (stained with CD68) (**Figure 13 B, D & E**) [3H]-DAA1106 binding did not overlap with GFAP labeled astrocytes in encephalitic brain tissue (**Figure 13 A, D & E**)

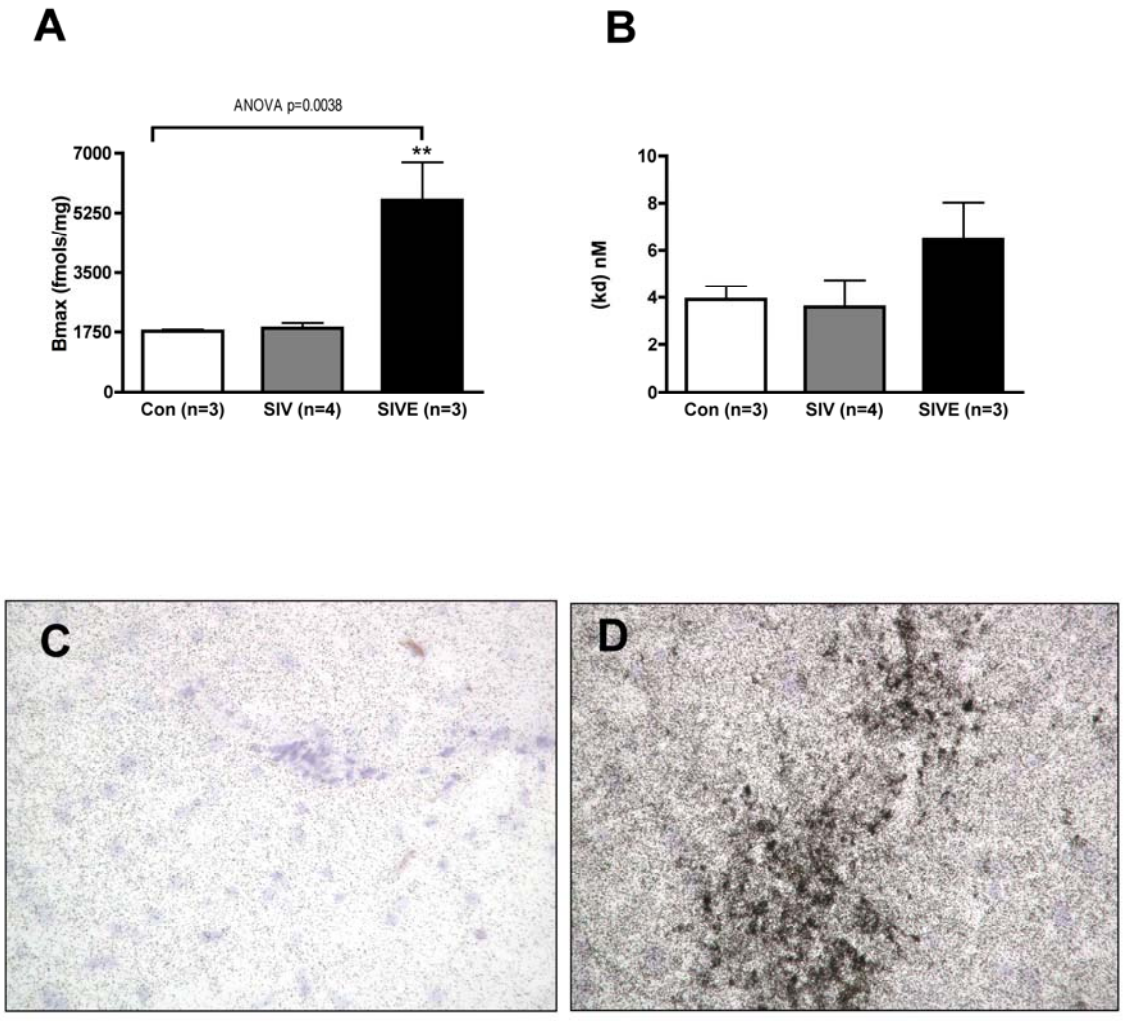

Figure 12 [3H]-DAA1106 binding is significantly higher in SIVE compared to controls.

(**A, B**) Filtration binding with [3H]-DAA1106 was assessed in frontal cortical brain tissue obtained from 3 SIVE, 4 SIV infected non-encephalitic (SIV) and 3 non-infected controls. The Bmax, reflective of the total number of binding sites was significantly higher in SIVE compared to controls (p=0.0038)

(A). The kd reflective of the binding affinity of the ligand to PBR did not significantly differ amongst the three conditions (p=0.2492). Data analyzed using one-sided ANOVA.

(**C, D**) [3H]-DAA1106 autoradiograms (black grains) of sections from frontal cortex show higher specific binding in SIVE (C) compared to SIV infected, non-encephalitic macaques (D).

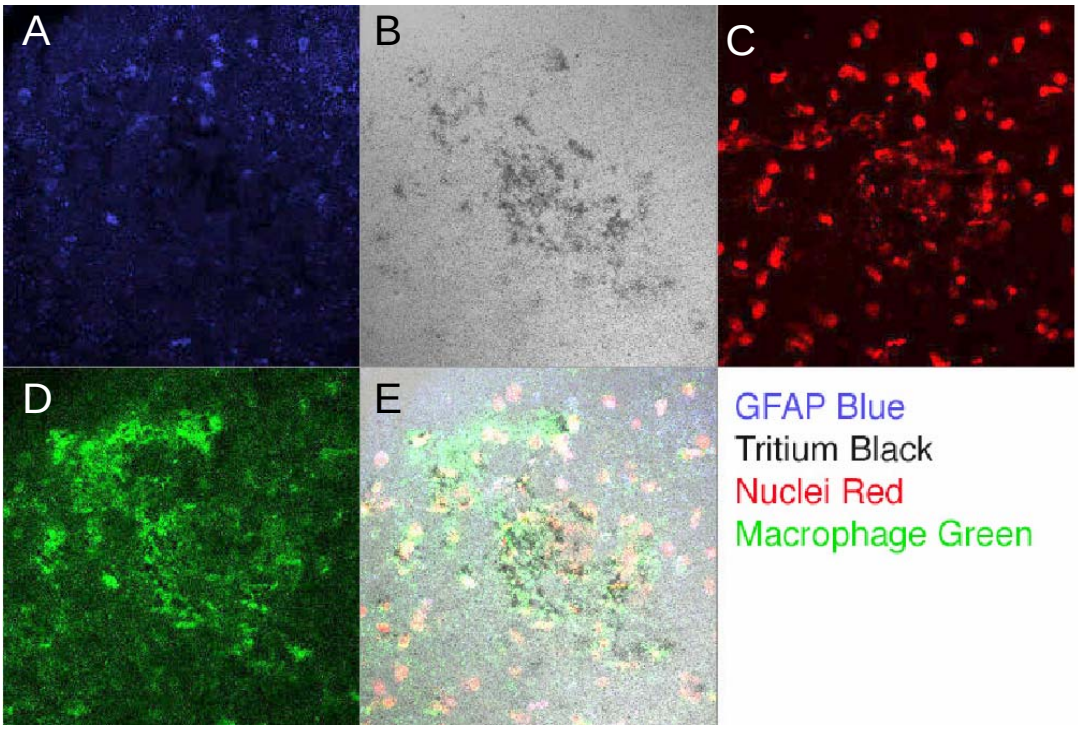

Figure 13 [3H]-DAA1106 binding corresponds to activated macrophages, but not astrocytes

(A-E) Sections obtained from the frontal cortex were stained with GFAP (Blue, A), processed for autoradiography with [3H]-DAA1106 (Black grains, B) and immunostained to label either nuclei with DAPI (Red, C) or activated macrophages with CD68 (Green C). Panel E shows a merged image of all the markers. [3H]-DAA1106 specific binding overlaps with CD68 and not with GFAP immunostaining.

[3H](R)-PK11195 binding is higher in HIV-1 infected macrophages compared to controls.

Primary macrophage cultures were infected with HIV-1 ADAM for 7, 14 and 21 days. Supernatants were collected at each of these time points and HIV-1 p24 levels were determined to assess productive HIV infection (data not shown). Supernatants derived

from macrophage cultures at 14 days post infection were used to treat primary astrocyte cultures. Saturation binding experiments with [3H](R)-PK11195 were performed on macrophage homogenates and at each of these post-infection time points and astrocyte cultures treated with macrophage supernatants. We found significant increases in Bmax, reflective of PBR expression, in HIV-1 ADAM infected macrophages at 7, 14 and 21 days post infection compared to non-infected controls and astrocytes treated with HIV-infected macrophage supernatants (**Figure 14 A**). We also found that the kd was significantly higher in HIV-1 infected macrophages at all time points post infection (**Figure 14 B**).

Increased [3H](R)-PK11195 binding in LPS activated macrophages is mediated by PI3K

We sought to determine the cellular signaling pathways that mediate increased [3H](R)-PK11195 binding in macrophages. Macrophages were pretreated with either the PI3-kinase inhibitor LY294002 (10μM) or the MAP-kinase inhibitor U0126 (10μM) for two hours after which they were activated with LPS for 48 hrs. Inhibition of PI3-kinase but not MAP-kinase reversed LPS induced increase in [3H](R)-PK11195 Bmax (**Figure 15 A**). The kd remained unchanged with either treatment (**Figure 15 B**).

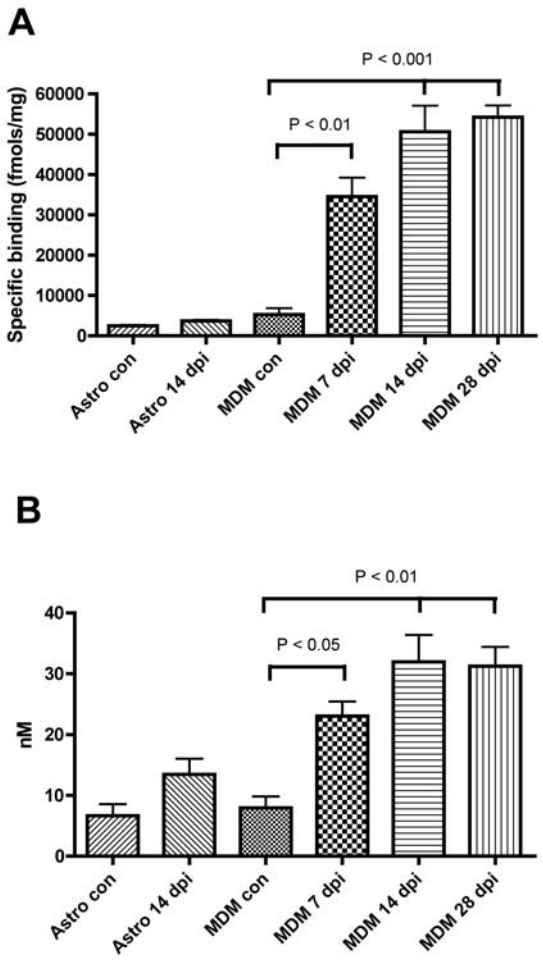

Figure 14 [3H](R)-PK11195 binding is increased in HIV infected macrophages.

Filtration binding was assessed in primary human macrophages (*denoted by MDM, monocyte derived macrophages*) and primary human astrocyte cultures with [3H](R)-PK11195. Macrophage (MDM) cultures were infected with HIV-1 ADAM for 7, 14 or 28 days. Astrocytes were treated with supernatants derived from macrophage cultures infected for 14 days with HIV-1 ADAM.

(**A**) The Bmax, reflective of the total number of binding sites is shown in the upper panel and was found to be significantly higher ($p<0.01$) in macrophages (MDM) infected for 7, 14 and 21 days compared to uninfected controls. Astrocytes treated with supernatants derived from macrophage cultures infected for 14 days with HIV-1 ADAM, did not show any difference from controls ($P=0.2403$). Data analyzed using one-sided ANOVA.

(**B**) The kd, reflective of the binding affinity of the ligand to PBR is shown in the lower panel and was significantly higher ($p<0.05$) in macrophages (MDM) infected for 7, 14 and 21 days compared to uninfected controls. Astrocytes treated with supernatants derived from macrophage cultures infected

for 14 days with HIV-1 ADAM, did not show any difference from controls (P=0.3315). Data analyzed using one-sided ANOVA.

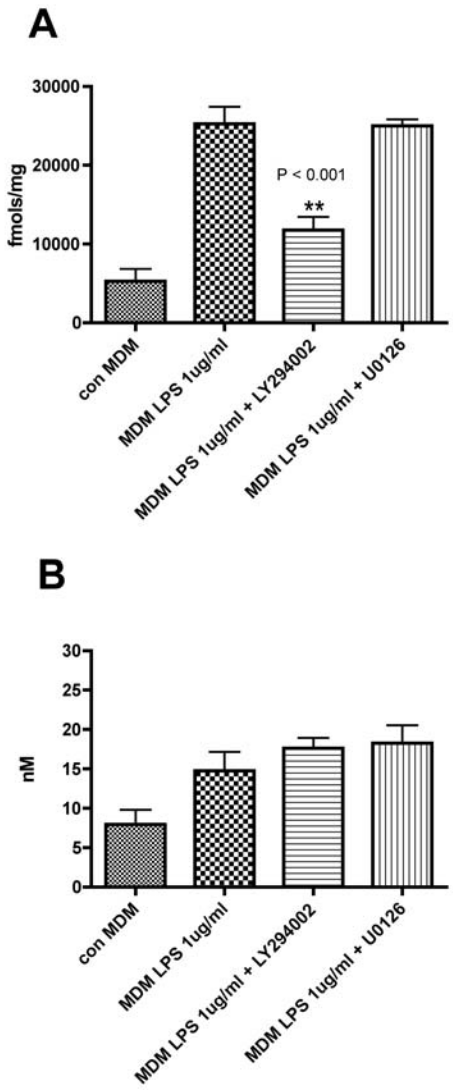

Figure 15 Pharmacologic inhibition on the PI3-Kinase pathway with LY29002 reverses LPS mediated increase in [3H](R)-PK11195 binding in macrophages.

Filtration binding with [3H](R)-PK11195 was assessed in primary human macrophages (MDM) activated with 1μg/ml LPS for 48 hrs pretreated for 3 hrs with 10μM of the PI3-kinase pathway inhibitor LY294002 or 10μM of the MEK-1/2 inhibitor U0126.

(**A**) LPS mediated increase in Bmax (reflective of the total number of binding sites) was reversed by the PI3-kinase pathway inhibitor LY294002 but not the MEK-1/2 inhibitor U0126, ($p<0.001$). Data analyzed using one-sided ANOVA.

(**B**) The kd (reflective of the binding affinity) shown in the lower panel, and was not significantly different in all the conditions (P=0.2284). Data analyzed using one-sided ANOVA.

3.2.5 Discussion

We examined expression of PBR in HIV encephalitis using the PBR-specific ligands [3H](R)-PK11195 and [3H]-DAA1106. HIVE brain tissue showed a significant increase in binding with both ligands compared to HIV infected, non-encephalitic controls and non-infected brain tissue. We also saw an increase in [3H]-DAA1106 binding in SIVE tissue compared to SIV infected, non-encephalitic and non-infected tissue. Increased expression was specific to macrophages as determined by combined immunohistochemistry and autoradiography in SIVE tissue. In tissue culture experiments, we found increased [3H](R)-PK11195 binding in macrophages activated with LPS or INF-γ compared to unactivated macrophages, astrocytes activated with dCAMP and unactivated astrocytes. Similar results were seen in mitochondrial fractions harvested from activated and unactivated macrophages and astrocytes using [3H]-DAA1106. Increase in [3H](R)-PK11195 binding was also seen in macrophages infected with HIV-1 ADAM, peaking at 14 days post infection and reaching a plateau by 21 days post infection. Astrocytes treated with supernatants derived from HIV-1 ADMA infected macrophages did not show a significant increase in [3H](R)-PK11195 binding compared to untreated cultures. Finally, the increase in [3H](R)-PK11195 binding in LPS treated macrophages was reversed using an inhibitor of PI3-kinase, but not of MEK-1/2.

Our results suggest that increased [3H](R)-PK11195 binding, reflective of increased PBR expression, is specific to macrophages in HIV encephalitis due to both activation and HIV infection. This increase in [3H](R)-PK11195 binding was dependent on PI3-kinase signaling in macrophages. These results are in agreement with previously published results suggesting that [3H](R)-PK11195 binding is increased in macrophages in SIVE (151). Direct implications of this study are that PK11195 and DAA1106 may be used to image macrophages in vivo using PET. Our data suggests that DAA1106 may be

a higher affinity ligand compared with PK11195 because of a significantly lower dissociation constant.

The functional significance of increased PBR in activated brain macrophages is not known. It is part of a hetero-oligomeric complex comprised of the voltage-dependent anion channel and an adenine nucleotide carrier forming the mitochondrial permeability transition pore (160). It is thought to be involved in neurosteroid synthesis by serving to transport cholesterol from the outer to the inner mitochondrial membranes (190). As a constituent of the mitochondrial permeability transition pore, it is thought to regulate cell death (160) and mitochondrial respiration (117). PBR overexpression in many cell types has also been shown to protect against various apoptotic insults including the cytopathic effects of sindbis and myxoma viral infections (80, 125). Forced PBR expression in neurons in *vivo* and jurkat cells *in vitro* protects these cells against apoptosis (125, 234). PBR upregulation in testicular leydig cells protects them from cytokine-induced toxicity (20, 237). This is also seen in blood phagocytic cells where PBR protects against oxidant induced cell death (44).

Several proteins involved in apoptosis including Bcl-2, Bcl-X_l and Bax have also been shown to physically interact with the voltage dependent anion channel and the adenine nucleotide carrier (62, 112). PBR can thus influence the cell death processes either by directly affecting the molecular components of the pore or through indirect effects by interfering with interactions of the voltage dependent anion channel and the adenine nucleotide carrier with proapoptotic proteins like Bax (46). These hypotheses draw support from kainic acid-injected rat where hippocampal PBR is increased by 20 fold with no significant increases in either the voltage dependent anion channel or the adenine nucleotide carrier (244). Increases in only the PBR component of the pore might result in altering both the channel properties and altering interactions of other pore proteins with proapoptoic mediators.

Very little is known about how macrophages survive in the brain in HIVE *in vivo*. In the SCID mouse model of HIV encephalitis, macrophages survive for several months in the brain (197). HIV infected macrophages also survive in culture for as long as 60 days (90). Since macrophages mediate the pathology of HIV encephalitis, it is conceivable that a longer life span of macrophages would lead to exacerbation of the

neurodegenerative process seen in HIVE. PBR expression in activated and HIV infected macrophages may prolong their life span by influencing mitochondrial permeability transition and preventing apoptosis of these cells in the CNS.

The biochemical mechanisms by which selective increase in expression or the role for this receptor in activated macrophages in several of these CNS diseases is not understood (91). In pancreatic islet cells, testicular leydig cells, the cytokines TNF-α, IFN-γ and IL-1β caused an increase in mitochondrial PBR mRNA and [3H](R)-PK11195 binding in a transcription dependent manner (20, 237). In the CNS, rats injected with IL-1, or TNF-α, or LPS resulted in increased [3H](R)-PK11195 binding to brain macrophages (31, 35). IL-1 and TNF-α also increase [3H](R)-PK11195 binding in cultured astrocytes (65). Finally, in Experimental Autoimmune Encephalitis, IL-6 and TNF-α expression profiles correlate with increase in spinal cord [3H](R)-PK11195 binding (5). These data suggest that cytokines increase PBR expression in various cell types including macrophages. However, the mechanisms mediating this increase are not known. It has been proposed that cellular upregulation of PBR in these systems may serve as a protective strategy against cytokine toxicity.

HIV infected macrophages are sources of cytokines in the brain. TNF-α can be detected in the CSF (107) and brain tissue (97) of HIV demented patients. In SIVE, TNF-α and IFN-γ are detected in brain tissue (186). These studies are complimented with *in vitro* data showing that cytokines including TNF-α and IL-6 are synthesized by HIV infected macrophages (29, 257). It is possible that PBR expression is increased in brain macrophages in HIVE in response to increased cytokines.

Interestingly, PI3K/Akt activation is an important survival-regulation pathway in brain macrophages (129), peripheral macrophages and other hemopoietic cell (169, 239). Activation of PI3K/Akt protects against toxicity induced by multiple cytokines (100, 169). Further, inhibition of PI3K pathway in peripheral macrophages causes cell death by loss of mitochondrial transmembrane potential by mechanisms not fully understood (144). Our data suggests that PBR is directly regulated by PI3K, and since PBR is a constituent of the permeability transition pore and may play a role in maintaining mitochondrial transmembrane potential, it is possible that PBR is an essential player in regulating macrophage cell survival in the CNS in HIVE.

3.3 PK11195 LABELS BRAIN MACROPHAGES IN ALZHEIMER'S DISEASE

3.3.1 Abstract

Prominent brain macrophage activation is seen around senile plaques and extracellular neurofibrillary tangles in Alzheimer's disease. Although the role of brain macrophage in the pathogenesis of Alzheimer's disease is not clearly established, activation of brain macrophage is associated with amyloid clearance and phagocytosis in Aβ immunization protocols in both animal models and humans. Imaging activated brain macrophage in vivo using positron emission tomography will help define the role of these cells in both Alzheimer's disease progression and therapeutic protocols targeted at modulating neuroinflammation. PK11195 is a ligand specific for the peripheral benzodiazepine receptor abundant on activated brain macrophages and expressed in low levels in the normal brain. We hypothesized that [11C](R)-PK11195 positron emission tomography (PET) could image brain macrophages in vivo in Alzheimer's disease. [3H](R)-PK11195 binding was assessed in postmortem brain tissue obtained from AD cases and age matched controls. [3H](R)-PK11195 binding was significantly higher in the frontal cortex but did not differ in the cerebellum of AD cases compared to controls suggesting that this increase was specific to regions of pathology. Mice expressing the APPSwe/PS1dE9 transgene were then scanned using positron emission tomography using [11C](R)-PK11195. Transgenic mice showed an age-dependent, moderate increase in [11C](R)-PK11195 and [3H](R)-PK11195 binding compared to controls. Histopathologic assessment showed significantly higher levels of brain macrophage activation in Alzheimer's disease compared to Tg mice. Further, significant correlation was observed between [3H](R)-PK11195 binding and activated brain macrophages in Alzheimer's disease but not in Tg mice. The extent of neuroinflammation is significantly lower in these transgenic mice as compared to Alzheimer's disease, which may undermine the utility of these mice in studying the role of neuroinflammation in the pathogenesis and treatment of Alzheimer's disease. However, our results suggest that PK11195 may be useful in labeling brain macrophages in vivo in AD.

3.3.2 Introduction

Alzheimer's disease is the leading cause of dementia characterized by the presence of plaques consisting of Aβ and intraneuronal neurofibrillary tangles (167). Aβ deposition leads to the formation of diffuse plaques that are believed to progress to neuritic plaques consisting of a dense core of Aβ, dystrophic neurites, astrocytes, and activated brain macrophages (161). While the biochemical processes related to Aβ processing have been studied extensively, the role of activated brain macrophages in the pathogenesis of AD is not well understood.

In AD and several other neurological disorders, activation of brain macrophages is thought to perpetuate the degenerative process. On activation, brain macrophage secrete substances such as TNFα and interleukins, free radicals generated by activation of NADPH oxidase, reactive nitrogen intermediates, and eicosanoids which are thought to trigger various cellular processes including cell death cascades in neurons (30, 225, 236).

On the other hand, several studies support the idea that activated brain macrophages may play a beneficial role in AD by promoting phagocytosis (150, 224). Further, brain macrophages may play a role in therapeutic strategies such as immunization. Immunization with Aβ is one of the most promising forms of AD therapeutics. Both active and passive immunizations in animal models have proved promising in clearing Aβ loads from the brain and improving behavioral/memory tests (22, 120, 171, 218). Several mechanisms have been proposed for Aβ clearance with immunization. However, the association of activated brain macrophages with the clearance of Aβ and "collapsed" plaques in both animal models and human-immunized subjects raises the possibility that the efficacy of immunizations may be related to the extent of activation of brain macrophages (22, 85, 179, 218).

Were it possible to image brain macrophages in vivo, then a better understanding of the role played by brain macrophages in Alzheimer's disease and therapies targeted at Aβ clearance may be obtained. We investigated the feasibility of imaging activated brain

macrophages using Positron Emission Tomography (PET) by taking advantage of elevated levels of peripheral benzodiazepine receptor expression (PBR) on brain macrophages. *We tested the hypothesis that PK11195, a selective ligand to PBR, will specifically label activated brain macrophage in AD postmortem tissue and in a mouse model of AD in vivo using PET.*

PK11195 is a lipid soluble isoquinoline carboxamide which crosses the blood brain barrier rapidly and has been extensively characterized (42). [11C](R)-PK11195 has been used to label activated brain macrophages in patients with multiple sclerosis (20, 69) Rasmussen's encephalitis (18), stroke (206), Herpes encephalitis (43), gliomas (191), Multiple System Atrophy (95) and AD (41). Studies in AD patients showed high [11C](R)-PK11195 binding in the entorhinal, temporoparietal and cingulate cortex, which are brain regions that show the highest degree of AD pathology (41). However, the relationship between PK11195 binding and the distribution of neuropathology was not assessed in this study (41). We used postmortem tissue from AD cases and a mouse model of AD to correlate the extent and distribution of neuropathology with the PK11195 binding. We also sought to determine if [11C](R)-PK11195 could image activated brain macrophages in the APP/PS1 transgenic mouse model of AD in vivo. We show that PK11195 binding is higher in AD tissue and significantly correlates with the distribution of activated brain macrophages in AD. Further, the extent of activated brain macrophages is significantly lower in APP/PS1 transgenic mice compared to AD tissue corresponding to moderate increases in PK11195 binding in vivo.

3.3.3 Methods

Animals

All animals were housed and maintained according to standards of the Association for Assessment and Accreditation of Laboratory Animal Care, and experiments were approved by the University of Pittsburgh Institutional Animal Care and Use Committee. APPSwe/PSEN1-DeltaE9 transgenic (Tg, n=9) heterozygote and control wild type (n=6) animals on a B6C3 background between the

ages of 7-9 months were obtained from *The Jackson Laboratory* (Maine, USA). 4/9 Tg and 1/6 wild type mice were part of a failed immunization experiment. In this study APPSwe/PS1dE9 and wild type mice beginning at the age of nine months mice were immunized i.p. with 100μg of Aβ42 emulsified in complete Freund's adjuvant, followed by a boost at 2 weeks with incomplete Freund's adjuvant and monthly thereafter for the next 3 immunizations according to established protocols (218). We assayed for the production of antibodies against Aβ42 at 1, 2, 3 and 4 months after immunization. Levels of antibody production were very low and did not differ in animals that were immunized with Aβ42 versus animals that were sham immunized (data not shown). Further, histopathologic assessment of immunized versus sham immunized or non-immunized animals did not show any differences in Aβ plaque deposition, brain macrophage activation, or the extent of astrocytosis (data not shown). Since immunization failed in these animals, PET data derived from these animals were grouped along with data obtained from their non-immunized counterparts.

PET imaging

High specific activity [11C](R)-PK11195 ([N-methyl-^{11}C]-PK11195) was produced at the UPMC PET Facility using methods similar to those previously described (245). Chemical and radiochemical purities were ≥95% with specific activities ≥2.0 Ci/μmol at the end of a 40 min synthesis. Typical end of synthesis yields of high purity [11C](R)-PK11195 was in the range of 40-100 mCi.

APPSwe/PS1dE9 (Tg) (n=9) and control wild type (n=6) mice were imaged using microPET with [11C](R)-PK11195 between ages 14-20 months. Data were reconstructed using the 3D Ordered Subsets Expectation Maximum (OSEM) algorithm for maximal image quality and image resolution. Regional brain radioactivity concentration were summed over the scan frames at various time points was normalized to both the injected dose of [11C](R)-PK11195 and the body mass of the animal (%ID/Kg*g) to represent a semi-quantitative measure of [11C](R)-PK11195 binding. Regions-of-interest (ROI) were defined on summed PET images and applied to the dynamic PET images to generate time-activity curves for both transgenic and control animals. Due to the spatial resolution limitations of microPET, it is not practical to define ROIs on small structures such as the

hippocampus within the mouse brain. Hence ROI parameters were defined in regions approximating the frontal cortex of the mouse brain and applied to all Tg and control animals.

Human Tissue

Brain tissue from the frontal cortex and the cerebellum of six AD postmortem cases and six age-matched controls were derived from the University of Pittsburgh Alzheimer's disease research center brain bank.

Tissue processing

After PET scans both transgenic and control animals were sacrificed to compare time activity curves for [11C](R)-PK11195 with the extent of activated brain macrophages, astrocytes and amyloid burden as determined by histopathology. After PET imaging, the brain was removed and the left hemisphere was fixed while the right hemisphere was frozen. Histopathology including amyloid burden and the extent of astrocytosis and brain macrophage activation was assessed using semi-quantitative laser confocal microscopy in the left hemisphere as described below. The right hemisphere was used to determine [3H](R)-PK11195 binding in six (3 Tg and 3 control) animals.

Filtration radioligand binding assays

Brain tissue from the frontal cortex and the cerebellum from AD cases and age-matched controls, and from the frontal cortex of 3 Tg and 3 control animals were dissected, weighed and homogenized in ice-cold 50 mM HEPES buffer (pH 7.4). Homogenates were washed four times by centrifugation at 40,000 g for 20 min at 4^0C. Saturation binding experiments were performed by incubating tissue (total protein concentration ranging from 150 to 200 μg determined using the BCA protein assay kit; Pierce, Rockford, IL) with 0.5-64 nM [3H](R)-PK11195 (sp. Act., 89.9 Ci/mmol; NEN Life Sciences Products, Boston, MA) at 4^0C for 2 hr in a final volume of 250 μl of HEPES. Nonspecific binding was determined by the inclusion of 10 μM PK11195. The reaction was terminated by the addition of ice-cold buffer in a vacuum cell harvester (Brandel, Gaithersburg, MD). All samples were run in duplicate. Bmax in fmoles per mg protein and kd in nM were determined using PRISM software (Graphpad, San Diego, CA).

Immunohistochemical labeling and confocal microscopic quantification

Immunostaining and laser confocal microscopic quantification was performed as described before (32, 126). Paraffin embedded sections obtained from transgenic mice and controls (whole brain sagital sections) or AD postmortem tissue and age-matched controls (sections from the frontal cortex) were stained with antibodies to GFAP (mouse monoclonal, DAKO, Carpinteria, CA) or Aβ (mouse monoclonal, DAKO, Carpinteria, CA) used at concentrations 1:1000**,** and 1:100 respectively. Brain macrophages were stained with F/4 80 (mouse monoclonal, DAKO) at a concentration of 1:1000 in mouse brain tissue or with CD68 (mouse monoclonal, DAKO) at a concentration of 1:100 in human tissue. Sections were then incubated with Cy5-conjugated goat anti-mouse or Cy3-conjugated anti-rabbit IgG at a concentration of 1:200 (Jackson Immunoresearch Laboratories Inc., West Grove, PA). The frontal cortex was identified using a dissection microscope and marked on the slides. Immunostained sections were scanned and quantified on a laser confocal microscope (LSM 150, Zeiss, Heidelberg, Germany). This scope is equipped with an argon laser with 458 nm, 477 nm, 488 nm and 514 nm primary emission lines. Each section was scanned along the *z*-axis to define the middle optical plane used in quantification (262,144 pixels/plane; 1 pixel= 0.25 μm^2). Image analysis was performed on a Silicon Graphics computer (Windows NT 4.0 operating system, Microsoft, Redmond, Washington) using the LSM software (version 3.0, Zeiss). Scanning parameters such as laser power aperture, gain, and photomultiplier tube settings were kept constant for each wavelength.

In each region, an individual blinded to the experimental design imaged 3 areas (40X) encompassing 106,100 μm^2. For each cell phenotype scanned, contribution to signal intensity from autofluorescence was minimized using a threshold that was kept constant. In each area the average pixel fluorescence along with the pixel counts for a given cell phenotype marker that exceeded the threshold were enumerated. The average pixel fluorescence was multiplied by the total number of pixels to measure the total florescence for that cell phenotype marker in that area. The total fluorescence values determined from the 3 scanned areas in one brain region were averaged to represent a measure of the cell phenotype in that brain region.

Statistical analysis

Data were analyzed using PRISM software (Graphpad, San Diego, CA). Student's *t* tests or one-way ANOVA tests with post-test Bonferroni correction and 95% confidence intervals were used to analyze data. Correlations using 95% confidence intervals were performed to quantify the relationship between [11C](R)-PK11195 binding and age of Tg or control mice. Results from correlation analyses are represented by *r,* the Pearson's coefficient.

3.3.4 Results

[3H](R)-PK11195 binding is higher in AD frontal cortex

We used saturation filtration binding to compare [3H](R)-PK11195 specific binding in AD with age-matched controls. Brain tissue from the frontal cortex and the cerebellum were dissected from five AD cases and five age matched controls. Tissue was weighed, homogenized and protein values were determined using the BCA protein assay kit (Pierce, Rockford, IL). Homogenized tissue was incubated with 0.5-64 nM [3H](R)-PK11195 to obtain total binding values. Nonspecific binding was determined in parallel by including 10μM PK11195. Specific binding at each given concentration of [3H](R)-PK11195 was defined as the difference between total binding and nonspecific binding. Bmax and kd values reflective of the total number of binding sites per mg protein and binding affinity of [3H](R)-PK11195 to PBR respectively were determined using PRISM software.

Bmax was significantly higher in the frontal cortex of AD brain tissue but did differ in the cerebellum (**Figure 16 A and B,** p=0.0002). This suggests that the increase in Bmax is specific to regions with pathology, as the cerebellum is not usually affected in AD until end stages of the disease (122). The affinity of [3H](R)-PK11195 to PBR reflected by the kd did not differ between AD and control brain tissue in either brain region (**Figure 16 C**).

[11C](R)-PK11195 PET imaging in APPSwe/PSEN1 (DeltaE9) transgenic mice

PET imaging using [11C](R)-PK11195 was assessed in 9 APPSwe/PSEN1-DeltaE9 transgenic mice (Tg) and 6 controls between the ages of 13 to 20 months. These mice show accelerated plaque deposition beginning at the age of 6 months (34). Both Tg and wild type control animals were injected i.v. with [11C](R)-PK11195. [11C](R)-PK11195 binding was followed over time (in minutes, X axis) and represented as radioactivity concentrations summed over the scan frames and normalized to both the injected dose of [11C](R)-PK11195 and the body mass of the animal (%ID/g*kg, y-axis). Tg animals showed an age dependent increase in retention of [11C](R)-PK11195 in the brain compared to controls in that, only Tg animals between the ages of 17-20 months showed increases in [11C](R)-PK11195 binding compared to controls (p=0.001) (**Figure 17**). This is consistent with the age-dependent progression of pathology in APP/PS1 and other Tg mice with age (34, 130).

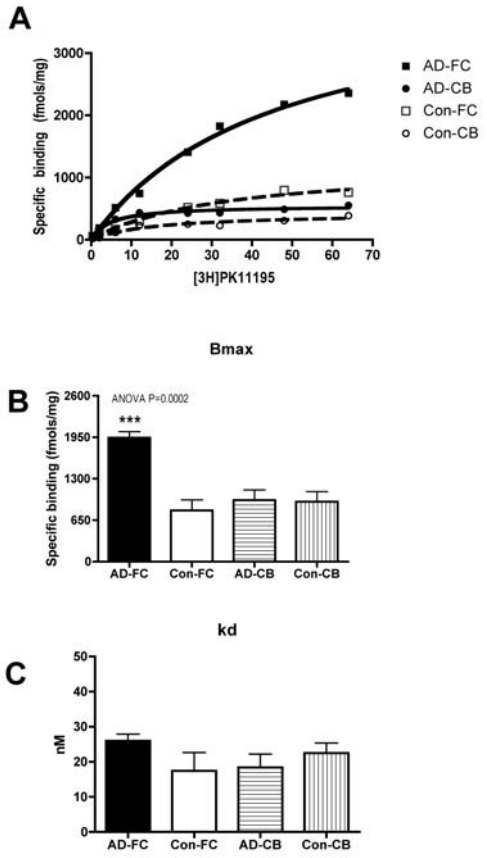

Figure 16 [3H](R)-PK11195 is higher in the AD frontal cortex

Filtration binding with [3H](R)-PK11195 was assessed in the frontal cortex (**FC**), cerebellum (**CB**) of 5 Alzheimer's disease (**AD**) and 5 age-matched controls (**Con**). Data was analyzed using one-way ANOVA with 95% confidence intervals.

(**A**) Shows representative curves from filtration [3H](R)-PK11195 binding experiments with brain tissue obtained from the frontal cortex (FC) and the cerebellum (CB) of AD and control cases. Frontal cortex (FC) brain tissue from AD showed significantly higher specific binding (per mg protein) than brain tissue obtained the cerebellum of AD cases, frontal cortical and cerebellar brain tissue obtained from controls.

(**B**) Bmax (reflective of the total number of binding sites) with [3H](R)-PK11195 was significantly higher in AD frontal cortical tissue compared with AD cerebellar tissue, frontal cortical and cerebellar tissue obtained from controls. (p=0.0002).

(**C**) The kd (reflective of the binding affinity) was not significantly different in all the conditions (P=0.3187).

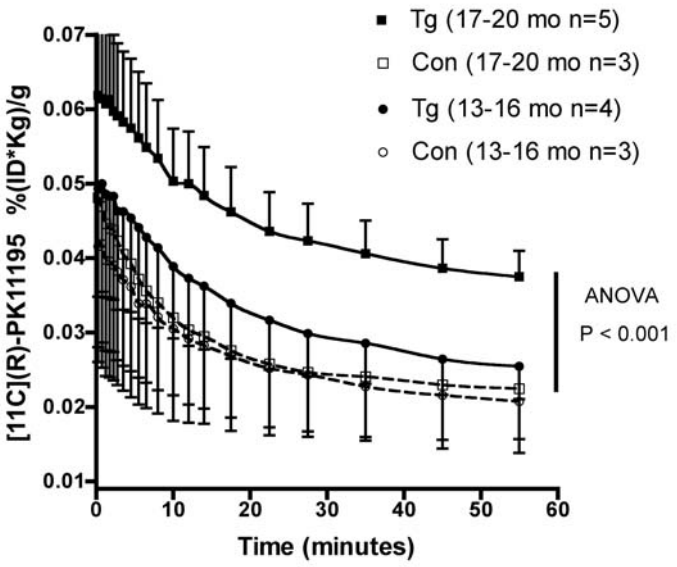

Figure 17 PET imaging with [11C](R)-PK11195 shows an age-dependent increase in APP/PS1 (Tg) mice, but not controls.

Time Activity curve of [11C](R)-PK11195 specific binding in APP/PS1 (**Tg**) and control (**Con**) represented as radioactivity concentrations summed over the scan frames and normalized to both the injected dose of [11C](R)-PK11195 and the body mass of the animal (%ID/g*kg, Y-axis) and is plotted against time in minutes (X-axis). Tg and control animals were divided into the age groups of 13-16 and 17-20 months (n shown in brackets). [11C](R)-PK11195 binding was not different between control and Tg mice in the 13-16 month age group. [11C](R)-PK11195 binding was higher in Tg mice compared to controls in the 17-20 month age group (p=0.001). Data was analyzed using one-way ANOVA with 95% confidence intervals.

[3H](R)-PK11195 binding in APPSwe/PSEN1 (DeltaE9) transgenic mice

We used saturation filtration binding to compare [3H](R)-PK11195 specific binding in TG with controls. Brain tissue from the frontal cortex was dissected from 3 Tg and 3 age wild type controls based on tissue availability. The ages of the Tg and control mice were 9, 11 and 19 months. [3H](R)-PK11195 and [11C](R)-PK11195 binding in Tg mice showed similar trends. Overall, the Bmax was moderately increased in the frontal cortex, but not significantly different in Tg mice compared to controls (**Figure 18 A & B**). However, the increase in [3H](R)-PK11195 binding was age dependent with 45%, 23% and 13% increases from controls in the 19, 11 and 9 month old Tg mice. The affinity of [3H](R)-PK11195 to PBR reflected by the kd did not differ between Tg and control brain tissue (**Figure 18 C**).

The extent of neuroinflammation is significantly higher in AD compared to Tg mice

After PET imaging, the animals were sacrificed and histopathology including amyloid burden, abundance of astrocyte activation and the extent of macrophage activation was assessed and measured using semi-quantitative laser confocal microscopy. Astrocytes, amyloid deposits and activated brain macrophages were immunostained for GFAP, Aβ and F4/80 respectively, and quantified in the frontal cortex of Tg and control brain tissue using laser confocal microscopy by an individual blinded to the experimental design. In Tg mice, GFAP and F4/80 staining was quantified in regions containing plaques as well as regions devoid of plaques. GFAP staining was significantly increased from controls in Tg mice in regions containing plaques, but did not differ from controls in regions devoid of plaques (**Figure 19 D-F and Figure 20 D**). Surprisingly, F4/80 staining for brain macrophages did not differ between Tg and controls in regions with or without plaque deposition (**Figure 19 D-F and Figure 20 C**).

Similarly, the abundance of GFAP staining, brain macrophage activation (as assessed by CD68 staining) and amyloid burden (by staining for Aβ) was assessed in the frontal cortex of AD postmortem tissue and age-matched controls. In contrast to the Tg mice, activated brain macrophages were significantly increased in AD in areas

surrounding plaques compared to areas with no plaques and age-matched controls (**Figure 19 A-C and Figure 20 A)**. GFAP staining was also significantly higher in regions with plaques compared to plaque free areas and control brain tissue (**Figure 19 A-C and Figure 20 B)**.

Increased PK11195 binding correlates with brain macrophages in AD postmortem tissue but not in Tg mice

We then determined the relationship between PK11195 binding and the abundance of activated brain macrophages and astrocytes. In Tg brain tissue, [11C](R)-PK11195 binding correlated poorly with the distribution of both brain macrophages and astrocytes, corresponding to moderate increases in PK11195 binding in these animals (**Table 4**). In contrast, [3H](R)-PK11195 binding correlated significantly with the abundance of brain macrophages and to a lesser extent the distribution of astrocytes in the frontal cortex of AD postmortem tissue (**Table 4**).

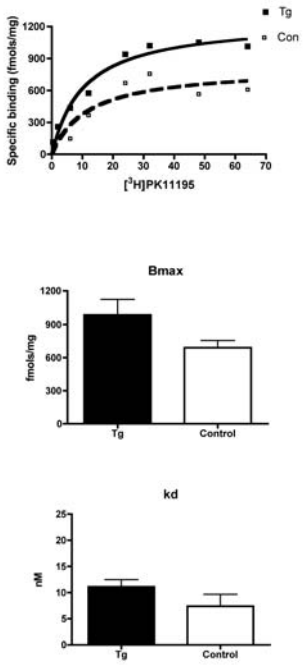

Figure 18 [3H](R)-PK11195 binding in APP/PS1 (Tg) mice.

Filtration binding with [3H](R)-PK11195 was assessed in the frontal cortex of 3 APP/PS1 (Tg) mice and 3age-matched controls (Con) aged 19, 11 and 9 months depending on tissue availability.

(**A**) Shows representative curves from filtration [3H](R)-PK11195 binding experiments in Tg and control cases. Brain tissue obtained from the frontal cortex of Tg showed moderately higher specific binding (per mg protein) than controls.

(**B**) Bmax (reflective of the total number of binding sites) with [3H](R)-PK11195 was higher, but not significantly different (p=0.1265) in Tg frontal cortical tissue compared with controls. However, the increase in [3H](R)-PK11195 binding was age dependent with 45%, 23% and 13% increases from controls in the 19, 11 and 9 month old Tg mice. Data analyzed using student's *t* test.

(**C**) The kd (reflective of the binding affinity) was not significantly different in all the conditions (P=0.2355). Data analyzed using student's *t* test.

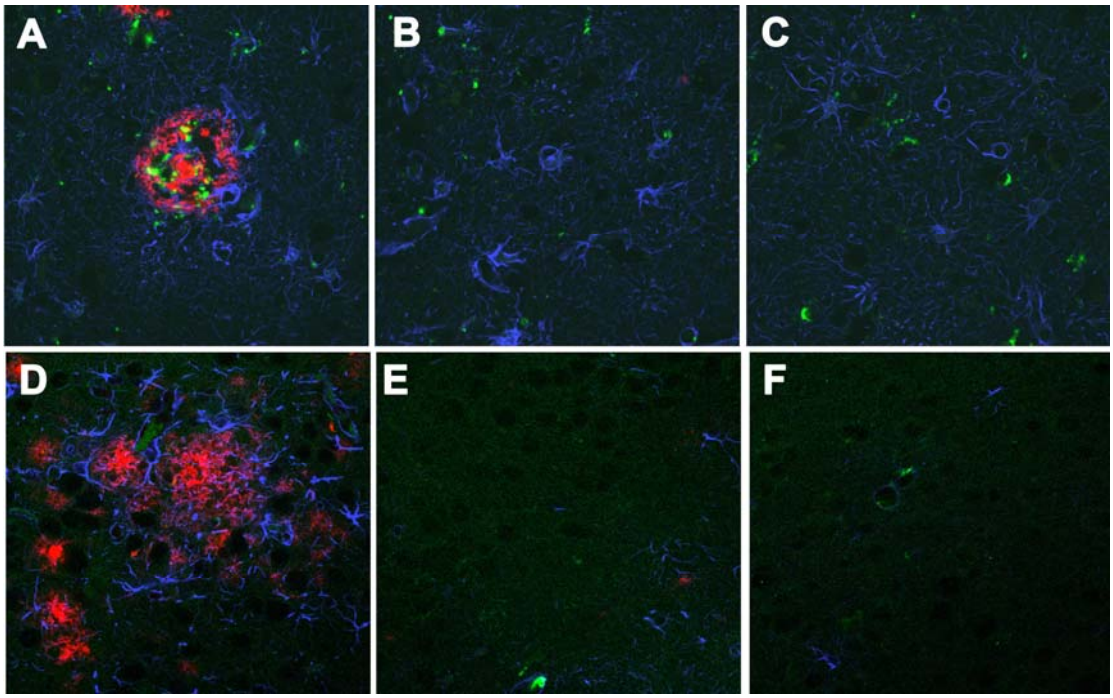

Figure 19 Immunohistochemical evaluation of neuroinflammation in AD and Tg mice

(**A-C**) Frontal tissue from AD and age-matched controls were stained for Aβ (red) brain macrophages (CD68, green) and astrocytes (GFAP, blue). In AD tissue, regions containing plaques (**A**) and plaque free areas (**B**) were compared with age matched controls (**C**).

(**D-F**) Frontal tissue from APP/PS1 (Tg) and control, wild type mice were stained for Aβ (red) brain macrophages (F 4/80, green) and astrocytes (GFAP, blue). In Tg tissue, regions containing plaques (**D**) and plaque free areas (**E**) were compared with age matched controls (**F**).

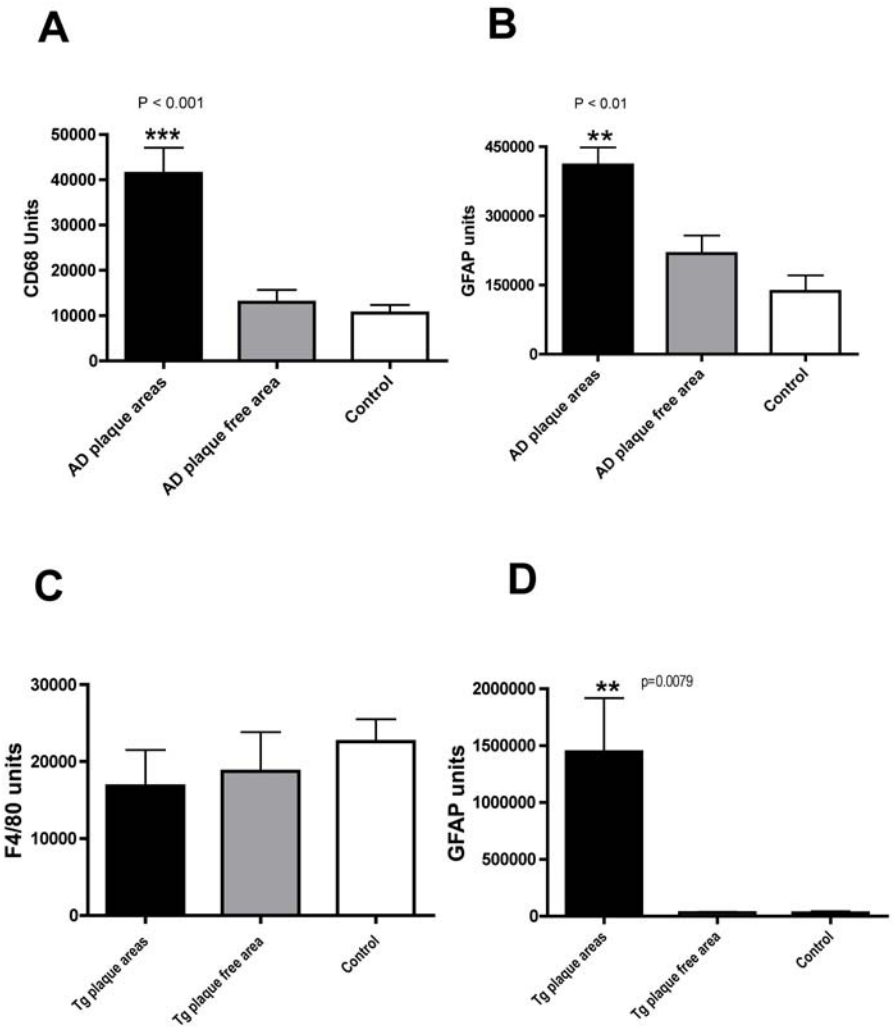

Figure 20 The extent of neuroinflammation is higher in AD in comparison to Tg brain tissue

(**A-B**) Frontal tissue from AD and age-matched controls were stained and quantified for brain macrophages (CD68) and astrocytes (GFAP). In AD tissue, regions containing plaques had significantly higher brain macrophages (**A**) and astrocytes (**B**) than regions without plaques and age matched controls.

(**C-D**) Frontal tissue from APP/PS1 Tg and wild type controls were stained and quantified for brain macrophages (F4/80) and astrocytes (GFAP). In Tg brain tissue, regions containing plaques had significantly higher astrocytes (**D**) but not macrophages (**C**) than regions without plaques and age matched controls.

Table 4 [3H](R)-PK11195 binding correlates best with brain macrophages in AD

Variable	Pearson's coefficient (r) with [3H](R)-PK11195 binding in AD post mortem tissue.	Pearson's coefficient (r) with [11C](R)-PK11195 binding in APP/PS1 in vivo.
	r value	r value
Astrocytes (GFAP)	0.6736*	0.4937
Brain macrophage (CD68 or F4/80)	**0.8432****	0.6062

Activated macrophages and astrocytes were quantified by immunostaining for CD68 or F4/80 in AD and Tg tissue respectively, or GFAP (astrocytic marker) in the frontal cortical tissue using confocal laser microscopy. Each cell phenotype marker was then correlated with [3H](R)-PK11195 binding in post mortem tissue in AD or [11C](R)-PK11195 PET binding in vivo in Tg mice in the corresponding brain regions in the same cases. PK11195 binding in post mortem tissue in AD correlated best with brain macrophages and did not correlate with either marker in Tg tissue, **p=0.002, *p=0.03.

3.3.5 Discussion

We sought to determine if [3H](R)-PK11195 could detect neuroinflammation in Alzheimer's disease. We first compared [3H](R)-PK11195 binding in Alzheimer's disease post mortem tissue with age-matched controls. We found increased [3H](R)-PK11195 binding in the frontal cortex but not the cerebellum, suggesting that the increase in [3H](R)-PK11195 binding was specific to regions of AD pathology. We then investigated the feasibility of [11C](R)-PK11195 to detect neuroinflammtion in vivo. We imaged mice expressing the APPSwe/PSEN1-DeltaE9 mutations with [11C](R)-PK11195 using PET. We found an age dependent increase in [11C](R)-PK11195 binding in Tg mice compared with controls. Immunohistochemical examination of brain tissue

from transgenic mice and AD showed significant differences in extent of neuroinflammation. AD postmortem tissue showed an increase in both brain macrophages and astrocytes, while brain tissue from Tg mice showed an increase in mainly astrocytes. This suggests that PK11195 binding in AD postmortem tissue may detect both activation of astrocytes and brain macrophages, while mainly labeling astrocytes in our Tg model of AD.

Alternatively, it is also possible that our microglial staining procedure in Tg mice using the F4/80 marker is not optimal. Our results suggest that activation of brain macrophages in mice expressing the APPSwe/PSEN1-DeltaE9 mutations is not different from control mice. While the deposition of Aβ has been well documented, the data suggesting activation of brain macrophages is in mice models is not so clear (72). Mice that model AD differ substantially with respect to the type and extent of transgene(s) overexpressed, which is further complicated by inconsistent results obtained from the various histologic markers currently available to detect activated brain macrophages in mice (reviewed in)(172). Some studies suggest that the extent of activation of brain macrophages in Tg mice is lower than that seen in the human disease, while other suggest comparable extent of brain macrophage activation. We utilized F4/80, a marker expressed on mature brain macrophages (118). Gordon et.al. suggest that that F4/80 is upregulated on brain macrophages in APP/PS1 Tg mice, but decreases with age, reaching levels comparable to controls in 15 month old Tg mice (103, 172). Sasaki et. al. also report low levels of brain macrophage activation using F4/80 in Tg2576 (APP) mice (215). Our F4/80 staining data in APP/PS1 mice are in agreement with these two studies. In contrast, other studies report robust brain macrophage activation in APP/PS1 mice utilizing markers such as Iba-1 (224), an actin cross linking protein in brain macrophages (127, 216). It is possible that different markers are expressed in brain macrophages in a time dependent manner in Tg mice and that we may be able to detect increases in brain macrophage staining in APP/PS1 Tg mice with other markers. We were unable to label brain macrophages using Iba1 in Tg mice tissue due to technical difficulties and are currently trouble-shooting the staining procedure.

Irrespective of the histologic detection of brain macrophages, the extent of PK11195 binding in APP/PS1 mice (~2 fold) was lower than that seen in AD (~4 fold).

This suggests that the extent of brain macrophage activation in Tg mice may be lower than seen in AD. APP/PS1 mice also show decreased retention of the PIB-amyloid PET ligand as compared to human AD subjects, which may be due to differences in the secondary structure of the deposited Aβ (133). It is possible that these differences in Aβ deposition and secondary structure may result in a lower degree of brain macrophage activation in APP/PS1 mice as compared to AD. While, genetically manipulated mice may have several advantages as model systems in AD and other neurodegenerative disorders, they may not be suitable in AD related PET studies.

PET imaging with [11C](R)-PK11195 shows increased ligand binding in 8 subjects with AD (41). Brain regions such as the temporal gyri, the cingulated cortex and the entorhinal cortex show increased [11C](R)-PK11195 retention. However, this study also reported high levels of [11C](R)-PK11195 binding in regions traditionally not involved in AD such as the thalamus and the brainstem (41). The authors interpret these findings arising due to a mechanism called "synaptic stripping" that may be the result of increased brain macrophage activation in regions connected by synapses to areas of pathology. It is also possible that these signals may arise from non-specific [11C](R)-PK11195 binding. In such cases it is vital that PET findings be compared to histopathology to confirm the presence of activated brain macrophages. It is obviously not possible to conduct such comparisons in human in vivo PET studies, which emphasize the need to compare human histopathologic data with ligand binding studies to determine if the underlying neuropathology corresponds to ligand binding.

The role of activated brain macrophages in AD is still not clearly understood (reviewed in (16, 219)). The neurotoxic role of brain macrophages draws support from several in vitro studies (reviewed in (27, 102)), while other studies suggest a beneficial role to brain macrophages in promoting phagocytosis of Aβ (150, 224). Moreover, clinical trials aimed at reducing the extent of neuroinflammation have suggested either reduction in the occurrence of the disease prior to the onset of AD (119, 233) or no effects in patients with mild-moderate AD (6). Brain macrophages may also play a role in immunization therapies by promoting phagocytosis of Aβ (22, 85, 179, 218). Detecting brain macrophages in vivo in AD may be of vital importance in defining the role of brain macrophages in progression of disease as well as the effectiveness of therapeutic

strategies targeted at modulating the immune system. Our studies suggest that PK11195 may be one such tool, which may help delineate the role of brain macrophages in the treatment and pathology of AD.

3.4 UTILITY OF THE PERIPHERAL BENZODIAZEPINE RECEPTOR LIGANDS DA1106 AND PK11195 TO IMAGE BRAIN MACROPHAGES IN RAT MODELS OF NEUROINFLAMMATION IN VIVO

3.4.1 Abstract

Activation of brain macrophages is seen in several neurological disorders and is thought to contribute to disease progression. Activated brain macrophages can be imaged in vivo using PET by taking advantage of increased expression of the peripheral benzodiazepine receptor in these cells in neuroinflammation. PK11195 is a ligand that binds specifically to the peripheral benzodiazepine receptor and has been used to image activated brain macrophages in a number of neuroinflammatory conditions. DAA1106 is a newer ligand that has been reported to bind to the peripheral benzodiazepine receptor with a higher affinity than PK11195. We compared the binding characteristics of both these ligands in normal brain tissue as well as rat models of neuroinflammation. [3H]-DAA1106 showed higher binding affinities compared with [3H](R)-PK11195 in brain tissue derived from normal rats and humans. [3H]-DAA1106 also bound with higher affinity when compared with [3H](R)-PK11195 in brain tissue derived from rats injected with 6-hydroxydopamine. Ex-vivo autoradiography showed greater retention of [11C]-DAA1106 compared to [11C](R)-PK11195 in the brains of rats injected with lipopolysaccaride. Further, PET imaging of rats lesioned with 6-hydroxydopamine showed increased retention of [11C]-DAA1106 compared to controls in vivo. These results indicate that DAA1106 binds with higher affinities to the site of lesion in animal models of neuroinflammation when compared with PK11195, suggesting that DAA1106 may be a better ligand to image activated brain macrophages in vivo.

3.4.2 Introduction

Activation of brain macrophages is a significant component of several neurodegenerative disorders. Phagocytic functions of these cells help in clearing debris at sites of neuronal death and damage (135). However, activated brain macrophages are also hypothesized to promote neurodegenerative in several disorders such as Alzheimer's disease, HIV associated dementia and Parkinson's diseases (102). On activation, brain macrophages are hypothesized to secrete neurotoxins such as interleukins (96, 208), tumor necrosis factor α (53), free radicals (52), nitric oxide (51), proteinases (61) and eicosanoids (114) which are thought to trigger various cellular processes including cell death cascades in neurons (235). In several of these disorders, therapeutic strategies are aimed at modulating the inflammatory process (132). If brain macrophage activation could be evaluated during life, it would be possible to identify developing neuroinflammatory damage and monitor efficacy of therapies targeted at decreasing neuroinflammation.

Several studies suggest that brain macrophages can be imaged in vivo using positron emission tomography with ligands specific to the peripheral benzodiazepine receptor (PBR) (17). Unlike the central benzodiazepine receptor, PBR is expressed at relatively low levels in the normal brain on resting brain macrophage and astrocytes (42, 45). *Ex vivo* autoradiography and *in vitro* studies show increased expression of PBR in activated brain macrophages in neurological diseases such as multiple sclerosis and experimental autoimmune encephalitis (20, 246), stroke (231) and in brain trauma (204).

Various ligands have been synthesized that bind specifically to PBR. Labeling these ligands with ^{3}H and ^{11}C has enabled their use in autoradiography and PET respectively. Of these ligands PK11195, a lipid soluble isoquinoline carboxamide shows rapid uptake into the central nervous system across the blood brain barrier and has been extensively characterized (17). [11C](R)-PK11195 has been used to label activated brain macrophage in patients with multiple sclerosis (20, 69) Rasmussen's encephalitis (18), stroke (206), Herpes encephalitis (43), gliomas (191), Multiple System Atrophy (95), animal models of HIV encephalitis (245) and AD (41).

A newer ligand, DAA1106 [N-(2,5-dimethoxybenzyl)-N-(4-uoro-2-phenoxyphenyl) acetamide] is an aryloxyanilide derivative, that binds selectively and

with higher affinity to PBR compared to PK11195 (47). This is reflected by its low dissociation constant (kd) assessed in mitochondrial fractions derived from the rat cerebral cortex (47). Due to high affinity, DAA1106 may serve as a more efficient ligand to label PBR in the brain in neuroinflammtion (149, 262). In this report our goal is to determine the utility of DAA1106 to image activated brain macrophages activation in animal models of neuroinflammation *in vivo*.

We first compare binding characteristics of [3H]-labeled PK11195 and DAA1106 in tissues using filtration binding techniques followed by in vivo binding comparisons utilizing [11C] labeled ligands. We report that DAA1106 displays higher binding affinity to PBR in comparison with PK11195 in normal brain tissue and brain tissue obtained from rats injected with either lipopolysaccharide (LPS) or 6-hydroxydopamine (6-OHDA). Ex vivo autoradiography showed that [11C]-DAA1106 was retained at higher levels compared to [11C](R)-PK11195 at the site of lesion in LPS-injected rats. PET imaging in 6-OHDA lesioned rats showed increased [11C]-DAA1106 compared to controls in vivo. These data suggest that DAA1106 binds to PBR with higher affinity compared to PK11195 and may be a better ligand in imaging brain macrophages in vivo with PET.

3.4.3 Methods

Animals

All animals were housed and maintained according to standards of the Association for Assessment and Accreditation of Laboratory Animal Care, and experiments were approved by the University of Pittsburgh Institutional Animal Care and Use Committee. Male Sprague-Dawley rats (300-350g) were injected with either 50μg lipopolysaccaride (LPS, Sigma, St Louis, MO) or 20μg 6-hydroxydopamine (6-OHDA, Sigma, St Louis, MO) into the striatum. Surgical procedures were conducted as described earlier (113). Briefly, animals were anesthetized with Equithesin [3.0 mg/kg; 258 mM chloral hydrate/20% (vol/vol) propylene glycol/86 mM MgSO4/20% (wt/vol) Nembutal (sodium pentobarbital)] and were injected sterotaxically with either 6-OHDA or LPS into the striatum with the help of a cannula

(coordinates: +0.8 mm anterior-posterior; +2.7 mm medial-lateral from bregma; -5.0 mm dorsal-ventral from dura). Animals were allowed to recover after surgery and were housed for 4 days following LPS injections or 21 days following 6-OHDA injections, following which they were imaged with PET.

Tissue processing

Following PET scans, animals were sacrificed and the brain was removed. Brian tissue was either processed to obtain frozen sections for autoradiography or paraffin sections for immunohistochemistry. Brain tissue from the cerebellum, occipital cortex and basal ganglia was dissected out from three control/normal rats. Similarly, tissue from the frontal cortex, cerebellum and basal ganglia was dissected out from three control/normal human brains obtained from the University of Pittsburgh Brain bank. In three animals injected with LPS and three animals injected with 6-OHDA the ipsilateral and contralateral striatum was dissected out. Brain tissue from each of these cases was then weighed and homogenized in ice-cold 50 mM HEPES buffer (pH 7.4). Homogenates were washed four times by centrifugation at 40,000 g for 20 min at 4^0C and protein values were estimated using the BCA protein assay kit before using homogenates in filtration binding experiments (Pierce, Rockford, IL).

Filtration radioligand binding assays

Tissue samples (total protein concentration ranging from 150 to 200 μg) were incubated with either 0.5-64 nM [3H](R)-PK11195 (sp. Act., 89.9 Ci/mmol; NEN Life Sciences Products, Boston, MA) or [3H]-DAA1106 (sp. Act., 80 Ci/mmol; American Radiolabeled Chemical, St Lousi, MO) at 4^0C for 2 hr in a final volume of 250 μl of HEPES. This was defined as total binding. Nonspecific binding was determined by the inclusion of 10 μM PK11195 or 10 μM DAA11106 respectively. The reaction was terminated by filtration through glass fiber filters harvester (Brandel, Gaithersburg, MD) presoaked in 0.3% polyethyleneimine by the addition of ice-cold HEPES in a vacuum cell harvester (Brandel, Gaithersburg, MD). Filter bound radioactivity was counted in a liquid scintillation spectrometer (Tricarb liquid scintillation counter, Perkin Elmer life sciences, Wellesley, MA) after the addition of 6 mls of liquid scintillation fluid (Perkin Elmer life

sciences, Wellesley, MA). Specific binding at each concentration of [3H]-ligand was defined as the difference between total binding and nonspecific binding and ranged from 80-90% of total binding. All samples were run in duplicate. Bmax in fmoles per mg protein and kd in nM were determined using PRISM software (Graphpad, San Diego, CA).

Immunohistochemistry

Immunostaining and laser confocal microscopic imaging was performed as described before (245). Paraffin embedded sections obtained from transgenic mice and controls were stained with antibodies to GFAP (mouse monoclonal, DAKO, Carpinteria, CA), or ED1 (anti-rat CD68, mouse monoclonal, Serotec, Raleigh, NC), or tyrosine hydroxylase (rabbit polyclonal, Covance research products, Denver, PA) used at concentrations 1:1000**,** 1:100 and 1:1000 respectively. Sections were then incubated with Cy5-conjugated goat anti-mouse or Cy3-conjugated anti-rabbit IgG at a concentration of 1:200 (Jackson Immunoresearch Laboratories Inc., West Grove, PA). Immunostained sections were then scanned on a laser confocal microscope (LSM 150, Zeiss, Heidelberg, Germany).

Ex-vivo autoradiography

Rats injected with LPS were anesthetized and injected intravenously with either of [11C]-DAA1106 or [11C](R)-PK11195 (1-2 mCi). The animals were sacrificed 30 minutes later and the brain was rapidly removed. The cortex was sectioned coronally into 2mm sections and mounted on a plastic film and apposed to a phosphor screen (PhosphorImager SI system, Molecular Dynamics, Sunnyvale, CA) for 20 minutes and then imaged on a phosphorimager (PhosphorImager SI system, Molecular Dynamics, Sunnyvale, CA). Brain sections were then fixed and processed for immunohistochemistry.

PET imaging

High specific activity [11C](R)-PK11195 ([N-methyl-^{11}C]-PK11195) and [11C]-DAA1106 ([N-methyl-^{11}C]-DAA1106) were produced at the UPMC PET Facility using methods similar to those previously described (245, 262). Chemical and radiochemical

purities were ≥95% with specific activities ≥2.0 Ci/μmol at the end of a 40 min synthesis. Typical end of synthesis yields of high purity [11C](R)-PK11195 was in the range of 40-100 mCi.

Rats were imaged using microPET with [11C](R)-PK11195 and [11C]-DAA1106 in succession. In ligand displacement studies, some animals were injected with a displacing dose of unlabeled DAA1106 (1.0 mg/kg) 15 min after injection of [11C](R)-PK11195 or [11C]-DAA1106. Data were reconstructed using the 3D Ordered Subsets Expectation Maximum (OSEM) algorithm for maximal image quality and image resolution. Regional brain radioactivity concentration were summed over the scan frames at various time points was normalized to both the injected dose of [11C]-ligand and the body mass of the animal (%ID/Kg*g) to represent a semi-quantitative measure of [11C]-ligand binding. Regions-of-interest (ROI) were defined on summed PET images and applied to the dynamic PET images to generate time-activity curves.

Autoradiography

Autoradiography was performed as described earlier (245). Briefly, 15 μm thick frozen brain sections were placed on Superfrost^{Tm} glass slides (Sigma, St Louis, MO) and incubated in ice-cold 50 mM TRIS-HEPES (pH 7.4) containing 1 nM [3H](R)-PK11195 (sp. Act., 89.9 Ci/mmol; NEN Life Sciences Products, Boston, MA) or 1 nM [3H]-DAA1106 for 30 min. Specificity of binding was ensured by the inclusion of 10 μM PK11195 (Sigma, St Louis, MO) or 10 μM DAA1106 in parallel sections. The sections were mounted with a layer of autoradiographic LM-1 emulsion (Amersham, UK), were developed after 4 weeks and imaged on the confocal microscope.

Statistical analysis

Data were analyzed using PRISM software (Graphpad, San Diego, CA). Student's *t* tests or one-way ANOVA tests with post-test Bonferroni correction and 95% confidence intervals were used to analyze data.

3.4.4 Results

[3H]-DAA1106 shows higher binding affinity compared to [3H](R)-PK11195 in normal human and rat brain tissue.

We used saturation filtration binding to compare [3H]-DAA1106 specific binding with that of [3H](R)-PK11195 in normal human (n=3) and rat (n=3) brain tissue. Brain tissue from the frontal cortex, cerebellum and basal ganglia were dissected from three postmortem samples of patients with no CNS pathology. Brain tissue from cerebellum, basal ganglia and the occipital cortex of three adult rats was dissected out. Tissue was weighed, homogenized in 50 mM HEPES (pH 7.4) and protein values were determined using the BCA protein assay kit. Homogenized tissue was incubated with either 0.5-64 nM [3H](R)-PK11195 or 0.2 to 20 nM [3H]-DAA1106 to obtain total binding values. Nonspecific binding was determined in parallel by including 10μM PK11195 or 10μM DAA1106 respectively. Specific binding at each given concentration of [3H]-ligand was defined as the difference between total binding and nonspecific binding. Bmax and kd values reflective of the total number of binding sites per mg protein and binding affinity of the ligand to PBR respectively were determined using PRISM software.

We first compared the affinity of binding of these two ligands to PBR reflected by an inverse proportionality to the dissociation constant kd. Binding affinity for [3H]-DAA1106 compared to [3H](R)-PK11195 was significantly higher reflected by a five to six fold lower kd in all brain regions assessed in normal human and rat brain tissue in (**Figure 21 B and D**). Bmax values were uniformly lower with [3H]-DAA1106 compared to [3H](R)-PK11195 in both human and rat brain tissue but did not approach statistical significance (**Figure 21 A and C**).

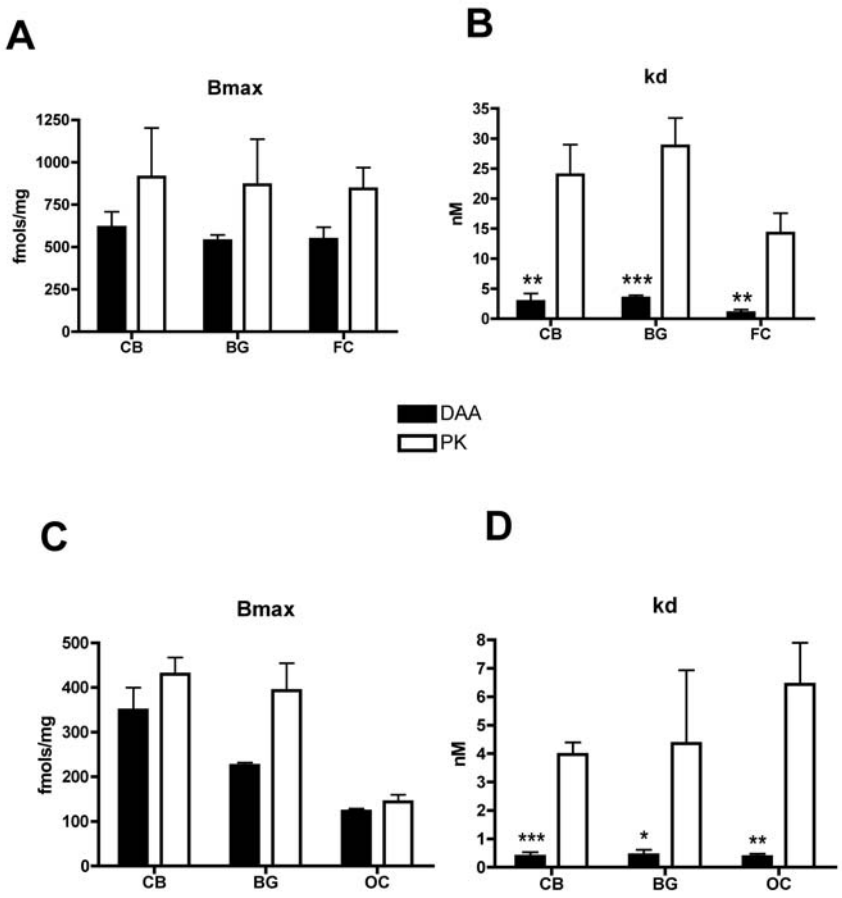

Figure 21 [3H]-DAA1106 shows higher binding affinity to PBR when compared with [3H](R)-PK11195

Filtration binding was assessed in normal human brain tissue (n=3, top panel) and normal rat brain tissue (n=3, lower panel) using [3H]-DAA1106 and [3H](R)-PK11195. The Bmax (fmols/mg), reflective of the total number of binding sites was calculated for both ligands is shown in the left panel (**A & C**) and the kd (nM) reflective of the binding affinity of the ligands to PBR is shown in the right panel (**B & D**). **CB**=Cerebellum, **FC**=Frontal Cortex, **BG**=Basal Ganglia, and **OC**=Occipital Cortex. Data analyzed using student's *t* test.

(**A, C**) Bmax with [3H]-DAA1106 assessed in normal human (A) and rat (C) brain tissue was uniformly lower than [3H](R)-PK11195 but did not approach statistical significance.

(**B, D**) kd with [3H]-DAA1106 was significantly lower with [3H]-DAA1106 than [3H](R)-PK11195 in all brain regions of both human (B) and rat (D) brain tissue , ***p<0.0001, **p<0.001, *p<0.01.

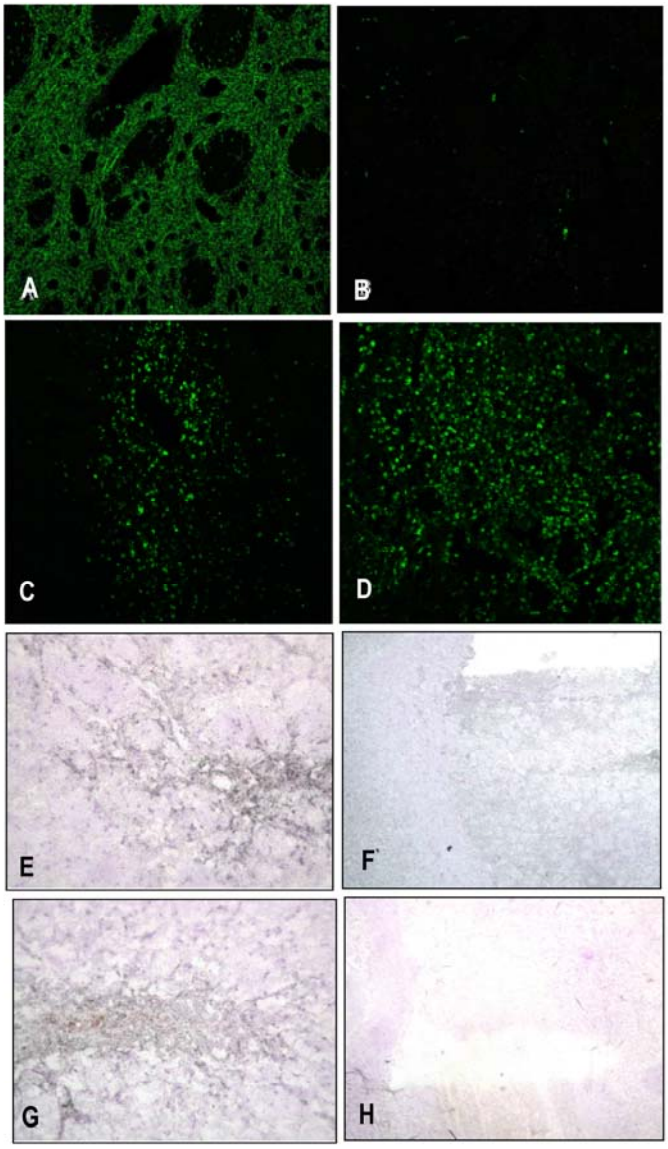

Figure 22 Rat models of neuroinflammation show increased [3H]-DAA1106 and [3H](R)-PK11195

(**A-D**) Rats were injected with either 20μg of 6-OHDA **(A-C**) or 50μg of LPS into the striatum (**D**). Brain sections were then stained with tyrosine hydroxylase (TH, marker for dopaminergic terminals, **A & B**) or CD68 (ED1, marker for rat brain macrophages, **C&D**). Rats injected with 6-OHDA showed a decrease in tyrosine hydroxylase staining in the ipsilateral (**B**) compared to contralateral side (**A**). Rats injected with 6-OHDA (**C**) and LPS (**D**) showed activated brain macrophages in the striatum.

(**E-F**) Brain sections obtained from 6-OHDA injected rats were incubated with 1nM [3H]-DAA1106 either without (**E**) or with 1μM DAA1106 (**F**). [3H]-DAA1106 binds to the lesioned area (**E**) and is competed out by DAA1106 (**F**), indicating that the binding is specific.

(**G-H**) Brain sections obtained from 6-OHDA injected rats were incubated with 1nM [3H](R)-PK11195 either without (**G**) or with 1μM PK11195 (**H**). [3H](R)-PK11195 binds to the lesioned area (**G**) and is competed out by DAA1106 (**H**), indicating that the binding is specific.

Rat models of neuroinflammation

PK11195 binding is higher in CNS tissue in response to neuroinflammatory lesions (17). We sought to determine if DAA1106 similarly shows an increase in specific binding in neuroinflammation. We also wanted to determine if the high binding affinity of DAA1106 observed in normal human tissue is seen in neuroinflammation. We used two well-characterized rat models of neuroinflammation. Rats were injected with 20 μg of 6-hydroxydopamine (6-OHDA) (as a model for Parkinson's disease) or 50 μg of lipopolysaccaride (LPS) into the striatum. Rats were sacrificed 3 weeks and 4 days post injection respectively, as maximal neuroinflammation was seen at these time points in each of the two models (data not shown). In 6-OHDA lesioned animals, tyrosine hydroxylase staining was significantly decreased (**Figure 22 A and B**) along with increased staining for the brain macrophage marker (rat CD68) on the ipsilateral side compared to the contralateral side (**Figure 22 C**). LPS injected rats showed increased staining for the activated brain macrophage marker (rat CD68) on the ipsilateral side compared to the contralateral side (**Figure 22 D**). PK11195 and DAA1106 binding characteristics were then compared in each of these two models.

[3H]-DAA1106 shows higher binding affinity compared to [3H](R)-PK11195 in brain tissue obtained from rats lesioned with 6-OHDA.

We assessed Bmax and kd values for each ligand in the ipsilateral and contralateral side of rats lesioned with 6-OHDA (n=3). Bmax values were significantly higher on the ipsilateral side compared with the contralateral side with either [3H]-DAA1106 or [3H](R)-PK11195 (**Figure 23 A**). On comparing the two ligands with each other, Bmax values did not differ significantly in the same brain region, but kd values were significantly lower with [3H]-DAA1106 (**Figure 23 A and B**). These results were

confirmed with autoradiography in frozen sections that showed specific binding of [3H]-DAA1106 (**Figure 22 E and F)** and [3H](R)-PK11195 at the site of the lesion in 6-OHDA lesioned rats (**Figure 22 G and H**). These results suggest that [3H]-DAA1106 binding sites (Bmax) increase in sites of brain inflammation similar to [3H](R)-PK11195. Further, [3H]-DAA1106 displays higher binding affinity compared with [3H](R)-PK11195 in neuroinflammation.

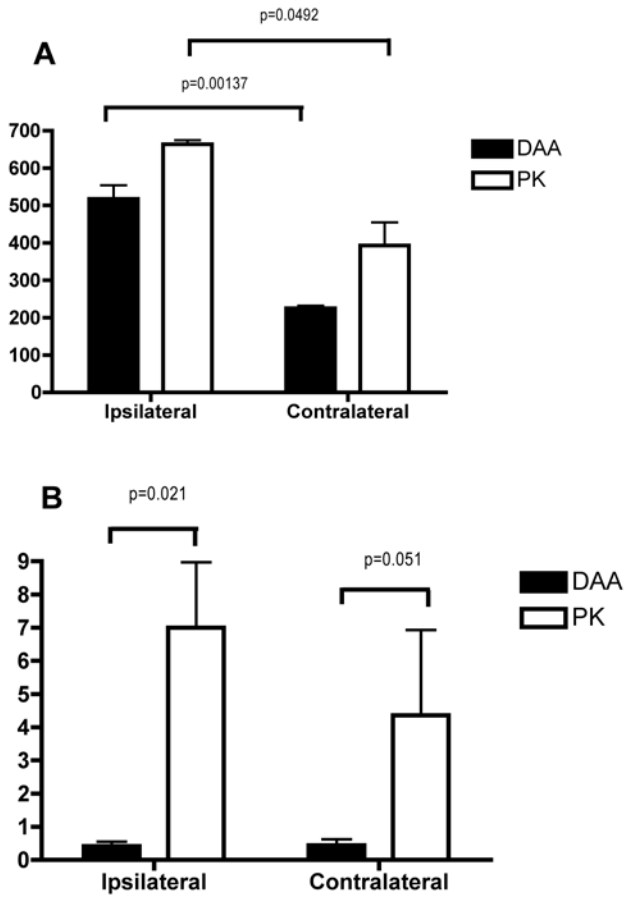

Figure 23 [3H]-DAA1106 shows higher affinity binding compared with [3H](R)-PK11195 in 6-OHDA injected rats.

Filtration binding was assessed in rat striatal brain tissue injected with 20μg 6-OHDA (n=3) using [3H]-DAA1106 and [3H](R)-PK11195.

(A) The Bmax (fmols/mg), reflective of the total number of binding sites was significantly higher in the area ipsilateral to the lesion compared with the area contralateral to the lesion with [3H]-DAA1106 and [3H](R)-PK11195. [3H]-DAA1106 and [3H](R)-PK11195 Bmax did not differ within the same area.

(B) The kd (nM), reflective of the ligand binding affinity was not different between the ipsilateral and the contralateral regions with the same ligand. However, the kd with [3H]-DAA1106 was significantly lower than with [3H](R)-PK11195 in both ipsillateral and contralateral regions.

Ex-vivo binding analysis shows increased brain retention of [11C]-DAA1106 compared to [11C](R)-PK11195 in rats lesioned with LPS.

[11C]-DAA1106 or [11C](R)-PK11195 (1-2mCi) was injected intravenously into rats lesioned with LPS (n=3, each). After a 30-minute uptake the animals were sacrificed, the brain was rapidly and sectioned coronally (2mm thick) and imaged on a phosphorimager. While both ligands showed retention, [11C]-DAA1106 binding was higher compared to [11C](R)-PK11195 at the site of the lesion (**Figure 24 A-D**). These results are consistent with the filtration binding studies suggesting that DAA1106 has higher binding affinity compared to PK11195 in neuroinflammation.

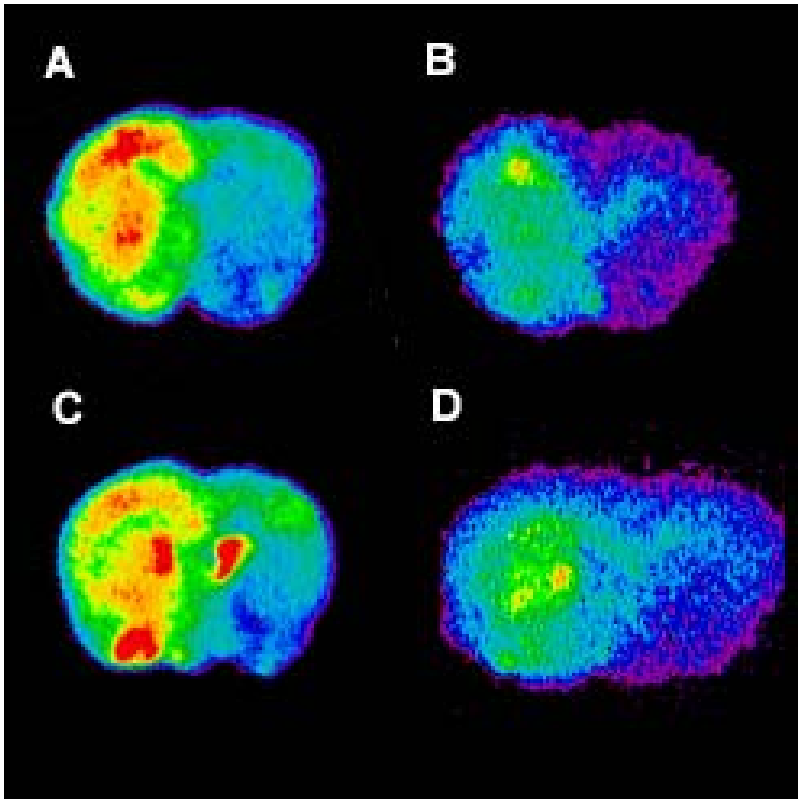

Figure 24 Ex vivo autoradiography shows higher [11C]-DAA1106 retention compared to [11C](R)-PK11195 in rats lesioned with LPS.

Rats (n=3) lesioned with 50μg LPS were injected with either [11C]-DAA1106 or [11C](R)-PK11195 (1-2mCi) intravenously. Brain sections were obtained after a 30-minute uptake and imaged on a phosphorimager.

(**A & C**) [11C]-DAA1106 retention was observed in lesioned area, but not the contralateral area.

(**B & D**) [11C](R)-PK11195 retention was also observed in lesioned area, but at lower levels when compared with [11C]-DAA1106.

PET imaging in with [11C]-DAA1106 in normal rats

We conducted a series of PET imaging experiments in normal rats to compare the kinetic behavior of [11C]-DAA1106 with [11C](R)-PK11195. We injected either [11C]-DAA1106 or [11C](R)-PK11195 into anesthetized animals and positioned them in the microPET scanner to image the brain, heart and lung. To demonstrate specific binding, we injected a displacing dose of unlabeled DAA1106 (1.0 mg/kg) 15 min after injection of [11C](R)-PK11195 or [11C]-DAA1106. Time-activity curves of radioactivity concentrations were expressed as percent-injected dose per gram normalized by body mass (%ID*kg/g, Y-axis) (**Figure 25**).

In rat myocardium where PBR sites are known to be abundant, kinetics of [11C](R)-PK11195 and [11C]-DAA1106 were similar and both were effectively displaced by unlabeled DAA1106 (**Figure 25 B,** black and red triangles). Clearance of [11C](R)-PK11195 from lung was much faster than [11C]-DAA1106, though both were displaced by unlabeled DAA1106 (**Figure 25 B,** black and red circles). In the rat brain [11C]-DAA1106 was effectively displaced by unlabeled DAA1106 (**Figure 25 A,** red triangles). [11C](R)-PK11195 showed an initial displacement followed by brief upswing before renewed clearance from brain (**Figure 25 A,** black triangles). This upswing may be the result of recirculation of [11C](R)-PK11195 displaced from peripheral tissues, such as the heart and lung (**Figure 25 B,** black triangles and circles) by the high affinity DAA1106 ligand. These studies complement blocking studies of [11C]-DAA1106 with unlabeled DAA1106 (1.0 mg/kg) and higher doses (5-10 mg/kg) of unlabeled PK11195 (149).

PET imaging with [11C]-DAA1106 shows increased brain retention compared to [11C](R)-PK11195 in 6-OHDA lesioned rats

[11C]-DAA1106 and [11C](R)-PK11195 were then used sequentially to image rats lesioned with 6-OHDA (n=2). When compared with [11C](R)-PK11195, [11C]-DAA1106 showed increased brain retention in 6-OHDA lesioned animals as compared to normal rats (**Figure 26**). However, due to limited resolution with PET imaging and the small size of the rat brain compared to the human brain, both ligands were unable to distinguish between the lesioned and the non-lesioned brain hemispheres in the same animal. However, ligand retention was significantly higher in the lesioned animals compared to controls. Further, [11C]-DAA1106 showed increased retention compared to [11C](R)-PK11195, consistent with our filtration binding and ex-vivo autoradiography results suggesting that DAA1106 shows higher affinity to PBR and hence, significantly higher retention at sites of neuroinflammation.

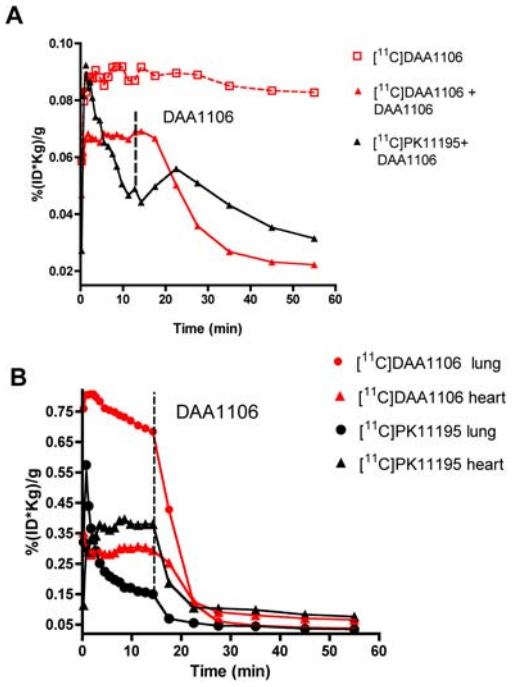

Figure 25 [11C]-DAA1106 specific binding in normal rats

The kinetics of [11C]-DAA1106 or [11C](R)-PK11195 injected in normal rats was followed in the brain, heart and lungs in vivo using PET. A displacing does of 1mg/ kg DAA1106 was injected 15 minutes (indicated by the dotted black line) after initial the [11C]-ligand administration. Time-activity curves of

radioactivity concentrations are expressed as percent-injected dose per gram normalized by body mass (%ID*kg/g, Y-axis) plotted against time (minutes, X-axis).

(A) PET imaging of the brain revealed [11C]-DAA1106 retention (red open squares), which was displaced by DAA1106 (red triangles), indicating that [11C]-DAA1106 binding was specific. [11C](R)-PK11195 binding showed an initial displacement followed by brief upswing before renewed clearance from brain.

(B) [11C]-DAA1106 retention in the lung (red circles) and myocardium (red triangles) were displaced by DAA1106 indicating specific binding in both these organs. Similarly, [11C](R)-PK11195 binding was displaced by DAA1106 in both the lung (black circles) and myocardium (black triangles).

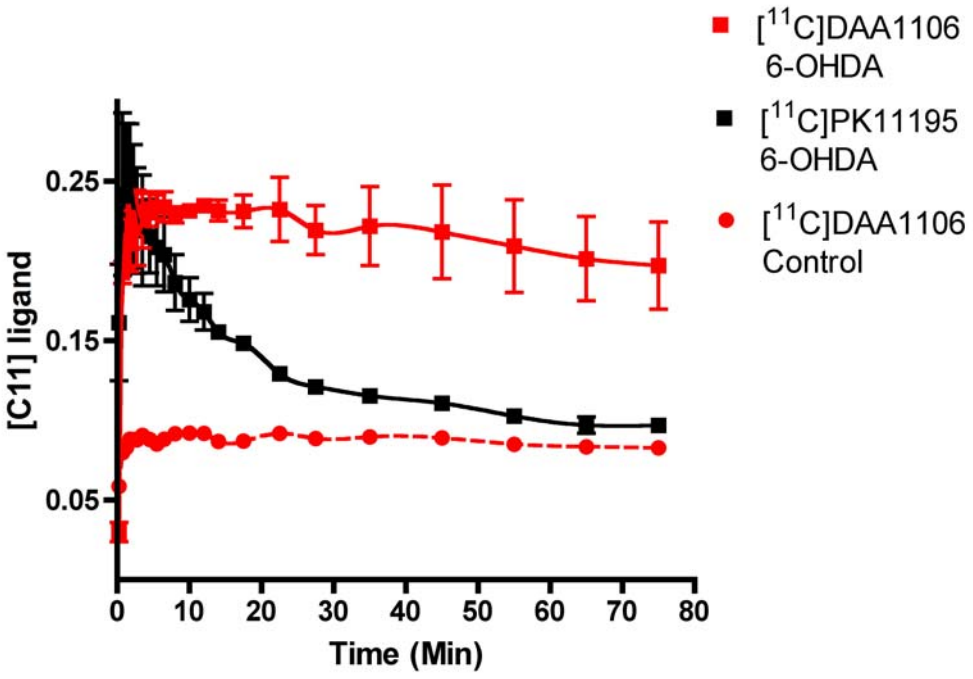

Figure 26 [11C]-DAA1106 binding is higher in 6-OHDA lesioned animals compared to controls

Rats lesioned with 6-OHDA were imaged sequentially with [11C]-DAA1106 and [11C](R)-PK11195 (n=2) and compared with control non-injected rats (n=1). [11C]-DAA1106 binding was significantly higher in 6-OHDA lesioned rats (red squares) compared to the control (red circles).

3.4.5 Discussion

PK11195 is a ligand that specifically binds to PBR expressed in low levels in the normal brain and is enriched in brain macrophages in neurological disorders (41, 45). PK11195 has been used to label brain macrophages in a number of neurodegenerative disorders (reviewed in (42)). In this study, we compared the binding characteristics of a newer PBR ligand DAA1106 with PK11195 in brain tissues and in rat models of neuroinflammation in vivo. We first used filtration binding analyses to compare the pharmacologic properties of DAA1106 with PK11195 in normal human and rat brain tissues, followed by binding studies in brain tissues obtained from rats lesioned with either LPS or 6-OHDA. In all the filtration binding experiments using [3H] labeled ligands, the binding affinity of DAA1106 to PBR was significantly higher than PK11195, reflected by a 5-6 fold lower dissociation constant (kd). The Bmax, reflective of the number of binding sites, was uniformly lower with DAA1106 but was not significantly different from PK11195. Ex-vivo autoradiography experiments utilizing [11C] labeled ligands, showed increased brain retention of DAA1106 compared to PK11195. DAA1106 thus shows similar properties as PK11195 and rapidly penetrates the blood brain barrier to enter the CNS. Further, [11C]-DAA1106 was displaced by DAA1106 in the brain suggesting [11C]-DAA1106 binding was specific. Finally, [11C]-DAA1106 showed increased retention in 6-OHDA lesioned animals compared to [11C](R)-PK11195 binding and controls. These data suggest that DAA1106 binds to PBR with higher affinity and can detect neuroinflammation in vivo using PET.

Our results showing higher PBR-ligand binding in rats injected with either LPS or 6-OHDA are consistent with previously published studies (31, 56, 212). However, Cicchetti et. al. report the ability to distinguish between the ipsilateral and contralateral regions of 6-OHDA lesioned animals using PET with [11C](R)-PK11195 (56). In our experience, the resolution of PET along with the small size of the rat brain did not enable us to distinguish between ipsilateral and contralateral regions with either [11C](R)-PK11195 or [11C]-DAA1106. However, animals lesioned with 6-OHDA showed increased brain retention of both ligands compared to controls. This binding was specific as it was displaced by cold DAA1106 in control animals.

[11C](R)-PK11195 has been used extensively to image neuroinflammation in vivo using PET (42). Studies in AD patients showed high [11C](R)-PK11195 binding in the entorhinal, temporoparietal and cingulate cortex, which are brain regions that show the highest degree of AD pathology (41). However, this study also reported high levels of [11C](R)-PK11195 binding in regions not involved in AD such as the thalamus and the brainstem (41). The authors interpret these findings arising due to a mechanism called "synaptic stripping" that may be the result of increased brain macrophage activation in regions synaptically connected to areas of pathology. It is also possible that these signals may arise from non-specific [11C](R)-PK11195 binding. Similarly, a recent report using [11C](R)-PK11195 to image activated brain macrophages in ALS patients showed high binding in the occipital cortex, regions of the prefrontal cortex, and the thalamus, which are areas that are not traditionally implicated in ALS pathology (238). Both these studies were not followed up by neuropathologic assessments with filtration binding analyses (to determine ligand-receptor binding characteristics), and the presence of activated brain macrophages in regions traditionally not involved in the disease pathology cannot be ruled out. However, these findings may be attributed to some degree of non-specific binding of PK11195, underscoring the importance of using a ligand with high specific binding to PBR. The higher affinity of DAA1106 to PBR may be able to address some of these concerns.

In conclusion, DAA1106 shows higher affinity to PBR, reflected by a 5-6 fold lowers kd, in comparison to PK11195 in both human and rat brain tissues. DAA1106 was also effectively crossed the blood brain barrier and was retained at higher levels in rats lesioned with either LPS or 6-OHDA. These results suggest that DAA1106 may be a better ligand than PK11195 to image neuroinflammation in vivo using PET.

4.0 OVERALL DISCUSSION

4.1.1 Summary

Neuroinflammation is seen in several neurodegenerative disorders and constitutes a significant component of the underlying pathology. In this body of work, we take advantage of increased PBR expression on brain macrophages to image these cells in vivo utilizing PET. We utilize two specific PBR ligands, PK11195 and DAA1106, to compare ligand binding in (1) human postmortem brain tissue and animal models of neuroinflammation (2) cell culture systems to dissect out relative contributions to ligand binding from macrophages and astrocytes and (3) animal models of disease utilizing PET.

Specifically, we found that SIV infected macaques that show higher levels of [11C](R)-PK11195 binding corresponded to the presence of SIV encephalitis on post mortem examination. Macaques that did not show an increase in [11C](R)-PK11195 binding did not exhibit SIVE. Brain post mortem [3H](R)-PK11195 binding was significantly higher in SIVE macaques from controls due to an increase in the number of binding sites (*Bmax*) with no significant changes in binding affinity (*Kd*) and correlated with in vivo binding measured with PET. Brain regions with elevated PK11195 binding on PET and filtration assays correlated with abundant activated macrophages but not with activated astrocytes or neurons quantified by laser confocal microscopy. Finally, combined autoradiography and immunostaining identified macrophages, but not astrocytes as the cells with highest [3H](R)-PK11195 binding.

HIV encephalitic brain tissue showed a significant increase in binding with both PK11195 and DAA1106 compared to HIV infected, non-encephalitic controls and non-infected brain tissue. We also saw an increase in [3H]-DAA1106 binding in SIVE tissue

compared to SIV infected, non-encephalitic and non-infected tissue. Increased expression was specific to macrophages as determined by combined immunohistochemistry and autoradiography in SIVE tissue. In tissue culture experiments, we found increased [3H](R)-PK11195 binding in macrophages activated with LPS or INF-γ compared to unactivated macrophages, astrocytes activated with dCAMP and unactivated astrocytes. Similar results were seen in mitochondrial fractions harvested from activated and unactivated macrophages and astrocytes using [3H]-DAA1106. Increase in [3H](R)-PK11195 binding was also seen in macrophages infected with HIV-1 ADAM, peaking at 14 days post infection and reaching a plateau by 21 days post infection. Astrocytes treated with supernatants derived from HIV-1 ADMA infected macrophages did not show a significant increase in [3H](R)-PK11195 binding compared to untreated cultures. The increase in [3H](R)-PK11195 binding in LPS treated macrophages was reversed using inhibitors of PI3-kinase, but not a MEK-1/2 inhibitor.

In postmortem brain tissue obtained from AD subjects we found increased [3H](R)-PK11195 binding in the frontal cortex but not the cerebellum, suggesting that the increase in [3H](R)-PK11195 binding was specific to regions of AD pathology. Mice expressing the APPSwe/PSEN1-DeltaE9 mutations showed an in vivo, age-dependent moderate increase in [11C](R)-PK11195 binding compared with controls. Immunohistochemical examination of brain tissue from transgenic mice and AD showed significant differences in extent of neuroinflammation. AD postmortem tissue showed an increase in both brain macrophages and astrocytes, while brain tissue from Tg mice showed an increase in mainly astrocytes.

On comparing the pharmacologic characteristics of DAA1106 with PK11195, we found that the binding affinity of DAA1106 to PBR was significantly higher than PK11195, reflected by a 5-6 fold lower dissociation constant (kd). The Bmax, reflective of the number of binding sites, was uniformly lower with DAA1106 but was not significantly different from PK11195. Ex-vivo autoradiography experiments utilizing [11C] labeled ligands, showed increased brain retention of DAA1106 compared to PK11195. In PET experiments, [11C]-DAA1106 was displaced by DAA1106 in the brain suggesting that in vivo [11C]-DAA1106 binding was specific. Finally, [11C]-DAA1106

showed increased retention in 6-OHDA lesioned animals compared to [11C](R)-PK11195 binding and controls.

These results taken together suggest that ligands to PBR specifically label brain macrophages and can be used to image these cells in vivo using PET in neuroinflammation.

4.1.2 Discussion and future directions

PBR can be used to label brain macrophages in vivo in neuroinflammation

We have shown that ligands to PBR can label brain macrophages in many neurodegenerative disorders including HIV encephalitis, Alzheimer's disease and animal models of Parkinson's disease. These data taken together suggest that increased expression of PBR is a common aspect of neuroinflammation and can be used to image brain macrophages in vivo. Our findings support the hypothesis that PBR-ligand binding may be a surrogate marker of activated brain macrophages and active loci of neuroinflammation in neurodegenerative disease. Although, the pathogenesis of these various diseases differ enormously, the common finding that PBR is expressed in brain macrophages in these diseases suggests that mechanisms and pathways responsible for brain macrophage activation are similar in these diseases.

In future experiments, we will expand on determining the biochemical processes that link PBR expression with brain macrophage activation. Our initial results suggest that PBR expression is mediated by the activation of the PI3K/Akt pathway. We will utilize cell culture systems to dissect out this pathway in relation to both brain macrophage activation and PBR expression in more detail.

What is the function of PBR in activated brain macrophages?

The functional significance of increased PBR in activated brain macrophages is not known. It is part of a hetero-oligomeric complex comprised of the voltage-dependent anion channel and an adenine nucleotide carrier forming the mitochondrial permeability transition pore (160). It is thought to be involved in neurosteroid synthesis by serving to transport cholesterol from the outer to the inner mitochondrial membranes (190). As a

constituent of the mitochondrial permeability transition pore it is thought to regulate cell death (160) and mitochondrial respiration (117). PBR overexpression in many cell types has also been shown to protect against various apoptotic insults including the cytopathic effects of sindbis and myxoma viral infections (80, 125). Forced PBR expression in neurons in *vivo* and jurkat cells *in vitro* protects these cells against apoptosis (125, 234). PBR upregulation in testicular leydig cells protects them from cytokine-induced toxicity (20, 237). This is also seen in blood phagocytic cells where PBR protects against oxidant induced cell death (44).

Several proteins involved in apoptosis including Bcl-2, Bcl-X_l and Bax have also been shown to physically interact with the voltage dependent anion channel and the adenine nucleotide carrier (62, 112). PBR can thus influence the cell death processes either by directly affecting the molecular components of the pore or through indirect effects by interfering with interactions of the voltage dependent anion channel and the adenine nucleotide carrier with pro-apoptotic proteins like Bax (46). These hypotheses draw support from kainic acid-injected rats, where hippocampal PBR is increased by 20 fold with no significant increases in either the voltage dependent anion channel or the adenine nucleotide carrier (244). Increases in only the PBR component of the pore might result in altering both the channel properties and altering interactions of other pore proteins with pro-apoptotic mediators.

The biochemical mechanisms by which selective increase in expression of PBR in activated brain macrophages in several of these CNS diseases is not understood (91). In pancreatic islet cells, testicular leydig cells, the cytokines TNF-α, IFN-γ and IL-1β caused an increase in mitochondrial PBR mRNA and [3H](R)-PK11195 binding in a transcription dependent manner (20, 237). In the CNS, rats injected with IL-1, or TNF-α, or LPS resulted in increased [3H](R)-PK11195 binding to brain macrophages (31, 35). IL-1 and TNF-α also increase [3H](R)-PK11195 binding in cultured astrocytes (65). Finally, in Experimental Autoimmune Encephalitis, IL-6 and TNF-α expression profiles correlate with increase in spinal cord [3H](R)-PK11195 binding (5). These data suggest that cytokines increase PBR expression in various cell types including macrophages. However, the mechanisms mediating this increase are not known. Cellular upregulation

of PBR in these systems may serve as a protective strategy against cytokine toxicity by altering mitochondrial permeability transition and consequent cell death.

Since brain macrophages are themselves sources of cytokines and several other toxic products, it is possible that the function of PBR in activated brain macrophages is to protect them from self-generated toxins by influencing mitochondrial permeability transition and preventing apoptosis of these cells in the CNS. We hypothesize that PBR expression in brain macrophages prevents these cells from undergoing toxin-induced cell death in neurodegenerative disorders.

To test this hypothesis, we will first determine the effects of increased PBR expression on mitochondrial permeability transition. We will also utilize RNA inhibition (RNAi) technologies to knock down PBR in brain macrophages. A prediction of this hypothesis is that PBR knockdown will increase cell death in brain macrophages. We will compare mitochondrial potential changes and cell death in macrophages that have been treated with RNAi with control untreated cells. These studies will help us better understand the role of PBR in activated brain macrophages. It is also conceivable that a longer life span of brain macrophages would lead to exacerbation of neuroinflammation and subsequently the neurodegenerative process. If PBR regulates cell survival in brain macrophages, it may prove a suitable target to decrease the viability of these cells in neuroinflammation.

Implications of detecting neuroinflammation in vivo

The clinical diagnosis of neurodegenerative disorders requires the presence of irreversible clinical symptoms and signs**.** Traditional imaging studies such as CT and MRI have not been of much assistance in the diagnosis of dementia in general (66)**.** Current methodologies, such as structural MRI assessment of brain volume are insensitive late measures of neurological damage and the diagnosis by neurocognitive tests is possible only after irreversible neuronal damage has occurred. Effective therapy requires early intervention at the onset of neuronal injury prior to the appearance of irreversible signs and symptoms. PET imaging of brain macrophages in neurodegenerative may enable early diagnosis and therapeutic interventions.

To design therapies for neurodegenerative disorders, it is critical to be able to monitor their success in arresting the progression of neurological disease. Monitoring therapeutic efficacy of any such treatments is also complicated by the fact that one can only assess absence of disease progression and not recovery of function. Any attempt to develop therapy targeted at neuroinflammation for diseases such as AIDS dementia, Alzheimer's disease or Multiple Sclerosis will require some means of monitoring the inflammatory pathogenic process, activated brain macrophages. Imaging brain macrophages may provide a better index of disease progression during treatment with antiinflammatory and other potentially neuroprotective drugs. PET imaging of brain macrophages with PBR ligands may be able to help in the early prediction of neuroinflammation, monitor the severity and progression of the disease, and help evaluate the effectiveness of CNS therapies aimed at decreasing neuroinflammation.

BIBLIOGRAPHY

1. 1996. Clinical confirmation of the American Academy of Neurology algorithm for HIV-1-associated cognitive/motor disorder. The Dana Consortium on Therapy for HIV Dementia and Related Cognitive Disorders. Neurology **47:**1247-53.
2. **Achim, C. L., M. P. Heyes, and C. A. Wiley.** 1993. Quantitation of human immunodeficiency virus, immune activation factors, and quinolinic acid in AIDS brains. J Clin Invest **91:**2769-75.
3. **Adamson, D. C., J. C. McArthur, T. M. Dawson, and V. L. Dawson.** 1999. Rate and severity of HIV-associated dementia (HAD): correlations with Gp41 and iNOS. Mol Med **5:**98-109.
4. **Adamson, D. C., B. Wildemann, M. Sasaki, J. D. Glass, J. C. McArthur, V. I. Christov, T. M. Dawson, and V. L. Dawson.** 1996. Immunologic NO synthase: elevation in severe AIDS dementia and induction by HIV-1 gp41. Science **274:**1917-21.
5. **Agnello, D., L. Carvelli, V. Muzio, P. Villa, B. Bottazzi, N. Polentarutti, T. Mennini, A. Mantovani, and P. Ghezzi.** 2000. Increased peripheral benzodiazepine binding sites and pentraxin 3 expression in the spinal cord during EAE: relation to inflammatory cytokines and modulation by dexamethasone and rolipram. J Neuroimmunol **109:**105-11.
6. **Aisen, P. S., K. A. Schafer, M. Grundman, E. Pfeiffer, M. Sano, K. L. Davis, M. R. Farlow, S. Jin, R. G. Thomas, and L. J. Thal.** 2003. Effects of rofecoxib or naproxen vs placebo on Alzheimer disease progression: a randomized controlled trial. Jama **289:**2819-26.
7. **Akiyama, H., C. Schwab, H. Kondo, H. Mori, F. Kametani, K. Ikeda, and P. L. McGeer.** 1996. Granules in glial cells of patients with Alzheimer's disease are immunopositive for C-terminal sequences of beta-amyloid protein. Neurosci Lett **206:**169-72.
8. **Albert, M. S., and D. A. Drachman.** 2000. Alzheimer's disease: what is it, how many people have it, and why do we need to know? Neurology **55:**166-8.
9. **Alkhatib, G., C. Combadiere, C. C. Broder, Y. Feng, P. E. Kennedy, P. M. Murphy, and E. A. Berger.** 1996. CC CKR5: a RANTES, MIP-1alpha, MIP-1beta receptor as a fusion cofactor for macrophage-tropic HIV-1. Science **272:**1955-8.
10. **Anders, K. H., W. F. Guerra, U. Tomiyasu, M. A. Verity, and H. V. Vinters.** 1986. The neuropathology of AIDS. UCLA experience and review. Am J Pathol **124:**537-58.
11. **Aquaro, S., P. Bagnarelli, T. Guenci, A. De Luca, M. Clementi, E. Balestra, R. Calio, and C. F. Perno.** 2002. Long-term survival and virus production in human primary macrophages infected by human immunodeficiency virus. J Med Virol **68:**479-88.

12. **Aquaro, S., E. Balestra, A. Cenci, M. Francesconi, R. Calio, and C. F. Perno.** 1997. HIV infection in macrophage: role of long-lived cells and related therapeutical strategies. J Biol Regul Homeost Agents **11:**69-73.
13. **Autran, B., G. Carcelain, T. S. Li, C. Blanc, D. Mathez, R. Tubiana, C. Katlama, P. Debre, and J. Leibowitch.** 1997. Positive effects of combined antiretroviral therapy on CD4+ T cell homeostasis and function in advanced HIV disease. Science **277:**112-6.
14. **Avison, M. J., A. Nath, and J. R. Berger.** 2002. Understanding pathogenesis and treatment of HIV dementia: a role for magnetic resonance? Trends Neurosci **25:**468-73.
15. **Aylward, E. H., J. D. Henderer, J. C. McArthur, P. D. Brettschneider, G. J. Harris, P. E. Barta, and G. D. Pearlson.** 1993. Reduced basal ganglia volume in HIV-1-associated dementia: results from quantitative neuroimaging. Neurology **43:**2099-104.
16. **Bamberger, M. E., and G. E. Landreth.** 2001. Microglial interaction with beta-amyloid: implications for the pathogenesis of Alzheimer's disease. Microsc Res Tech **54:**59-70.
17. **Banati, R. B.** 2002. Visualising microglial activation in vivo. Glia **40:**206-17.
18. **Banati, R. B., G. W. Goerres, R. Myers, R. N. Gunn, F. E. Turkheimer, G. W. Kreutzberg, D. J. Brooks, T. Jones, and J. S. Duncan.** 1999. [11C](R)-PK11195 positron emission tomography imaging of activated microglia in vivo in Rasmussen's encephalitis. Neurology **53:**2199-203.
19. **Banati, R. B., R. Myers, and G. W. Kreutzberg.** 1997. PK ('peripheral benzodiazepine')--binding sites in the CNS indicate early and discrete brain lesions: microautoradiographic detection of [3H]PK11195 binding to activated microglia. J Neurocytol **26:**77-82.
20. **Banati, R. B., J. Newcombe, R. N. Gunn, A. Cagnin, F. Turkheimer, F. Heppner, G. Price, F. Wegner, G. Giovannoni, D. H. Miller, G. D. Perkin, T. Smith, A. K. Hewson, G. Bydder, G. W. Kreutzberg, T. Jones, M. L. Cuzner, and R. Myers.** 2000. The peripheral benzodiazepine binding site in the brain in multiple sclerosis: quantitative in vivo imaging of microglia as a measure of disease activity. Brain **123 (Pt 11):**2321-37.
21. **Bard, F., R. Barbour, C. Cannon, R. Carretto, M. Fox, D. Games, T. Guido, K. Hoenow, K. Hu, K. Johnson-Wood, K. Khan, D. Kholodenko, C. Lee, M. Lee, R. Motter, M. Nguyen, A. Reed, D. Schenk, P. Tang, N. Vasquez, P. Seubert, and T. Yednock.** 2003. Epitope and isotype specificities of antibodies to beta -amyloid peptide for protection against Alzheimer's disease-like neuropathology. Proc Natl Acad Sci U S A **100:**2023-8.
22. **Bard, F., C. Cannon, R. Barbour, R. L. Burke, D. Games, H. Grajeda, T. Guido, K. Hu, J. Huang, K. Johnson-Wood, K. Khan, D. Kholodenko, M. Lee, I. Lieberburg, R. Motter, M. Nguyen, F. Soriano, N. Vasquez, K. Weiss, B. Welch, P. Seubert, D. Schenk, and T. Yednock.** 2000. Peripherally administered antibodies against amyloid beta-peptide enter the central nervous system and reduce pathology in a mouse model of Alzheimer disease. Nat Med **6:**916-9.
23. **Barre-Sinoussi, F., J. C. Chermann, F. Rey, M. T. Nugeyre, S. Chamaret, J. Gruest, C. Dauguet, C. Axler-Blin, F. Vezinet-Brun, C. Rouzioux, W. Rozenbaum, and L. Montagnier.** 1983. Isolation of a T-lymphotropic retrovirus from a patient at risk for acquired immune deficiency syndrome (AIDS). Science **220:**868-71.

24. **Baskin, G. B., M. Murphey-Corb, E. D. Roberts, P. J. Didier, and L. N. Martin.** 1992. Correlates of SIV encephalitis in rhesus monkeys. J Med Primatol **21:**59-63.
25. **Bauer, J., T. Sminia, F. G. Wouterlood, and C. D. Dijkstra.** 1994. Phagocytic activity of macrophages and microglial cells during the course of acute and chronic relapsing experimental autoimmune encephalomyelitis. J Neurosci Res **38:**365-75.
26. **Bennett, D. A.** 2000. Part II. Clinical diagnosis and course of Alzheimer's disease. Dis Mon **46:**666-86.
27. **Benveniste, E. N., V. T. Nguyen, and G. M. O'Keefe.** 2001. Immunological aspects of microglia: relevance to Alzheimer's disease. Neurochem Int **39:**381-91.
28. **Benzing, W. C., J. R. Wujek, E. K. Ward, D. Shaffer, K. H. Ashe, S. G. Younkin, and K. R. Brunden.** 1999. Evidence for glial-mediated inflammation in aged APP(SW) transgenic mice. Neurobiol Aging **20:**581-9.
29. **Bergamini, A., E. Faggioli, F. Bolacchi, S. Gessani, L. Cappannoli, I. Uccella, F. Demin, M. Capozzi, R. Cicconi, R. Placido, S. Vendetti, G. M. Colizzi, and G. Rocchi.** 1999. Enhanced production of tumor necrosis factor-alpha and interleukin-6 due to prolonged response to lipopolysaccharide in human macrophages infected in vitro with human immunodeficiency virus type 1. J Infect Dis **179:**832-42.
30. **Bianca, V. D., S. Dusi, E. Bianchini, I. Dal Pra, and F. Rossi.** 1999. beta-amyloid activates the O-2 forming NADPH oxidase in microglia, monocytes, and neutrophils. A possible inflammatory mechanism of neuronal damage in Alzheimer's disease. J Biol Chem **274:**15493-9.
31. **Biegon, A., M. Alvarado, T. F. Budinger, R. Grossman, K. Hensley, M. S. West, Y. Kotake, M. Ono, and R. A. Floyd.** 2002. Region-selective effects of neuroinflammation and antioxidant treatment on peripheral benzodiazepine receptors and NMDA receptors in the rat brain. J Neurochem **82:**924-34.
32. **Bissel, S. J., G. Wang, M. Ghosh, T. A. Reinhart, S. Capuano, 3rd, K. Stefano Cole, M. Murphey-Corb, M. Piatak Jr, Jr., J. D. Lifson, and C. A. Wiley.** 2002. Macrophages relate presynaptic and postsynaptic damage in simian immunodeficiency virus encephalitis. Am J Pathol **160:**927-41.
33. **Bleich, S., J. Wiltfang, and J. Kornhuber.** 2003. Memantine in moderate-to-severe Alzheimer's disease. N Engl J Med **349:**609-10; author reply 609-10.
34. **Borchelt, D. R., T. Ratovitski, J. van Lare, M. K. Lee, V. Gonzales, N. A. Jenkins, N. G. Copeland, D. L. Price, and S. S. Sisodia.** 1997. Accelerated amyloid deposition in the brains of transgenic mice coexpressing mutant presenilin 1 and amyloid precursor proteins. Neuron **19:**939-45.
35. **Bourdiol, F., S. Toulmond, A. Serrano, J. Benavides, and B. Scatton.** 1991. Increase in omega 3 (peripheral type benzodiazepine) binding sites in the rat cortex and striatum after local injection of interleukin-1, tumour necrosis factor-alpha and lipopolysaccharide. Brain Res **543:**194-200.
36. **Bradbury, J.** 2005. Hope for AD with NGF gene-therapy trial. Lancet Neurol **4:**335.
37. **Brew, B. J.** 1999. AIDS dementia complex. Neurol Clin **17:**861-81.
38. **Brew, B. J., M. Rosenblum, K. Cronin, and R. W. Price.** 1995. AIDS dementia complex and HIV-1 brain infection: clinical-virological correlations. Ann Neurol **38:**563-70.
39. **Budka, H.** 1991. Neuropathology of human immunodeficiency virus infection. Brain Pathol **1:**163-75.

40. **Budka, H., G. Costanzi, S. Cristina, A. Lechi, C. Parravicini, R. Trabattoni, and L. Vago.** 1987. Brain pathology induced by infection with the human immunodeficiency virus (HIV). A histological, immunocytochemical, and electron microscopical study of 100 autopsy cases. Acta Neuropathol (Berl) **75:**185-98.
41. **Cagnin, A., D. J. Brooks, A. M. Kennedy, R. N. Gunn, R. Myers, F. E. Turkheimer, T. Jones, and R. B. Banati.** 2001. In-vivo measurement of activated microglia in dementia. Lancet **358:**461-7.
42. **Cagnin, A., A. Gerhard, and R. B. Banati.** 2002. In vivo imaging of neuroinflammation. Eur Neuropsychopharmacol **12:**581-6.
43. **Cagnin, A., R. Myers, R. N. Gunn, A. D. Lawrence, T. Stevens, G. W. Kreutzberg, T. Jones, and R. B. Banati.** 2001. In vivo visualization of activated glia by [11C] (R)-PK11195-PET following herpes encephalitis reveals projected neuronal damage beyond the primary focal lesion. Brain **124:**2014-27.
44. **Carayon, P., M. Portier, D. Dussossoy, A. Bord, G. Petitpretre, X. Canat, G. Le Fur, and P. Casellas.** 1996. Involvement of peripheral benzodiazepine receptors in the protection of hematopoietic cells against oxygen radical damage. Blood **87:**3170-8.
45. **Casellas, P., S. Galiegue, and A. S. Basile.** 2002. Peripheral benzodiazepine receptors and mitochondrial function. Neurochem Int **40:**475-86.
46. **Castedo, M., J. L. Perfettini, and G. Kroemer.** 2002. Mitochondrial apoptosis and the peripheral benzodiazepine receptor: a novel target for viral and pharmacological manipulation. J Exp Med **196:**1121-5.
47. **Chaki, S., T. Funakoshi, R. Yoshikawa, S. Okuyama, T. Okubo, A. Nakazato, M. Nagamine, and K. Tomisawa.** 1999. Binding characteristics of [3H]DAA1106, a novel and selective ligand for peripheral benzodiazepine receptors. Eur J Pharmacol **371:**197-204.
48. **Chan, A., R. Seguin, T. Magnus, C. Papadimitriou, K. V. Toyka, J. P. Antel, and R. Gold.** 2003. Phagocytosis of apoptotic inflammatory cells by microglia and its therapeutic implications: termination of CNS autoimmune inflammation and modulation by interferon-beta. Glia **43:**231-42.
49. **Chang, L., T. Ernst, M. Leonido-Yee, I. Walot, and E. Singer.** 1999. Cerebral metabolite abnormalities correlate with clinical severity of HIV-1 cognitive motor complex. Neurology **52:**100-8.
50. **Chang, L., O. Speck, E. N. Miller, J. Braun, J. Jovicich, C. Koch, L. Itti, and T. Ernst.** 2001. Neural correlates of attention and working memory deficits in HIV patients. Neurology **57:**1001-7.
51. **Chao, C. C., S. Hu, T. W. Molitor, E. G. Shaskan, and P. K. Peterson.** 1992. Activated microglia mediate neuronal cell injury via a nitric oxide mechanism. J Immunol **149:**2736-41.
52. **Chao, C. C., S. Hu, and P. K. Peterson.** 1995. Modulation of human microglial cell superoxide production by cytokines. J Leukoc Biol **58:**65-70.
53. **Chao, C. C., S. Hu, W. S. Sheng, and P. K. Peterson.** 1995. Tumor necrosis factor-alpha production by human fetal microglial cells: regulation by other cytokines. Dev Neurosci **17:**97-105.
54. **Chen, M. K., K. Baidoo, T. Verina, and T. R. Guilarte.** 2004. Peripheral benzodiazepine receptor imaging in CNS demyelination: functional implications of anatomical and cellular localization. Brain **127:**1379-92.

55. **Cherner, M., E. Masliah, R. J. Ellis, T. D. Marcotte, D. J. Moore, I. Grant, and R. K. Heaton.** 2002. Neurocognitive dysfunction predicts postmortem findings of HIV encephalitis. Neurology **59:**1563-7.
56. **Cicchetti, F., A. L. Brownell, K. Williams, Y. I. Chen, E. Livni, and O. Isacson.** 2002. Neuroinflammation of the nigrostriatal pathway during progressive 6-OHDA dopamine degeneration in rats monitored by immunohistochemistry and PET imaging. Eur J Neurosci **15:**991-8.
57. **Cinque, P., P. Scarpellini, L. Vago, A. Linde, and A. Lazzarin.** 1997. Diagnosis of central nervous system complications in HIV-infected patients: cerebrospinal fluid analysis by the polymerase chain reaction. Aids **11:**1-17.
58. **Cinque, P., L. Vago, M. Mengozzi, V. Torri, D. Ceresa, E. Vicenzi, P. Transidico, A. Vagani, S. Sozzani, A. Mantovani, A. Lazzarin, and G. Poli.** 1998. Elevated cerebrospinal fluid levels of monocyte chemotactic protein-1 correlate with HIV-1 encephalitis and local viral replication. Aids **12:**1327-32.
59. **Citron, M.** 2004. Strategies for disease modification in Alzheimer's disease. Nat Rev Neurosci **5:**677-85.
60. **Cleij MC, A. F., Baron JC, Clark JC.** 2003. Presented at the 15th International Symposium on Radiopharmaceutical Chemistry.
61. **Colton, C. A., J. E. Keri, W. T. Chen, and W. L. Monsky.** 1993. Protease production by cultured microglia: substrate gel analysis and immobilized matrix degradation. J Neurosci Res **35:**297-304.
62. **Crompton, M.** 1999. The mitochondrial permeability transition pore and its role in cell death. Biochem J **341 (Pt 2):**233-49.
63. **Czub, S., J. G. Muller, M. Czub, and H. K. Muller-Hermelink.** 1996. Impact of various simian immunodeficiency virus variants on induction and nature of neuropathology in macaques. Res Virol **147:**165-70.
64. **D'Aversa, T. G., K. M. Weidenheim, and J. W. Berman.** 2002. CD40-CD40L interactions induce chemokine expression by human microglia: implications for human immunodeficiency virus encephalitis and multiple sclerosis. Am J Pathol **160:**559-67.
65. **Dal Pan, G. J., J. H. McArthur, E. Aylward, O. A. Selnes, T. E. Nance-Sproson, A. J. Kumar, E. D. Mellits, and J. C. McArthur.** 1992. Patterns of cerebral atrophy in HIV-1-infected individuals: results of a quantitative MRI analysis. Neurology **42:**2125-30.
66. **Das, P., V. Howard, N. Loosbrock, D. Dickson, M. P. Murphy, and T. E. Golde.** 2003. Amyloid-beta immunization effectively reduces amyloid deposition in FcRgamma-/- knock-out mice. J Neurosci **23:**8532-8.
67. **Davalos, D., J. Grutzendler, G. Yang, J. V. Kim, Y. Zuo, S. Jung, D. R. Littman, M. L. Dustin, and W. B. Gan.** 2005. ATP mediates rapid microglial response to local brain injury in vivo. Nat Neurosci **8:**752-8.
68. **Davis, L. E., B. L. Hjelle, V. E. Miller, D. L. Palmer, A. L. Llewellyn, T. L. Merlin, S. A. Young, R. G. Mills, W. Wachsman, and C. A. Wiley.** 1992. Early viral brain invasion in iatrogenic human immunodeficiency virus infection. Neurology **42:**1736-9.
69. **Debruyne, J. C., J. Versijpt, K. J. Van Laere, F. De Vos, J. Keppens, K. Strijckmans, E. Achten, G. Slegers, R. A. Dierckx, J. Korf, and J. L. De Reuck.** 2003. PET visualization of microglia in multiple sclerosis patients using [11C]PK11195. Eur J Neurol **10:**257-64.

70. **Del Rio Hortega, P.** 1932. Cytology and Cellular Pathology of the Nervous system, Penfield, W., ed. ed. Hoeber, New York.
71. **DeMattos, R. B., K. R. Bales, D. J. Cummins, J. C. Dodart, S. M. Paul, and D. M. Holtzman.** 2001. Peripheral anti-A beta antibody alters CNS and plasma A beta clearance and decreases brain A beta burden in a mouse model of Alzheimer's disease. Proc Natl Acad Sci U S A **98:**8850-5.
72. **Dickson, D. W.** 1999. Microglia in Alzheimer's disease and transgenic models. How close the fit? Am J Pathol **154:**1627-31.
73. **Doody, R. S.** 1999. Therapeutic standards in Alzheimer disease. Alzheimer Dis Assoc Disord **13 Suppl 2:**S20-6.
74. **Dore, G. J., P. K. Correll, Y. Li, J. M. Kaldor, D. A. Cooper, and B. J. Brew.** 1999. Changes to AIDS dementia complex in the era of highly active antiretroviral therapy. Aids **13:**1249-53.
75. **Dragic, T., V. Litwin, G. P. Allaway, S. R. Martin, Y. Huang, K. A. Nagashima, C. Cayanan, P. J. Maddon, R. A. Koup, J. P. Moore, and W. A. Paxton.** 1996. HIV-1 entry into CD4+ cells is mediated by the chemokine receptor CC-CKR-5. Nature **381:**667-73.
76. **Du, Y., Z. Ma, S. Lin, R. C. Dodel, F. Gao, K. R. Bales, L. C. Triarhou, E. Chernet, K. W. Perry, D. L. Nelson, S. Luecke, L. A. Phebus, F. P. Bymaster, and S. M. Paul.** 2001. Minocycline prevents nigrostriatal dopaminergic neurodegeneration in the MPTP model of Parkinson's disease. Proc Natl Acad Sci U S A **98:**14669-74.
77. **Ekdahl, C. T., J. H. Claasen, S. Bonde, Z. Kokaia, and O. Lindvall.** 2003. Inflammation is detrimental for neurogenesis in adult brain. Proc Natl Acad Sci U S A **100:**13632-7.
78. **Ernst, T., L. Chang, and S. Arnold.** 2003. Increased glial metabolites predict increased working memory network activation in HIV brain injury. Neuroimage **19:**1686-93.
79. **Everall, I. P., R. K. Heaton, T. D. Marcotte, R. J. Ellis, J. A. McCutchan, J. H. Atkinson, I. Grant, M. Mallory, and E. Masliah.** 1999. Cortical synaptic density is reduced in mild to moderate human immunodeficiency virus neurocognitive disorder. HNRC Group. HIV Neurobehavioral Research Center. Brain Pathol **9:**209-17.
80. **Everett, H., M. Barry, X. Sun, S. F. Lee, C. Frantz, L. G. Berthiaume, G. McFadden, and R. C. Bleackley.** 2002. The myxoma poxvirus protein, M11L, prevents apoptosis by direct interaction with the mitochondrial permeability transition pore. J Exp Med **196:**1127-39.
81. **Everett, H., and G. McFadden.** 2001. Viruses and apoptosis: meddling with mitochondria. Virology **288:**1-7.
82. **Fauci, A. S., G. Pantaleo, S. Stanley, and D. Weissman.** 1996. Immunopathogenic mechanisms of HIV infection. Ann Intern Med **124:**654-63.
83. **Fedoroff, S., R. Zhai, and J. P. Novak.** 1997. Microglia and astroglia have a common progenitor cell. J Neurosci Res **50:**477-86.
84. **Feng, Y., C. C. Broder, P. E. Kennedy, and E. A. Berger.** 1996. HIV-1 entry cofactor: functional cDNA cloning of a seven-transmembrane, G protein-coupled receptor. Science **272:**872-7.
85. **Ferrer, I., M. Boada Rovira, M. L. Sanchez Guerra, M. J. Rey, and F. Costa-Jussa.** 2004. Neuropathology and pathogenesis of encephalitis following amyloid-beta immunization in Alzheimer's disease. Brain Pathol **14:**11-20.

86. **Fetler, L., and S. Amigorena.** 2005. Neuroscience. Brain under surveillance: the microglia patrol. Science **309:**392-3.
87. **Frackowiak, J., H. M. Wisniewski, J. Wegiel, G. S. Merz, K. Iqbal, and K. C. Wang.** 1992. Ultrastructure of the microglia that phagocytose amyloid and the microglia that produce beta-amyloid fibrils. Acta Neuropathol (Berl) **84:**225-33.
88. **Frautschy, S. A., G. M. Cole, and A. Baird.** 1992. Phagocytosis and deposition of vascular beta-amyloid in rat brains injected with Alzheimer beta-amyloid. Am J Pathol **140:**1389-99.
89. **Frautschy, S. A., F. Yang, M. Irrizarry, B. Hyman, T. C. Saido, K. Hsiao, and G. M. Cole.** 1998. Microglial response to amyloid plaques in APPsw transgenic mice. Am J Pathol **152:**307-17.
90. **Garaci, E., M. C. Caroleo, L. Aloe, S. Aquaro, M. Piacentini, N. Costa, A. Amendola, A. Micera, R. Calio, C. F. Perno, and R. Levi-Montalcini.** 1999. Nerve growth factor is an autocrine factor essential for the survival of macrophages infected with HIV. Proc Natl Acad Sci U S A **96:**14013-8.
91. **Gavish, M., I. Bachman, R. Shoukrun, Y. Katz, L. Veenman, G. Weisinger, and A. Weizman.** 1999. Enigma of the peripheral benzodiazepine receptor. Pharmacol Rev **51:**629-50.
92. **Gehlert, D. R., D. T. Stephenson, D. A. Schober, K. Rash, and J. A. Clemens.** 1997. Increased expression of peripheral benzodiazepine receptors in the facial nucleus following motor neuron axotomy. Neurochem Int **31:**705-13.
93. **Gehrmann, J., Y. Matsumoto, and G. W. Kreutzberg.** 1995. Microglia: intrinsic immuneffector cell of the brain. Brain Res Brain Res Rev **20:**269-87.
94. **Geraci, A. P., and D. M. Simpson.** 2001. Neurological manifestations of HIV-1 infection in the HAART era. Compr Ther **27:**232-41.
95. **Gerhard, A., R. B. Banati, G. B. Goerres, A. Cagnin, R. Myers, R. N. Gunn, F. Turkheimer, C. D. Good, C. J. Mathias, N. Quinn, J. Schwarz, and D. J. Brooks.** 2003. [(11)C](R)-PK11195 PET imaging of microglial activation in multiple system atrophy. Neurology **61:**686-9.
96. **Giulian, D., T. J. Baker, L. C. Shih, and L. B. Lachman.** 1986. Interleukin 1 of the central nervous system is produced by ameboid microglia. J Exp Med **164:**594-604.
97. **Glass, J. D., H. Fedor, S. L. Wesselingh, and J. C. McArthur.** 1995. Immunocytochemical quantitation of human immunodeficiency virus in the brain: correlations with dementia. Ann Neurol **38:**755-62.
98. **Glass, J. D., S. L. Wesselingh, O. A. Selnes, and J. C. McArthur.** 1993. Clinical-neuropathologic correlation in HIV-associated dementia. Neurology **43:**2230-7.
99. **Goedert, M.** 1993. Tau protein and the neurofibrillary pathology of Alzheimer's disease. Trends Neurosci **16:**460-5.
100. **Gold, M. R., V. Duronio, S. P. Saxena, J. W. Schrader, and R. Aebersold.** 1994. Multiple cytokines activate phosphatidylinositol 3-kinase in hemopoietic cells. Association of the enzyme with various tyrosine-phosphorylated proteins. J Biol Chem **269:**5403-12.
101. **Gonzalez, E., B. H. Rovin, L. Sen, G. Cooke, R. Dhanda, S. Mummidi, H. Kulkarni, M. J. Bamshad, V. Telles, S. A. Anderson, E. A. Walter, K. T. Stephan, M. Deucher, A. Mangano, R. Bologna, S. S. Ahuja, M. J. Dolan, and S. K. Ahuja.** 2002. HIV-1 infection and AIDS dementia are influenced by a mutant MCP-1 allele linked to

increased monocyte infiltration of tissues and MCP-1 levels. Proc Natl Acad Sci U S A **99:**13795-800.

102. **Gonzalez-Scarano, F., and G. Baltuch.** 1999. Microglia as mediators of inflammatory and degenerative diseases. Annu Rev Neurosci **22:**219-40.
103. **Gordon, M. N., L. A. Holcomb, P. T. Jantzen, G. DiCarlo, D. Wilcock, K. W. Boyett, K. Connor, J. Melachrino, J. P. O'Callaghan, and D. Morgan.** 2002. Time course of the development of Alzheimer-like pathology in the doubly transgenic PS1+APP mouse. Exp Neurol **173:**183-95.
104. **Gorry, P. R., G. Bristol, J. A. Zack, K. Ritola, R. Swanstrom, C. J. Birch, J. E. Bell, N. Bannert, K. Crawford, H. Wang, D. Schols, E. De Clercq, K. Kunstman, S. M. Wolinsky, and D. Gabuzda.** 2001. Macrophage tropism of human immunodeficiency virus type 1 isolates from brain and lymphoid tissues predicts neurotropism independent of coreceptor specificity. J Virol **75:**10073-89.
105. **Gray, F., F. Chretien, A. V. Vallat-Decouvelaere, and F. Scaravilli.** 2003. The changing pattern of HIV neuropathology in the HAART era. J Neuropathol Exp Neurol **62:**429-40.
106. **Gray, F., and C. Keohane.** 2003. The neuropathology of HIV infection in the era of Highly Active AntiRetroviral Therapy (HAART). Brain Pathol **13:**79-83.
107. **Grimaldi, L. M., G. V. Martino, D. M. Franciotta, R. Brustia, A. Castagna, R. Pristera, and A. Lazzarin.** 1991. Elevated alpha-tumor necrosis factor levels in spinal fluid from HIV-1-infected patients with central nervous system involvement. Ann Neurol **29:**21-5.
108. **Gunn, R. N., A. A. Lammertsma, S. P. Hume, and V. J. Cunningham.** 1997. Parametric imaging of ligand-receptor binding in PET using a simplified reference region model. Neuroimage **6:**279-87.
109. **Gunn, R. N., P. A. Sargent, C. J. Bench, E. A. Rabiner, S. Osman, V. W. Pike, S. P. Hume, P. M. Grasby, and A. A. Lammertsma.** 1998. Tracer kinetic modeling of the 5-HT1A receptor ligand [carbonyl-11C]WAY-100635 for PET. Neuroimage **8:**426-40.
110. **Hansen, L. A., and R. D. Terry.** 1997. Position paper on diagnostic criteria for Alzheimer disease. Neurobiol Aging **18:**S71-3.
111. **Hardy, J., and D. J. Selkoe.** 2002. The amyloid hypothesis of Alzheimer's disease: progress and problems on the road to therapeutics. Science **297:**353-6.
112. **Harris, M. H., and C. B. Thompson.** 2000. The role of the Bcl-2 family in the regulation of outer mitochondrial membrane permeability. Cell Death Differ **7:**1182-91.
113. **Hastings, T. G., D. A. Lewis, and M. J. Zigmond.** 1996. Role of oxidation in the neurotoxic effects of intrastriatal dopamine injections. Proc Natl Acad Sci U S A **93:**1956-61.
114. **Heyes, M. P., C. L. Achim, C. A. Wiley, E. O. Major, K. Saito, and S. P. Markey.** 1996. Human microglia convert l-tryptophan into the neurotoxin quinolinic acid. Biochem J **320 (Pt 2):**595-7.
115. **Heyes, M. P., B. J. Brew, A. Martin, R. W. Price, A. M. Salazar, J. J. Sidtis, J. A. Yergey, M. M. Mouradian, A. E. Sadler, J. Keilp, and et al.** 1991. Quinolinic acid in cerebrospinal fluid and serum in HIV-1 infection: relationship to clinical and neurological status. Ann Neurol **29:**202-9.

116. **Hickey, W. F., K. Vass, and H. Lassmann.** 1992. Bone marrow-derived elements in the central nervous system: an immunohistochemical and ultrastructural survey of rat chimeras. J Neuropathol Exp Neurol **51:**246-56.
117. **Hirsch, J. D., C. F. Beyer, L. Malkowitz, B. Beer, and A. J. Blume.** 1989. Mitochondrial benzodiazepine receptors mediate inhibition of mitochondrial respiratory control. Mol Pharmacol **35:**157-63.
118. **Hirsch, S., J. M. Austyn, and S. Gordon.** 1981. Expression of the macrophage-specific antigen F4/80 during differentiation of mouse bone marrow cells in culture. J Exp Med **154:**713-25.
119. **in t' Veld, B. A., A. Ruitenberg, A. Hofman, L. J. Launer, C. M. van Duijn, T. Stijnen, M. M. Breteler, and B. H. Stricker.** 2001. Nonsteroidal antiinflammatory drugs and the risk of Alzheimer's disease. N Engl J Med **345:**1515-21.
120. **Janus, C., J. Pearson, J. McLaurin, P. M. Mathews, Y. Jiang, S. D. Schmidt, M. A. Chishti, P. Horne, D. Heslin, J. French, H. T. Mount, R. A. Nixon, M. Mercken, C. Bergeron, P. E. Fraser, P. St George-Hyslop, and D. Westaway.** 2000. A beta peptide immunization reduces behavioural impairment and plaques in a model of Alzheimer's disease. Nature **408:**979-82.
121. **Jayakumar, A. R., K. S. Panickar, and M. D. Norenberg.** 2002. Effects on free radical generation by ligands of the peripheral benzodiazepine receptor in cultured neural cells. J Neurochem **83:**1226-34.
122. **Joachim, C. L., J. H. Morris, and D. J. Selkoe.** 1989. Diffuse senile plaques occur commonly in the cerebellum in Alzheimer's disease. Am J Pathol **135:**309-19.
123. **Joe, B. N., M. B. Fukui, C. C. Meltzer, Q. S. Huang, R. S. Day, P. J. Greer, and M. E. Bozik.** 1999. Brain tumor volume measurement: comparison of manual and semiautomated methods. Radiology **212:**811-6.
124. **Johnson, L. A., J. D. Pearlman, C. A. Miller, T. I. Young, and K. R. Thulborn.** 1993. MR quantification of cerebral ventricular volume using a semiautomated algorithm. AJNR Am J Neuroradiol **14:**1373-8.
125. **Johnston, C., W. Jiang, T. Chu, and B. Levine.** 2001. Identification of genes involved in the host response to neurovirulent alphavirus infection. J Virol **75:**10431-45.
126. **Jordan-Sciutto, K. L., G. Wang, M. Murphey-Corb, and C. A. Wiley.** 2002. Cell cycle proteins exhibit altered expression patterns in lentiviral-associated encephalitis. J Neurosci **22:**2185-95.
127. **Kanazawa, H., K. Ohsawa, Y. Sasaki, S. Kohsaka, and Y. Imai.** 2002. Macrophage/microglia-specific protein Iba1 enhances membrane ruffling and Rac activation via phospholipase C-gamma -dependent pathway. J Biol Chem **277:**20026-32.
128. **Kaul, M., G. A. Garden, and S. A. Lipton.** 2001. Pathways to neuronal injury and apoptosis in HIV-associated dementia. Nature **410:**988-94.
129. **Kim, W. K., S. Y. Hwang, E. S. Oh, H. Z. Piao, K. W. Kim, and I. O. Han.** 2004. TGF-beta1 represses activation and resultant death of microglia via inhibition of phosphatidylinositol 3-kinase activity. J Immunol **172:**7015-23.
130. **Kitazawa, M., S. Oddo, T. R. Yamasaki, K. N. Green, and F. M. LaFerla.** 2005. Lipopolysaccharide-induced inflammation exacerbates tau pathology by a cyclin-dependent kinase 5-mediated pathway in a transgenic model of Alzheimer's disease. J Neurosci **25:**8843-53.

131. **Klatzmann, D., E. Champagne, S. Chamaret, J. Gruest, D. Guetard, T. Hercend, J. C. Gluckman, and L. Montagnier.** 1984. T-lymphocyte T4 molecule behaves as the receptor for human retrovirus LAV. Nature **312:**767-8.
132. **Klegeris, A., and P. L. McGeer.** 2005. Non-steroidal anti-inflammatory drugs (NSAIDs) and other anti-inflammatory agents in the treatment of neurodegenerative disease. Curr Alzheimer Res **2:**355-65.
133. **Klunk, W. E., B. J. Lopresti, M. D. Ikonomovic, I. M. Lefterov, R. P. Koldamova, E. E. Abrahamson, M. L. Debnath, D. P. Holt, G. F. Huang, L. Shao, S. T. DeKosky, J. C. Price, and C. A. Mathis.** 2005. Binding of the positron emission tomography tracer Pittsburgh compound-B reflects the amount of amyloid-beta in Alzheimer's disease brain but not in transgenic mouse brain. J Neurosci **25:**10598-606.
134. **Kosik, K. S.** 1990. Tau protein and Alzheimer's disease. Curr Opin Cell Biol **2:**101-4.
135. **Kreutzberg, G. W.** 1996. Microglia: a sensor for pathological events in the CNS. Trends Neurosci **19:**312-8.
136. **Kuhlmann, A. C., and T. R. Guilarte.** 2000. Cellular and subcellular localization of peripheral benzodiazepine receptors after trimethyltin neurotoxicity. J Neurochem **74:**1694-704.
137. **Lackner, A. A., M. O. Smith, R. J. Munn, D. J. Martfeld, M. B. Gardner, P. A. Marx, and S. Dandekar.** 1991. Localization of simian immunodeficiency virus in the central nervous system of rhesus monkeys. Am J Pathol **139:**609-21.
138. **Lammertsma, A. A., and S. P. Hume.** 1996. Simplified reference tissue model for PET receptor studies. Neuroimage **4:**153-8.
139. **Langford, T. D., S. L. Letendre, G. J. Larrea, and E. Masliah.** 2003. Changing patterns in the neuropathogenesis of HIV during the HAART era. Brain Pathol **13:**195-210.
140. **Lemere, C. A., A. Beierschmitt, M. Iglesias, E. T. Spooner, J. K. Bloom, J. F. Leverone, J. B. Zheng, T. J. Seabrook, D. Louard, D. Li, D. J. Selkoe, R. M. Palmour, and F. R. Ervin.** 2004. Alzheimer's disease abeta vaccine reduces central nervous system abeta levels in a non-human primate, the Caribbean vervet. Am J Pathol **165:**283-97.
141. **Levy, J. A.** 1994. HIV and the Pathogenesis of AIDS, Washington D.C.
142. **Lewandowska, E., E. Bertrand, J. Kulczycki, W. Lipczynska-Lojkowska, W. Lechowicz, and J. Stankiewicz.** 1999. Microglia and neuritic plaques in familial Alzheimer's disease induced by a new mutation of presenilin-1 gene. An ultrastructural study. Folia Neuropathol **37:**243-6.
143. **Lim, G. P., F. Yang, T. Chu, P. Chen, W. Beech, B. Teter, T. Tran, O. Ubeda, K. H. Ashe, S. A. Frautschy, and G. M. Cole.** 2000. Ibuprofen suppresses plaque pathology and inflammation in a mouse model for Alzheimer's disease. J Neurosci **20:**5709-14.
144. **Liu, H., H. Perlman, L. J. Pagliari, and R. M. Pope.** 2001. Constitutively activated Akt-1 is vital for the survival of human monocyte-differentiated macrophages. Role of Mcl-1, independent of nuclear factor (NF)-kappaB, Bad, or caspase activation. J Exp Med **194:**113-26.
145. **Lockhart, A., B. Davis, J. C. Matthews, H. Rahmoune, G. Hong, A. Gee, D. Earnshaw, and J. Brown.** 2003. The peripheral benzodiazepine receptor ligand PK11195 binds with high affinity to the acute phase reactant alpha1-acid glycoprotein:

implications for the use of the ligand as a CNS inflammatory marker(1). Nucl Med Biol **30:**199-206.

146. **Logan, J., J. S. Fowler, N. D. Volkow, G. J. Wang, Y. S. Ding, and D. L. Alexoff.** 1996. Distribution volume ratios without blood sampling from graphical analysis of PET data. J Cereb Blood Flow Metab **16:**834-40.
147. **Loy, R., D. Heyer, M. Clagett-Dame, and P. S. DiStefano.** 1990. Localization of NGF receptors in normal and Alzheimer's basal forebrain with monoclonal antibodies against the truncated form of the receptor. J Neurosci Res **27:**651-64.
148. **Lue, L. F., D. G. Walker, and J. Rogers.** 2001. Modeling microglial activation in Alzheimer's disease with human postmortem microglial cultures. Neurobiol Aging **22:**945-56.
149. **Maeda, J., T. Suhara, M. R. Zhang, T. Okauchi, F. Yasuno, Y. Ikoma, M. Inaji, Y. Nagai, A. Takano, S. Obayashi, and K. Suzuki.** 2004. Novel peripheral benzodiazepine receptor ligand [11C]DAA1106 for PET: An imaging tool for glial cells in the brain. Synapse **52:**283-91.
150. **Malm, T. M., M. Koistinaho, M. Parepalo, T. Vatanen, A. Ooka, S. Karlsson, and J. Koistinaho.** 2005. Bone-marrow-derived cells contribute to the recruitment of microglial cells in response to beta-amyloid deposition in APP/PS1 double transgenic Alzheimer mice. Neurobiol Dis **18:**134-42.
151. **Mankowski, J. L., S. E. Queen, P. J. Tarwater, R. J. Adams, and T. R. Guilarte.** 2003. Elevated peripheral benzodiazepine receptor expression in simian immunodeficiency virus encephalitis. J Neurovirol **9:**94-100.
152. **Mann, D. M.** 1985. The neuropathology of Alzheimer's disease: a review with pathogenetic, aetiological and therapeutic considerations. Mech Ageing Dev **31:**213-55.
153. **Masliah, E., C. L. Achim, N. Ge, R. DeTeresa, R. D. Terry, and C. A. Wiley.** 1992. Spectrum of human immunodeficiency virus-associated neocortical damage. Ann Neurol **32:**321-9.
154. **Masliah, E., R. M. DeTeresa, M. E. Mallory, and L. A. Hansen.** 2000. Changes in pathological findings at autopsy in AIDS cases for the last 15 years. Aids **14:**69-74.
155. **Masliah, E., L. Hansen, A. Adame, L. Crews, F. Bard, C. Lee, P. Seubert, D. Games, L. Kirby, and D. Schenk.** 2005. Abeta vaccination effects on plaque pathology in the absence of encephalitis in Alzheimer disease. Neurology **64:**129-31.
156. **Masliah, E., R. K. Heaton, T. D. Marcotte, R. J. Ellis, C. A. Wiley, M. Mallory, C. L. Achim, J. A. McCutchan, J. A. Nelson, J. H. Atkinson, and I. Grant.** 1997. Dendritic injury is a pathological substrate for human immunodeficiency virus-related cognitive disorders. HNRC Group. The HIV Neurobehavioral Research Center. Ann Neurol **42:**963-72.
157. **Masters, C. L., G. Multhaup, G. Simms, J. Pottgiesser, R. N. Martins, and K. Beyreuther.** 1985. Neuronal origin of a cerebral amyloid: neurofibrillary tangles of Alzheimer's disease contain the same protein as the amyloid of plaque cores and blood vessels. Embo J **4:**2757-63.
158. **McArthur, J. C.** 1997. NeuroAIDS: diagnosis and management. Hosp Pract (Off Ed) **32:**73-4, 77-9, 84 passim.
159. **McArthur, J. C., A. J. Kumar, D. W. Johnson, O. A. Selnes, J. T. Becker, C. Herman, B. A. Cohen, and A. Saah.** 1990. Incidental white matter hyperintensities on

magnetic resonance imaging in HIV-1 infection. Multicenter AIDS Cohort Study. J Acquir Immune Defic Syndr **3:**252-9.

160. **McEnery, M. W., A. M. Snowman, R. R. Trifiletti, and S. H. Snyder.** 1992. Isolation of the mitochondrial benzodiazepine receptor: association with the voltage-dependent anion channel and the adenine nucleotide carrier. Proc Natl Acad Sci U S A **89:**3170-4.
161. **McGeer, P. L., S. Itagaki, B. E. Boyes, and E. G. McGeer.** 1988. Reactive microglia are positive for HLA-DR in the substantia nigra of Parkinson's and Alzheimer's disease brains. Neurology **38:**1285-91.
162. **McGeer, P. L., S. Itagaki, H. Tago, and E. G. McGeer.** 1988. Occurrence of HLA-DR reactive microglia in Alzheimer's disease. Ann N Y Acad Sci **540:**319-23.
163. **McLaurin, J., R. Cecal, M. E. Kierstead, X. Tian, A. L. Phinney, M. Manea, J. E. French, M. H. Lambermon, A. A. Darabie, M. E. Brown, C. Janus, M. A. Chishti, P. Horne, D. Westaway, P. E. Fraser, H. T. Mount, M. Przybylski, and P. St George-Hyslop.** 2002. Therapeutically effective antibodies against amyloid-beta peptide target amyloid-beta residues 4-10 and inhibit cytotoxicity and fibrillogenesis. Nat Med **8:**1263-9.
164. **McManus, C. M., C. F. Brosnan, and J. W. Berman.** 1998. Cytokine induction of MIP-1 alpha and MIP-1 beta in human fetal microglia. J Immunol **160:**1449-55.
165. **Meda, L., M. A. Cassatella, G. I. Szendrei, L. Otvos, Jr., P. Baron, M. Villalba, D. Ferrari, and F. Rossi.** 1995. Activation of microglial cells by beta-amyloid protein and interferon-gamma. Nature **374:**647-50.
166. **Merrill, J. E., and I. S. Chen.** 1991. HIV-1, macrophages, glial cells, and cytokines in AIDS nervous system disease. Faseb J **5:**2391-7.
167. **Mesulam, M. M.** 1999. Neuroplasticity failure in Alzheimer's disease: bridging the gap between plaques and tangles. Neuron **24:**521-9.
168. **Minghetti, L., and G. Levi.** 1998. Microglia as effector cells in brain damage and repair: focus on prostanoids and nitric oxide. Prog Neurobiol **54:**99-125.
169. **Minshall, C., S. Arkins, G. G. Freund, and K. W. Kelley.** 1996. Requirement for phosphatidylinositol 3'-kinase to protect hemopoietic progenitors against apoptosis depends upon the extracellular survival factor. J Immunol **156:**939-47.
170. **Monje, M. L., H. Toda, and T. D. Palmer.** 2003. Inflammatory blockade restores adult hippocampal neurogenesis. Science **302:**1760-5.
171. **Morgan, D., D. M. Diamond, P. E. Gottschall, K. E. Ugen, C. Dickey, J. Hardy, K. Duff, P. Jantzen, G. DiCarlo, D. Wilcock, K. Connor, J. Hatcher, C. Hope, M. Gordon, and G. W. Arendash.** 2000. A beta peptide vaccination prevents memory loss in an animal model of Alzheimer's disease. Nature **408:**982-5.
172. **Morgan, D., M. N. Gordon, J. Tan, D. Wilcock, and A. M. Rojiani.** 2005. Dynamic complexity of the microglial activation response in transgenic models of amyloid deposition: implications for Alzheimer therapeutics. J Neuropathol Exp Neurol **64:**743-53.
173. **Muhleisen, H., J. Gehrmann, and R. Meyermann.** 1995. Reactive microglia in Creutzfeldt-Jakob disease. Neuropathol Appl Neurobiol **21:**505-17.
174. **Murman, D. L., and C. C. Colenda.** 2005. The economic impact of neuropsychiatric symptoms in Alzheimer's disease: can drugs ease the burden? Pharmacoeconomics **23:**227-42.

175. **Murphy, G. M., Jr., X. C. Jia, Y. Song, E. Ong, R. Shrivastava, V. Bocchini, Y. L. Lee, and L. F. Eng.** 1995. Macrophage inflammatory protein 1-alpha mRNA expression in an immortalized microglial cell line and cortical astrocyte cultures. J Neurosci Res **40:**755-63.
176. **Myers, R., L. G. Manjil, B. M. Cullen, G. W. Price, R. S. Frackowiak, and J. E. Cremer.** 1991. Macrophage and astrocyte populations in relation to [3H]PK 11195 binding in rat cerebral cortex following a local ischaemic lesion. J Cereb Blood Flow Metab **11:**314-22.
177. **Nath, A.** 2002. Human immunodeficiency virus (HIV) proteins in neuropathogenesis of HIV dementia. J Infect Dis **186 Suppl 2:**S193-8.
178. **Navia, B. A., E. S. Cho, C. K. Petito, and R. W. Price.** 1986. The AIDS dementia complex: II. Neuropathology. Ann Neurol **19:**525-35.
179. **Nicoll, J. A., D. Wilkinson, C. Holmes, P. Steart, H. Markham, and R. O. Weller.** 2003. Neuropathology of human Alzheimer disease after immunization with amyloid-beta peptide: a case report. Nat Med **9:**448-52.
180. **Nimmerjahn, A., F. Kirchhoff, and F. Helmchen.** 2005. Resting microglial cells are highly dynamic surveillants of brain parenchyma in vivo. Science **308:**1314-8.
181. **Nottet, H. S., Y. Persidsky, V. G. Sasseville, A. N. Nukuna, P. Bock, Q. H. Zhai, L. R. Sharer, R. D. McComb, S. Swindells, C. Soderland, and H. E. Gendelman.** 1996. Mechanisms for the transendothelial migration of HIV-1-infected monocytes into brain. J Immunol **156:**1284-95.
182. **O'Neil, S. P., C. Suwyn, D. C. Anderson, G. Niedziela, J. Bradley, F. J. Novembre, J. G. Herndon, and H. M. McClure.** 2004. Correlation of acute humoral response with brain virus burden and survival time in pig-tailed macaques infected with the neurovirulent simian immunodeficiency virus SIVsmmFGb. Am J Pathol **164:**1157-72.
183. **Oddo, S., A. Caccamo, J. D. Shepherd, M. P. Murphy, T. E. Golde, R. Kayed, R. Metherate, M. P. Mattson, Y. Akbari, and F. M. LaFerla.** 2003. Triple-transgenic model of Alzheimer's disease with plaques and tangles: intracellular Abeta and synaptic dysfunction. Neuron **39:**409-21.
184. **Oh, Y. J., J. W. Francis, G. J. Markelonis, and T. H. Oh.** 1992. Interleukin-1-beta and tumor necrosis factor-alpha increase peripheral-type benzodiazepine binding sites in cultured polygonal astrocytes. J Neurochem **58:**2131-8.
185. **Okuyama, S., S. Chaki, R. Yoshikawa, S. Ogawa, Y. Suzuki, T. Okubo, A. Nakazato, M. Nagamine, and K. Tomisawa.** 1999. Neuropharmacological profile of peripheral benzodiazepine receptor agonists, DAA1097 and DAA1106. Life Sci **64:**1455-64.
186. **Orandle, M. S., A. G. MacLean, V. G. Sasseville, X. Alvarez, and A. A. Lackner.** 2002. Enhanced expression of proinflammatory cytokines in the central nervous system is associated with neuroinvasion by simian immunodeficiency virus and the development of encephalitis. J Virol **76:**5797-802.
187. **Osaki, M., M. Oshimura, and H. Ito.** 2004. PI3K-Akt pathway: its functions and alterations in human cancer. Apoptosis **9:**667-76.
188. **Padmanabhan, J., D. Clayton, and M. L. Shelanski.** 1999. Dibutyryl cyclic AMP-induced process formation in astrocytes is associated with a decrease in tyrosine phosphorylation of focal adhesion kinase and paxillin. J Neurobiol **39:**407-22.

189. **Pantaleo, G., and A. S. Fauci.** 1996. Immunopathogenesis of HIV infection. Annu Rev Microbiol **50:**825-54.
190. **Papadopoulos, V., H. Amri, H. Li, N. Boujrad, B. Vidic, and M. Garnier.** 1997. Targeted disruption of the peripheral-type benzodiazepine receptor gene inhibits steroidogenesis in the R2C Leydig tumor cell line. J Biol Chem **272:**32129-35.
191. **Pappata, S., P. Cornu, Y. Samson, C. Prenant, J. Benavides, B. Scatton, C. Crouzel, J. J. Hauw, and A. Syrota.** 1991. PET study of carbon-11-PK 11195 binding to peripheral type benzodiazepine sites in glioblastoma: a case report. J Nucl Med **32:**1608-10.
192. **Paresce, D. M., H. Chung, and F. R. Maxfield.** 1997. Slow degradation of aggregates of the Alzheimer's disease amyloid beta-protein by microglial cells. J Biol Chem **272:**29390-7.
193. **Pascal, S., L. Resnick, W. W. Barker, D. Loewenstein, F. Yoshii, J. Y. Chang, T. Boothe, J. Sheldon, and R. Duara.** 1991. Metabolic asymmetries in asymptomatic HIV-1 seropositive subjects: relationship to disease onset and MRI findings. J Nucl Med **32:**1725-9.
194. **Paul, R., R. Cohen, B. Navia, and K. Tashima.** 2002. Relationships between cognition and structural neuroimaging findings in adults with human immunodeficiency virus type-1. Neurosci Biobehav Rev **26:**353-9.
195. **Peluso, R., A. Haase, L. Stowring, M. Edwards, and P. Ventura.** 1985. A Trojan Horse mechanism for the spread of visna virus in monocytes. Virology **147:**231-6.
196. **Perry, V. H., and S. Gordon.** 1991. Macrophages and the nervous system. Int Rev Cytol **125:**203-44.
197. **Persidsky, Y., M. Buttini, J. Limoges, P. Bock, and H. E. Gendelman.** 1997. An analysis of HIV-1-associated inflammatory products in brain tissue of humans and SCID mice with HIV-1 encephalitis. J Neurovirol **3:**401-16.
198. **Portegies, P., R. H. Enting, J. de Gans, P. R. Algra, M. M. Derix, J. M. Lange, and J. Goudsmit.** 1993. Presentation and course of AIDS dementia complex: 10 years of follow-up in Amsterdam, The Netherlands. Aids **7:**669-75.
199. **Post, M. J., B. E. Levin, J. R. Berger, R. Duncan, R. M. Quencer, and G. Calabro.** 1992. Sequential cranial MR findings of asymptomatic and neurologically symptomatic HIV+ subjects. AJNR Am J Neuroradiol **13:**359-70.
200. **Post, M. J., L. G. Tate, R. M. Quencer, G. T. Hensley, J. R. Berger, W. A. Sheremata, and G. Maul.** 1988. CT, MR, and pathology in HIV encephalitis and meningitis. AJR Am J Roentgenol **151:**373-80.
201. **Power, C., P. A. Kong, T. O. Crawford, S. Wesselingh, J. D. Glass, J. C. McArthur, and B. D. Trapp.** 1993. Cerebral white matter changes in acquired immunodeficiency syndrome dementia: alterations of the blood-brain barrier. Ann Neurol **34:**339-50.
202. **Price, R. W., C. T. Yiannoutsos, D. B. Clifford, L. Zaborski, A. Tselis, J. J. Sidtis, B. Cohen, C. D. Hall, A. Erice, and K. Henry.** 1999. Neurological outcomes in late HIV infection: adverse impact of neurological impairment on survival and protective effect of antiviral therapy. AIDS Clinical Trial Group and Neurological AIDS Research Consortium study team. Aids **13:**1677-85.
203. **Pulvirenti, J. J.** 2005. Inpatient care of the HIV infected patient in the highly active antiretroviral therapy (HAART) era. Curr HIV Res **3:**133-45.

204. **Raghavendra Rao, V. L., A. Dogan, K. K. Bowen, and R. J. Dempsey.** 2000. Traumatic brain injury leads to increased expression of peripheral-type benzodiazepine receptors, neuronal death, and activation of astrocytes and microglia in rat thalamus. Exp Neurol **161:**102-14.
205. **Raininko, R., I. Elovaara, A. Virta, L. Valanne, M. Haltia, and S. L. Valle.** 1992. Radiological study of the brain at various stages of human immunodeficiency virus infection: early development of brain atrophy. Neuroradiology **34:**190-6.
206. **Ramsay, S. C., C. Weiller, R. Myers, J. E. Cremer, S. K. Luthra, A. A. Lammertsma, and R. S. Frackowiak.** 1992. Monitoring by PET of macrophage accumulation in brain after ischaemic stroke. Lancet **339:**1054-5.
207. **Rey, C., C. Mauduit, O. Naureils, M. Benahmed, P. Louisot, and F. Gasnier.** 2000. Up-regulation of mitochondrial peripheral benzodiazepine receptor expression by tumor necrosis factor alpha in testicular leydig cells. Possible involvement in cell survival. Biochem Pharmacol **60:**1639-46.
208. **Righi, M., L. Mori, G. De Libero, M. Sironi, A. Biondi, A. Mantovani, S. D. Donini, and P. Ricciardi-Castagnoli.** 1989. Monokine production by microglial cell clones. Eur J Immunol **19:**1443-8.
209. **Rogers, J., and L. F. Lue.** 2001. Microglial chemotaxis, activation, and phagocytosis of amyloid beta-peptide as linked phenomena in Alzheimer's disease. Neurochem Int **39:**333-40.
210. **Rosci, M. A., F. Pigorini, A. Bernabei, F. M. Pau, V. Volpini, D. E. Merigliano, and M. F. Meligrana.** 1992. Methods for detecting early signs of AIDS dementia complex in asymptomatic HIV-1-infected subjects. Aids **6:**1309-16.
211. **Sacktor, N., M. P. McDermott, K. Marder, G. Schifitto, O. A. Selnes, J. C. McArthur, Y. Stern, S. Albert, D. Palumbo, K. Kieburtz, J. A. De Marcaida, B. Cohen, and L. Epstein.** 2002. HIV-associated cognitive impairment before and after the advent of combination therapy. J Neurovirol **8:**136-42.
212. **Sanchez-Pernaute, R., A. Ferree, O. Cooper, M. Yu, A. L. Brownell, and O. Isacson.** 2004. Selective COX-2 inhibition prevents progressive dopamine neuron degeneration in a rat model of Parkinson's disease. J Neuroinflammation **1:**6.
213. **Sanders, V. J., C. A. Pittman, M. G. White, G. Wang, C. A. Wiley, and C. L. Achim.** 1998. Chemokines and receptors in HIV encephalitis. Aids **12:**1021-6.
214. **Sargsyan, S. A., P. N. Monk, and P. J. Shaw.** 2005. Microglia as potential contributors to motor neuron injury in amyotrophic lateral sclerosis. Glia **51:**241-53.
215. **Sasaki, A., M. Shoji, Y. Harigaya, T. Kawarabayashi, M. Ikeda, M. Naito, E. Matsubara, K. Abe, and Y. Nakazato.** 2002. Amyloid cored plaques in Tg2576 transgenic mice are characterized by giant plaques, slightly activated microglia, and the lack of paired helical filament-typed, dystrophic neurites. Virchows Arch **441:**358-67.
216. **Sasaki, Y., K. Ohsawa, H. Kanazawa, S. Kohsaka, and Y. Imai.** 2001. Iba1 is an actin-cross-linking protein in macrophages/microglia. Biochem Biophys Res Commun **286:**292-7.
217. **Schenk, D.** 2002. Amyloid-beta immunotherapy for Alzheimer's disease: the end of the beginning. Nat Rev Neurosci **3:**824-8.
218. **Schenk, D., R. Barbour, W. Dunn, G. Gordon, H. Grajeda, T. Guido, K. Hu, J. Huang, K. Johnson-Wood, K. Khan, D. Kholodenko, M. Lee, Z. Liao, I. Lieberburg, R. Motter, L. Mutter, F. Soriano, G. Shopp, N. Vasquez, C. Vandevert, S. Walker,**

M. Wogulis, T. Yednock, D. Games, and P. Seubert. 1999. Immunization with amyloid-beta attenuates Alzheimer-disease-like pathology in the PDAPP mouse. Nature **400:**173-7.

219. **Schenk, D. B., and T. Yednock.** 2002. The role of microglia in Alzheimer's disease: friend or foe? Neurobiol Aging **23:**677-9; discussion 683-4.
220. **Schmitz, J. E., M. J. Kuroda, S. Santra, V. G. Sasseville, M. A. Simon, M. A. Lifton, P. Racz, K. Tenner-Racz, M. Dalesandro, B. J. Scallon, J. Ghrayeb, M. A. Forman, D. C. Montefiori, E. P. Rieber, N. L. Letvin, and K. A. Reimann.** 1999. Control of viremia in simian immunodeficiency virus infection by CD8+ lymphocytes. Science **283:**857-60.
221. **Selkoe, D. J.** 1994. Cell biology of the amyloid beta-protein precursor and the mechanism of Alzheimer's disease. Annu Rev Cell Biol **10:**373-403.
222. **Shah, F., S. P. Hume, V. W. Pike, S. Ashworth, and J. McDermott.** 1994. Synthesis of the enantiomers of [N-methyl-11C]PK 11195 and comparison of their behaviours as radioligands for PK binding sites in rats. Nucl Med Biol **21:**573-81.
223. **Sharer, L. R., E. S. Cho, and L. G. Epstein.** 1985. Multinucleated giant cells and HTLV-III in AIDS encephalopathy. Hum Pathol **16:**760.
224. **Simard, A. R., D. Soulet, G. Gowing, J. P. Julien, and S. Rivest.** 2006. Bone marrow-derived microglia play a critical role in restricting senile plaque formation in Alzheimer's disease. Neuron **49:**489-502.
225. **Smith, M. A., P. L. Richey Harris, L. M. Sayre, J. S. Beckman, and G. Perry.** 1997. Widespread peroxynitrite-mediated damage in Alzheimer's disease. J Neurosci **17:**2653-7.
226. **Solomon, B., R. Koppel, D. Frankel, and E. Hanan-Aharon.** 1997. Disaggregation of Alzheimer beta-amyloid by site-directed mAb. Proc Natl Acad Sci U S A **94:**4109-12.
227. **Sonnerborg, A., J. Saaf, B. Alexius, O. Strannegard, L. O. Wahlund, and L. Wetterberg.** 1990. Quantitative detection of brain aberrations in human immunodeficiency virus type 1-infected individuals by magnetic resonance imaging. J Infect Dis **162:**1245-51.
228. **Stalder, M., T. Deller, M. Staufenbiel, and M. Jucker.** 2001. 3D-Reconstruction of microglia and amyloid in APP23 transgenic mice: no evidence of intracellular amyloid. Neurobiol Aging **22:**427-34.
229. **Stalder, M., A. Phinney, A. Probst, B. Sommer, M. Staufenbiel, and M. Jucker.** 1999. Association of microglia with amyloid plaques in brains of APP23 transgenic mice. Am J Pathol **154:**1673-84.
230. **Starosta-Rubinstein, S., B. J. Ciliax, J. B. Penney, P. McKeever, and A. B. Young.** 1987. Imaging of a glioma using peripheral benzodiazepine receptor ligands. Proc Natl Acad Sci U S A **84:**891-5.
231. **Stephenson, D. T., D. A. Schober, E. B. Smalstig, R. E. Mincy, D. R. Gehlert, and J. A. Clemens.** 1995. Peripheral benzodiazepine receptors are colocalized with activated microglia following transient global forebrain ischemia in the rat. J Neurosci **15:**5263-74.
232. **Stephenson, F. A.** 1995. The GABAA receptors. Biochem J **310 (Pt 1):**1-9.
233. **Stewart, W. F., C. Kawas, M. Corrada, and E. J. Metter.** 1997. Risk of Alzheimer's disease and duration of NSAID use. Neurology **48:**626-32.
234. **Stoebner, P. E., P. Carayon, P. Casellas, M. Portier, T. Lavabre-Bertrand, P. Cuq, J. P. Cano, J. Meynadier, and L. Meunier.** 2001. Transient protection by peripheral

benzodiazepine receptors during the early events of ultraviolet light-induced apoptosis. Cell Death Differ **8:**747-53.

235. **Stoll, G., and S. Jander.** 1999. The role of microglia and macrophages in the pathophysiology of the CNS. Prog Neurobiol **58:**233-47.
236. **Tan, J., T. Town, D. Paris, T. Mori, Z. Suo, F. Crawford, M. P. Mattson, R. A. Flavell, and M. Mullan.** 1999. Microglial activation resulting from CD40-CD40L interaction after beta-amyloid stimulation. Science **286:**2352-5.
237. **Trincavelli, M. L., L. Marselli, A. Falleni, V. Gremigni, E. Ragge, F. Dotta, C. Santangelo, P. Marchetti, A. Lucacchini, and C. Martini.** 2002. Upregulation of mitochondrial peripheral benzodiazepine receptor expression by cytokine-induced damage of human pancreatic islets. J Cell Biochem **84:**636-44.
238. **Turner, M. R., A. Cagnin, F. E. Turkheimer, C. C. Miller, C. E. Shaw, D. J. Brooks, P. N. Leigh, and R. B. Banati.** 2004. Evidence of widespread cerebral microglial activation in amyotrophic lateral sclerosis: an [11C](R)-PK11195 positron emission tomography study. Neurobiol Dis **15:**601-9.
239. **Tyner, J. W., O. Uchida, N. Kajiwara, E. Y. Kim, A. C. Patel, M. P. O'Sullivan, M. J. Walter, R. A. Schwendener, D. N. Cook, T. M. Danoff, and M. J. Holtzman.** 2005. CCL5-CCR5 interaction provides antiapoptotic signals for macrophage survival during viral infection. Nat Med **11:**1180-7.
240. **Ulvestad, E., K. Williams, R. Matre, H. Nyland, A. Olivier, and J. Antel.** 1994. Fc receptors for IgG on cultured human microglia mediate cytotoxicity and phagocytosis of antibody-coated targets. J Neuropathol Exp Neurol **53:**27-36.
241. **UNAIDS.** 2004. AIDS epidemic update: 2004 Joint United Nations Programme on HIV/AIDS and Worls Health Organization.
242. **Valcour, V. G., C. M. Shikuma, M. R. Watters, and N. C. Sacktor.** 2004. Cognitive impairment in older HIV-1-seropositive individuals: prevalence and potential mechanisms. Aids **18 Suppl 1:**S79-86.
243. **Vassar, R., and M. Citron.** 2000. Abeta-generating enzymes: recent advances in beta- and gamma-secretase research. Neuron **27:**419-22.
244. **Veenman, L., S. Leschiner, I. Spanier, G. Weisinger, A. Weizman, and M. Gavish.** 2002. PK 11195 attenuates kainic acid-induced seizures and alterations in peripheral-type benzodiazepine receptor (PBR) protein components in the rat brain. J Neurochem **80:**917-27.
245. **Venneti, S., B. J. Lopresti, G. Wang, S. J. Bissel, C. A. Mathis, C. C. Meltzer, F. Boada, S. Capuano, 3rd, G. J. Kress, D. K. Davis, J. Ruszkiewicz, I. J. Reynolds, M. Murphey-Corb, A. M. Trichel, S. R. Wisniewski, and C. A. Wiley.** 2004. PET imaging of brain macrophages using the peripheral benzodiazepine receptor in a macaque model of neuroAIDS. J Clin Invest **113:**981-9.
246. **Vowinckel, E., D. Reutens, B. Becher, G. Verge, A. Evans, T. Owens, and J. P. Antel.** 1997. PK11195 binding to the peripheral benzodiazepine receptor as a marker of microglia activation in multiple sclerosis and experimental autoimmune encephalomyelitis. J Neurosci Res **50:**345-53.
247. **Webster, S. D., M. D. Galvan, E. Ferran, W. Garzon-Rodriguez, C. G. Glabe, and A. J. Tenner.** 2001. Antibody-mediated phagocytosis of the amyloid beta-peptide in microglia is differentially modulated by C1q. J Immunol **166:**7496-503.

248. **Weissman, B. A., G. T. Bolger, L. Isaac, S. M. Paul, and P. Skolnick.** 1984. Characterization of the binding of [3H]Ro 5-4864, a convulsant benzodiazepine, to guinea pig brain. J Neurochem **42:**969-75.
249. **Wenserski, F., H. J. von Giesen, H. J. Wittsack, A. Aulich, and G. Arendt.** 2003. Human immunodeficiency virus 1-associated minor motor disorders: perfusion-weighted MR imaging and H MR spectroscopy. Radiology **228:**185-92.
250. **Wesselingh, S. L., and K. A. Thompson.** 2001. Immunopathogenesis of HIV-associated dementia. Curr Opin Neurol **14:**375-9.
251. **Westmoreland, S. V., E. Halpern, and A. A. Lackner.** 1998. Simian immunodeficiency virus encephalitis in rhesus macaques is associated with rapid disease progression. J Neurovirol **4:**260-8.
252. **Wiley, C. A., and C. Achim.** 1994. Human immunodeficiency virus encephalitis is the pathological correlate of dementia in acquired immunodeficiency syndrome. Ann Neurol **36:**673-6.
253. **Wiley, C. A., C. L. Achim, C. Christopherson, Y. Kidane, S. Kwok, E. Masliah, J. Mellors, L. Radhakrishnan, G. Wang, and V. Soontornniyomkij.** 1999. HIV mediates a productive infection of the brain. Aids **13:**2055-9.
254. **Wiley, C. A., E. Masliah, M. Morey, C. Lemere, R. DeTeresa, M. Grafe, L. Hansen, and R. Terry.** 1991. Neocortical damage during HIV infection. Ann Neurol **29:**651-7.
255. **Wiley, C. A., R. D. Schrier, J. A. Nelson, P. W. Lampert, and M. B. Oldstone.** 1986. Cellular localization of human immunodeficiency virus infection within the brains of acquired immune deficiency syndrome patients. Proc Natl Acad Sci U S A **83:**7089-93.
256. **Williams, K. C., and W. F. Hickey.** 2002. Central nervous system damage, monocytes and macrophages, and neurological disorders in AIDS. Annu Rev Neurosci **25:**537-62.
257. **Wilt, S. G., E. Milward, J. M. Zhou, K. Nagasato, H. Patton, R. Rusten, D. E. Griffin, M. O'Connor, and M. Dubois-Dalcq.** 1995. In vitro evidence for a dual role of tumor necrosis factor-alpha in human immunodeficiency virus type 1 encephalopathy. Ann Neurol **37:**381-94.
258. **Wong, P. C., H. Cai, D. R. Borchelt, and D. L. Price.** 2002. Genetically engineered mouse models of neurodegenerative diseases. Nat Neurosci **5:**633-9.
259. **Woods, R. P., S. R. Cherry, and J. C. Mazziotta.** 1992. Rapid automated algorithm for aligning and reslicing PET images. J Comput Assist Tomogr **16:**620-33.
260. **Yan, Q., J. Zhang, H. Liu, S. Babu-Khan, R. Vassar, A. L. Biere, M. Citron, and G. Landreth.** 2003. Anti-inflammatory drug therapy alters beta-amyloid processing and deposition in an animal model of Alzheimer's disease. J Neurosci **23:**7504-9.
261. **Zhang, K., G. A. McQuibban, C. Silva, G. S. Butler, J. B. Johnston, J. Holden, I. Clark-Lewis, C. M. Overall, and C. Power.** 2003. HIV-induced metalloproteinase processing of the chemokine stromal cell derived factor-1 causes neurodegeneration. Nat Neurosci **6:**1064-71.
262. **Zhang, M. R., T. Kida, J. Noguchi, K. Furutsuka, J. Maeda, T. Suhara, and K. Suzuki.** 2003. [(11)C]DAA1106: radiosynthesis and in vivo binding to peripheral benzodiazepine receptors in mouse brain. Nucl Med Biol **30:**513-9.
263. **Zink, M. C., J. P. Spelman, R. B. Robinson, and J. E. Clements.** 1998. SIV infection of macaques--modeling the progression to AIDS dementia. J Neurovirol **4:**249-59.
264. **Zink, M. C., K. Suryanarayana, J. L. Mankowski, A. Shen, M. Piatak, Jr., J. P. Spelman, D. L. Carter, R. J. Adams, J. D. Lifson, and J. E. Clements.** 1999. High

viral load in the cerebrospinal fluid and brain correlates with severity of simian immunodeficiency virus encephalitis. J Virol **73:**10480-8.